LIGHT-SCATTERING STUDY OF THE GLASS TRANSITION AND THE GLASSY STATE IN LUBRICATING OILS

A THESIS

Presented to

The Faculty of the Division of Graduate Studies

By

Mohammed Ahmed Alsaad

In Partial Fulfillment

of the Requirements for the Degree

Doctor of Philosophy in the

School of Mechanical Engineering

Georgia Institute of Technology

August, 1976

LIGHT-SCATTERING STUDY OF THE GLASS TRANSITION AND THE GLASSY STATE IN LUBRICATING OILS

Approved:

Ward O. Winer, Chairman

Donald C. O'Shea

John T. Berry

George M. Rentzepis

David M. Sanborn

Date approved by Chairman: August 76

ACKNOWLEDGMENTS

The author is most grateful to his thesis committee for their time, continuous interest, counsel and suggestions throughout the period of this research. The advice and assistance from the chairman of the doctoral committee, Professor Ward O. Winer, is particularly appreciated. His constant advice and discussion made this thesis continually interesting.

The author is thankful to Dr. Donald C. O'Shea of the Physics Department for his authorization of using the light scattering equipment. The author also wishes to thank Dr. Fernando D. Medina, of the Physics Department, for his assistance in the light scattering experimental and for the design of some high pressure equipment needed in this investigation.

The research reported herein was supported by NASA Grant Number NGR 11-002-133 and NSF Grant Number ENG74-21002.

Finally, this research would have been impossible without the support and encouragement of my parents, Mr. and Mrs. Ahmed Alsaad.

TABLE OF CONTENTS

TABLE OF CONTENTS (Continued)

LIST OF TABLES

LIST OF TABLES (Continued)

LIST OF TABLES (Continued)

LIST OF TABLES (Continued)

LIST OF ILLUSTRATIONS

LIST OF ILLUSTRATIONS (Continued)

LIST OF ILLUSTRATIONS (Continued)

LIST OF ILLUSTRATIONS (Continued)

SUMMARY

This thesis reports the glass transition temperature as a function of pressure for four lubricants (polyphenyl ether, cycloaliphatic hydrocarbon, naphthenic base oil, and naphthenic base oil blended with 2.2 percent high molecular weight polymer) as measured by the light-scattering technique. The light source was a CRL Argon ion laser having a power of about 200 m watt in single frequency operation at 5145 Å. This technique allows the measurements of the sound velocity in materials as a function of pressure and temperature. The change in slope of the sound velocity as a function of pressure or temperature allows the determination of the glass transition. The maximum pressure attained was 100 kpsi (0.69 GN/m^2) and the temperature range varied from 76 to 210F (25 to 100C).

Two formation histories were used to form the glass. In both histories, all measurements were commenced in the liquid state and the glassy state was reached either by decreasing the temperature at a specified pressure (history A) or by increasing the pressure at room temperature (history B). The glass transition data were used to construct a phase diagram (glassy-liquid states) for each lubricant.

The glass transition data obtained were in good agreement with glass transition measurements of other techniques. The data indicated that the glass transition temperature increased with increasing pressure at a rate which ranged from 1.50 to 2.45 F per kpsi (120 to 200 C per GN/m^2). Data taken from literature indicated that lubricants, under some temperature and pressure conditions of elastohydrodynamic (EHD) contacts,

were in the glassy state (by using the phase diagrams).

The importance of this research lies in the fact that at present many workers in the field of elastohydrodynamic lubrication assume that the lubricant in EHD contacts remains in the viscous liquid state. Adjustment to the existing theory will be necessary if the physical state of a lubricating oil in the EHD contact indicates that it falls in or near the glassy state. In that case, the solid-like properties of the lubricant will be the controlling material characteristics.

NOMENCLATURE

C_p = Specific Heat

E = Electric Field Intensity of Incident Light

E_s = Electric Field Intensity of Scattered Light

E_o = Amplitude of the Electric Field of the Scattered Light

FSR = Free Spectral Range

G = Shear Modulus

G_t = The 97.5 percent point of the t-distribution

I_i = Intensity of the Incident Light

I_c = Intensity of the Central Unshifted Component

I_s = Intensity of the Scattered Light

I_B = Intensity of Brillouin Component

K = Cooling Rate

M = Longitudinal Modulus

N = Number of Molecules in the Scattering Volume

P = Pressure

Pg = Glass Transition Pressure

ΔP = Adiabatic Fluctuation of Pressure

ΔPg = Confidence Limit of Pg

S = Entropy

S_p = A Quantity defined as $\left\{ \sum_{i=1}^{n} (T_i - T_{av_i})^2 \right\}^{1/2}$

T = Temperature

T_{av} = Average Temperature

T_1 = Temperature at which solidification ends

T_2 = Temperature at which solidification starts

T_g = Glass Transition Temperature

ΔT_g = Confidence Limit of Tg

V = Velocity of Sound

V_L = Velocity of Sound in the Liquid State

V_ℓ = Longitudinal Velocity of Sound

V_g = Velocity of Sound in the Glassy State

V_t = Transverse Velocity of Sound

a = Least-Square Estimator (intercept)

b = Least-Square Estimator (slope)

c = Speed of Light

d = Separation Distance between the Mirrors of the Fabry-Perot

K = Wave Number of the Elastic Waves

$\vec{K}$ = Wave Vector of Sound

$\vec{K}_i$ = Wave Vector of Incident Light

$\vec{K}_s$ = Wave Vector of Scattered Light

f = Frequency of Light

m = Order of Interference (an Integer)

n = Number of Experimental Points

n_i = Index of Refraction

r = Distance from an Arbitrary Fixed Point to any element Inside the Scattering Medium

s = Standard Derivation of the Residuals of V

s_p = Pooled Variance Defined by Equation 33

t = Time

v = Specific Volume

ρ = Density

α = Isobaric Coefficient of Expansion

β = Isothermal Compressibility

γ = Specific Heat Ratio

ϵ = Dielectric Constant

$\bar{\epsilon}$ = Average Dielectric Constant

$\Delta\epsilon$ = Fluctuation in the Dielectric Constant

τ = Relaxation Time

θ = Scattering Angle

φ = Phase Angle

λ = Wavelength of Light in Free Space

Λ = Wavelength of Sound in the Medium

ω_o = Frequency of Incident Light

ω_B = Frequency Shift or Brillouin Shift

$\omega_{B\ell}$ = Longitudinal Frequency Shift

ω_{Bt} = Transverse Frequency Shift

$\bar{\eta}$ = Apparent Viscosity

Φ = Modulation Function of the Scattered Light

Φ_o = Amplitude of the Modulation Function

Ω = Frequency of Sound (Equal to ω_B)

Σ = Slide-to-roll speed ratio

CHAPTER I

INTRODUCTION

Recent investigations of elastohydrodynamic lubrication have indicated the importance of lubricant rheology. Lubricants serve multiple functions in the operation of an elastohydrodynamic (EHD) contact. One function of major importance is the separation of rolling or sliding surfaces in an EHD contact by the lubricant film. If total separation of the EHD contact surfaces can be achieved, the life of bearings and gear components can be expected to be very long, being limited principally by fatigue of the material surfaces. Therefore, the practical importance of the mechanism of elastohydrodynamic lubrication lies in the thickness of the lubricant film generated between the contact surfaces.

A thorough understanding of the lubricant rheology in the EHD contact is still lacking. As this thesis will demonstrate, the glass transition of lubricants and therefore the rheological behavior in the glassy state play a significant role in determining the rheological behavior in EHD lubrication.

Elastohydrodynamic Lubrication

Elastohydrodynamic lubrication deals with nonconforming surfaces that are elastically deformed by loads which must be carried over small areas. The load gives rise to a pressure which is distributed over the small contact area. Typical maximum pressure found in bearings and gear

contacts are on the order of 200,000 to 500,000 psi. Such nonconforming surfaces may be represented by a sphere or cylinder loaded against a flat surface where the load causes the surfaces to elastically deform over a small region.

An EHD contact can move by rolling, by sliding, or a combination of the two. Sliding generates frictional heat and imposes large shear forces on the lubricant film. These films are usually only a few microinches thick in the contact area. For such a thin film to permit relative motion of the surfaces, it must undergo shearing at very high rate.

The conjunction zone of a typical EHD contact can be divided up into three general regions: the inlet region, the Hertzian region, and the outlet region. The pressure and temperature in the contact build up gradually over the inlet region to high values in the Hertzian area. The pressure has a spike before dropping sharply to zero at the outlet region. Therefore, the properties of the lubricant, while passing through these regions, change within a matter of millisecond. The properties in each region are determined by the temperature, pressure, and relaxation time that exist in each region. The physical state of the lubricant is important to investigate since the behavior of the lubricant, as governed by pressure and temperature conditions within the inlet region, influence the film thickness. This film thickness is controlled by the rate at which the lubricant is drawn into the conjunction zone and by the viscosity of the lubricant in the inlet zone which can be increased significantly by pressure. The lubricant behavior in the Hertzian zone is important primarily in determining

sliding friction or traction. The simultaneous existence of extremes of high pressure and temperature in thin lubricant films and short residence times make the elastohydrodynamic contact a most unusual physical system.

The mechanical behavior of a lubricant as it passes through an EHD contact has been assumed by many workers to be viscous in nature. The proposition that this behavior might not be that of a viscous liquid but an elastic solid was first presented by Smith[1] in 1960. In 1973 Johnson and Roberts[2] devised a rolling contact experiment to make direct observations of viscoelastic behavior under conditions of elastohydrodynamic lubrication. Their results demonstrate a transition from a predominantly viscous to predominantly elastic response with increasing pressure at constant temperature and with decreasing temperature at constant pressure. Results obtained from disc machines on a typical high viscosity mineral oil (Shell Turbo 33), obtained by Johnson and Cameron[3], show that the plot of log ($\bar{\eta}$) versus pressure exhibits a marked change in slope at viscosities above 10^4 poise, where $\bar{\eta}$ is the apparent viscosity determined from the measured traction. These authors remarked that this change indicates a change in physical properties of the oil at high pressure. In a recent paper[5] on a five ring polyphenyl ether, it was concluded that this oil behaves elastically and that the criterion of elastic behavior is not the magnitude of the pressure but of apparent viscosity.

It is important to note that most hydrocarbon lubricating oils contain linear and highly branched hydrocarbons as well as ring structures. Thus, a lubricant can display both a glass transition temperature which

is associated with the non-crystallized part of the oil and a phase transition which is associated with the wax in the oil[6,7]. In the early stages of this research, glass transition temperatures at atmospheric pressure were measured by the technique of Differential Scanning Calorimetry (DSC) for two lubricating oils: naphthenic base oil R-620-15, designated as N1 and five ring polyphenyl ether, 5P4E. The instrument employed was a Perkin-Elmer Model DSC-2. Glass transition temperatures were -74 F (-59 C) for N-1 sample and -6 F (-21 C) for 5P4E. Since these values are low compared to the operating temperatures in a typical EHD contact, the occurrence of the glass transition phenomena and the existence of the glassy state in the contact were not investigated earlier by other researchers in this field. However, because of the fact that the glass transition temperature increases with pressure, and because of the existence of high pressures in the EHD contacts, the glass transition temperature can be greater than the operating temperature in the contact. The ASME Pressure-Viscosity-Report[8] was used to obtain an estimate of the variation of Tg with pressure. The solidification points indicated in the ASME report were taken as the glass transition points. Since these are reported as pressures at several different temperatures, they premit an estimate of the change of glass transition temperature with pressure. Also, according to McKinny[14], the glass transition is an isoviscous state. The change in temperature with pressure required to maintain constant viscosity gives results that are consistent with the results based on solidification. For typical lubricants, the glass transition temperature increases with pressure at a rate ranging from 1.0 to 4.0 F per kpsi. Thus, it would be

expected that lubricants will be in the glassy state in an EHD contact with average pressures of 100,000 psi or higher at room temperature. Therefore, it would be expected that many lubricants are in the glassy state for a significant portion of the time they are in the contact. The temperatures and pressures at which glass transition occurs and the mechanical properties of the lubricant in the glassy state may influence the two most important dependent operating variables of an EHD contact: the film thickness and the traction. Since the relaxation time of a material in the glassy state is long compared to the residence time in the contact, it is possible that once in the glassy state, the lubricant will remain in the glassy state on the moving surface while the surface moves from one EHD contact to the next. This may happen in spite of the fact that the pressure causing the glassy state formation has been removed. It is also possible that the glassy lubricant does not have time to flow while in the EHD contact but cleaves somewhere in the film so that solid layers of lubricant adhere to the contact surfaces and slid upon each other. Therefore, the glass transition temperature as a function of pressure, is a significant material property of lubricants. The mechanical and thermal properties of a substance in the glassy state are known to be functions of Tg and Pg which in turn are functions of temperature, pressure, and rate of temperature and pressure changes prior to entering the glassy state .

Glass Transition Temperature and the Glassy State

Glass transition is characterized by certain experimental observations which occur on the isobaric cooling or isothermal

compression of a material. At the glass transition, many material properties change in a characteristic manner. As the temperature is reduced in the liquid region, the material contracts and the viscosity increases. If the material is capable of crystallization, a point will be reached where crystallization starts. If crystallization does not occur or can be avoided, the viscosity will continue to increase until some level of 10^{8}-10^{13} poise is reached[10,35,48]. At this point, the material becomes solid and the thermal expansion coefficient falls by about one-half to one-third of its value in the melt or liquid state as shown in Figure 1. Glass transition is also accompanied by a change in the specific heat, C_p, isothermal compressibility, β, and other secondary properties. It corresponds to a change in slope of a plot of specific volume versus temperature as shown in Figure 2. Thus, glass transition phenomena are a characteristic of any liquid which can be supercooled to a sufficiently low temperature without crystallization. Glass transition phenomena are often referred to as an apparent second-order transition since it is characterized by a discontinuous change in the secondary thermodynamic quantities. These changes occur over a range of temperatures and are not strictly discontinuous. Ferry[11] and Haward[9] showed that glass transition phenomena is not a true second-order thermodynamic transition since the substance at Tg is not in thermodynamic equilibrium. This is due to the slowness of molecular rearrangements at this temperature. This absence of thermodynamic equilibrium is part of the definition of the glassy state. Below Tg, the degree of order will appear fixed and will not vary with temperature or pressure during any reasonable length of time. Because

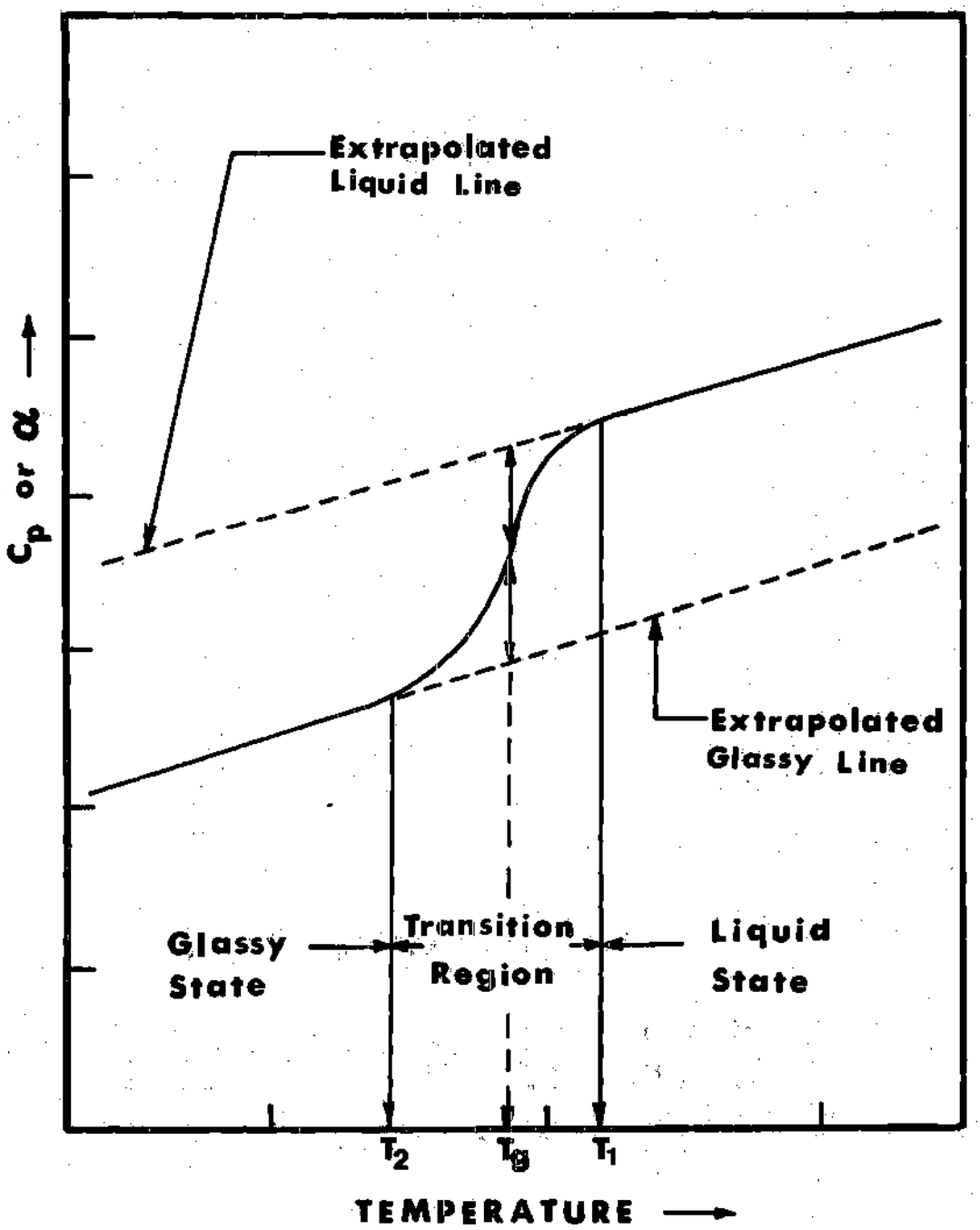

Figure 1. Thermal Expansion Coefficient or Specific Heat for a Typical Glassy Material.

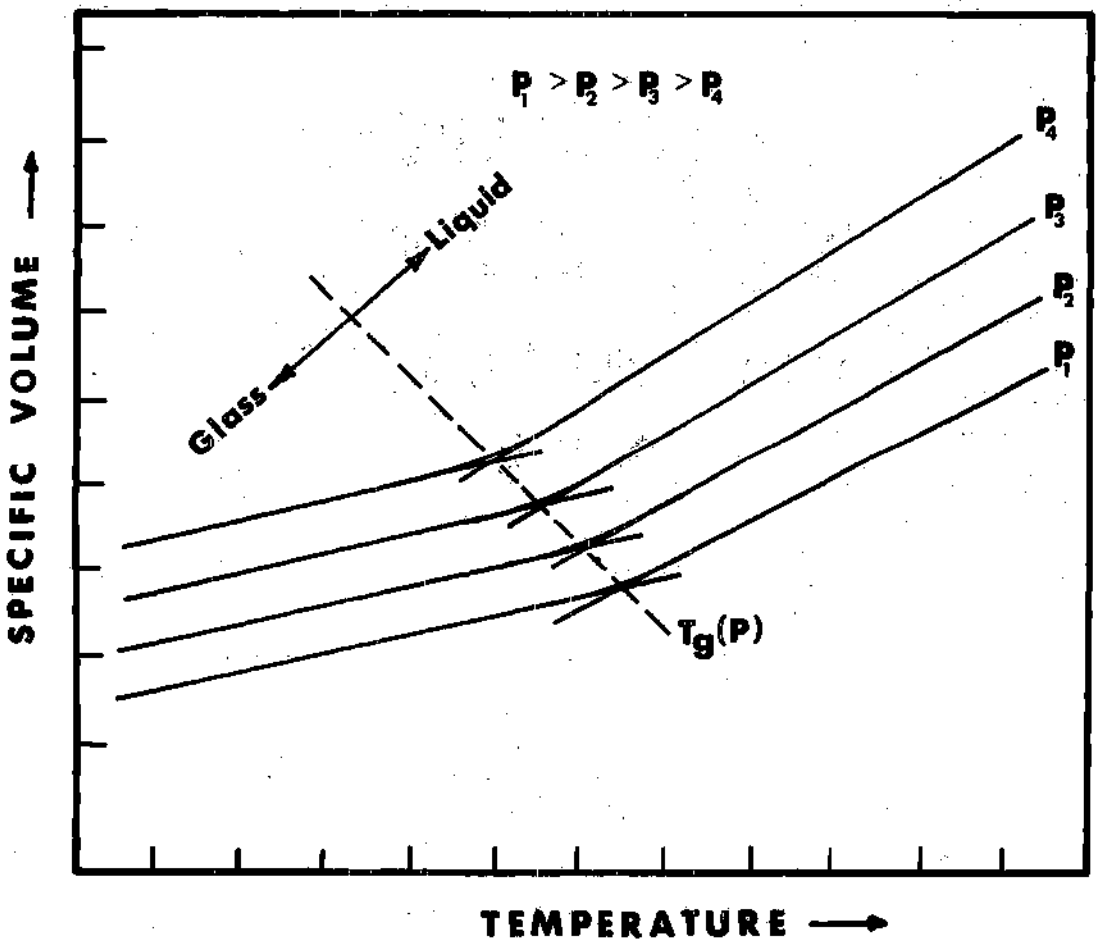

Figure 2. Typical Plot of Specific Volume Versus Temperature for a Glassy Material at Different Formation Pressures.

of this, the structural degrees of freedom are said to be frozen-in and therefore, the structural contribution to α, C_p and β are absent in the glassy state.

The effect of pressure on Tg is shown in Figure 2. The glass transition temperature shifts upward as the pressure is increased. The increase in Tg with pressure will be sufficient to maintain an isoviscous state. A sufficiently high pressure can induce a transition from the liquid state to the glassy state without requiring a decrease in the temperature.

As a result of the non-equilibrium state, the thermodynamic history of a glass forming liquid has considerable influence on the structure, the transition and the properties in the glassy state. Glass transition can be reached either by isobaric cooling or by isothermal compression. The influence of the rate of cooling, K, on the shift of the glass transition temperature of poly(vinyl acetate) has been studied over a wide range of rates by Kovacs[12]. The volume-temperature response obtained from different constant rates of cooling of a glass-forming substance is shown in Figure 3. Since decreasing the rate of cooling increases the effective experimental time, the glass transition temperature will be shifted to lower values. Matsouka and Maxwell[13] studied the effect of rate of compression on the compressibility curves of polysterene at 250 F. Their results indicate that glass transition pressure, Pg, shifts to lower values when a greater rate of pressure application is employed. If the pressure is increased slowly, the molecules of the material will have enough time to rearrange and the glass transition will take place at a higher pressure. On the other

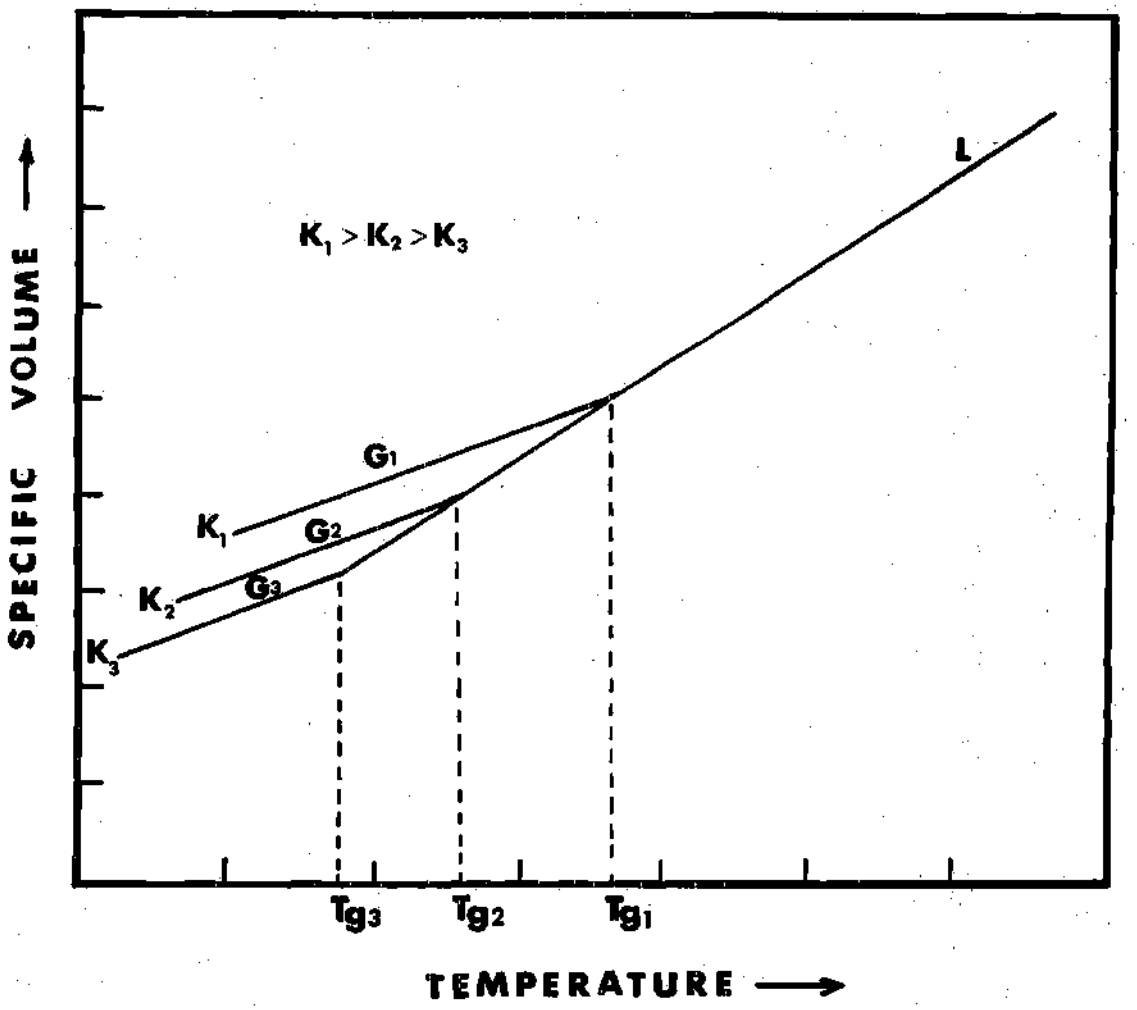

Figure 3. Dependence of the Glass Transition Temperature on the Cooling Rate, K_i. L = Liquid and G = Glass.

hand, if the rate of pressurization is increased, the time for any structural changes is smaller and the glass transition occurs at a lower pressure.

The influence of thermodynamic history on glass transition of poly(vinyl acetate) was studied by McKinney and Goldstein[14] by using three different thermodynamic histories: variable formation history (isobaric cooling at different pressures), and two constant formation histories (cooling at atmospheric pressure or 800 bar followed by pressure changes in the glassy state). Comparisons were made between data obtained from different histories used to form the glass.

Several techniques are employed for the determination of the glass transition temperature such as dilatometry[14,35,36], differential scanning calorimetry[6,37,38]. Thermomechanical analysis (TMA), and, dielectric[39,40] and light-scattering techniques[20-25,27-31]. Depending on the technique used, various methods exist for specifying the glass transition temperature within the transition region. The usual dilatometric technique is to cool the liquid at a constant rate and extrapolate the linear portions of the volume-temperature relation above and below the transition region to their intersection. The temperature of this intersection[14] is taken as the glass transition temperature as shown in Figure 2. If Tg is measured by the change in the expansion coefficient or the specific heat, then Tg is taken as the mid-point in the step-change as measured from the extensions of the glass and liquid base lines as shown in Figure 1. While the choice is somewhat arbitrary, and other authors have suggested alternate techniques, the above methods are the most commonly used.

The first step in the study of the importance of the glassy state in EHD contacts is to determine if the lubricant is in or near the glassy state while in an EHD contact. This requires the determination of the glass transition temperature as a function of pressure for typical lubricants. From these data, a phase diagram showing the liquid and the glassy state can be constructed based on the operating temperatures and pressures in the contact. This will require the knowledge of the temperature and pressure distributions in the contact. Winer and co-workers[15] measured the temperature distribution for a naphthenic base lubricant (N1) in the contact by using the infrared radiation emitted by the EHD conjunction. The prediction of the elastohydrodynamic pressure distribution in the contact requires extensive numerical analysis. This distribution can be obtained from an analytical technique being investigated at the Tribology and Rheology Laboratory, School of Mechanical Engineering, Georgia Institute of Technology. This technique employs the measured film thickness distribution in the EHD contact in solving an inverse elasticity problem. However, a satisfactory first approximation to the pressure distribution of highly loaded EHD contacts would be the Hertzian pressure distribution resulting from dry contacts of the surfaces.

Knowing the temperature and pressure distributions in the EHD contact, the constructed phase diagram will determine whether or not lubricants in EHD contacts are ever in the glassy state, approximately what operating conditions result in the glassy state behavior, and over what fraction of the contact area the glassy state exists.

In this research, the glass transition temperature as a function

of pressure will be determined for four typical lubricants by the light-scattering technique. A phase diagram which shows the liquid state and the glassy state for each lubricant will be constructed. These phase diagrams will be used to determine if a lubricating oil, under the operating conditions of pressure and temperature in the EHD contact, passes through a glassy state or remain in the liquid state.

CHAPTER II

RESEARCH TECHNIQUE

The basic concepts of the light-scattering technique and the description of experimental equipment used for measuring the glass transition temperature are discussed in the first section of this chapter. The second section contains a description of the experimental fluids chosen for this research.

Theory of Light-Scattering for Measuring Glass Transition

This section will be divided into two parts. The light-scattering theory will be presented in the first part. The concept of measuring the glass transition from the sound velocity data will be discussed in the second part.

Theory

When a laser beam passes through a transparent medium, a small portion of the light is scattered in all directions. This light scattering is a result of optical inhomogeneities in the scattering medium. The optical inhomogeneities are the result of fluctuations of the dielectric constant brought about by the fluctuation of the density of the medium due to random thermal motion of the molecules[16].

The dielectric constant, ϵ, of a liquid can be considered as

$$\epsilon = \bar{\epsilon} + \Delta\epsilon \qquad (1)$$

where $\bar{\epsilon}$ is the average dielectric constant and $\Delta\epsilon$ represents the

fluctuation in ϵ. Assuming the entropy, S, and the pressure, P, are independent variables, one can write $\Delta\epsilon$ as a sum of two terms

$$\Delta\epsilon = \left(\frac{\partial\epsilon}{\partial S}\right)_P \Delta S + \left(\frac{\partial\epsilon}{\partial P}\right)_S \Delta P \qquad (2)$$

The first term is the result of entropy fluctuations at constant pressure (isobaric) while the second term is the result of pressure fluctuations at constant entropy (adiabatic). The convenience of this choice of independent variables is obvious if one realizes that thermal sound waves are adiabatic pressure fluctuations. These pressure fluctuations represent random local compressions or rarefactions which, as a consequence of the elastic properties of the medium, do not remain fixed in position but travel throughout the volume of the sample. These adiabatic fluctuations can be described by means of plane sound waves of thermal origin propagating in all possible directions.

The study of the specific heat of a solid lead Debye[17] to the conclusion that the energy which one must have in all 3N degrees of freedom associated with the atomic oscillations of the solid can be considered as the energy of 3N normal elastic waves. Thus, Debye considered the energy of thermal motion of a solid as the energy of elastic waves. The Debye representation of the energy of thermal motion can also be extended to liquids and dense gas if the damping of thermal waves is small.

A major advancement in the development of light-scattering theory was achieved when Brillouin[18] established the fact that sound waves and the Debye thermal elastic waves were the same phenomena.

Thermal fluctuations do not remain "frozen", but change continuously in time and therefore, they can modulate the scattered light. If we let the modulation function be $\Phi(t)$ and the monochromatic light wave undergoing modulation be given by

$$E_s(t) = E_o \exp(i\omega_o t) \tag{3}$$

where $E_s(t)$ is the electric field intensity of the scattered light and E_o is its amplitude, the resulting vibration of the scattered light will have the form

$$E_s'(t) = E_s(t) \cdot \Phi(t) \tag{4}$$

Consider the modulation of the scattered light by adiabatic fluctuations of pressure. The change of pressure with time satisfies the wave equation. Neglecting the absorption of the elastic waves, we can write the wave equation in the form[16]

$$\ddot{\Phi} - V^2\nabla^2\Phi = 0 \tag{5}$$

where V represent the velocity of propagation of the elastic waves. The solution of equation (5) is given by

$$\Phi(t) = \Phi_o \cos[\Omega t - \vec{k}\cdot\vec{r}] \tag{6}$$

where Ω is the frequency of the elastic wave and equal to $\vec{V}\cdot\vec{k}$ where $\vec{k}$ is the wave vector of the elastic wave. Thus, the vibration in the scattered light wave with wave vector $\vec{k}_s$ diffracted by the elastic wave with wave vector $\vec{k}$ in the direction of $\vec{k}_s$ is given by

$$E_s'(t) = \frac{\Phi_o E_o}{2} \{\exp[i(\omega_o + \Omega)t - \vec{k}\cdot\vec{r}] + \exp[i(\omega_o - \Omega)t + \vec{k}\cdot\vec{r}]\} \qquad (7)$$

The above result shows that there are two doublets in the spectrum of the scattered light with frequencies $(\omega_o + \Omega)$ and $(\omega_o - \Omega)$ symmetrically located on the two sides of the incident frequency, ω_o.

All 3N Debye waves in a body propagate in all possible directions. If such a body is irradiated by a parallel light beam with wave vector $\vec{k}_i$ and the scattered light is observed in the direction of the wave vector of the scattered light, $\vec{k}_s$, making an angle θ with $\vec{k}_i$ as shown in Figure 4, then the maximum intensity of the scattered light along $\vec{k}_s$ will occur when the wave vector $\vec{k}$ of the elastic wave together with the vectors $\vec{k}_s$ and $\vec{k}_i$ satisfy the Bragg condition

$$\vec{k}_i \mp \vec{k} = \vec{k}_s$$

or

$$|\vec{k}| \equiv k = \mp |\vec{k}_s - \vec{k}_i| = 2n_i k_i \sin\frac{\theta}{2} \qquad (8)$$

where n_i is the refractive index of the scattering medium at the incident wave length. Since the wave number is the reciprocal of the wave length, equation (8) can be rewritten as

$$\Lambda = \frac{\lambda}{2n_i \sin\theta/2} = \frac{V}{\Omega} \qquad (9)$$

where Λ is the wave length of the sound wave and λ is that of the incident light.

Moreover, as a consequence of the movement of the sound wave, the frequency of the incident light is altered by the Doppler effect

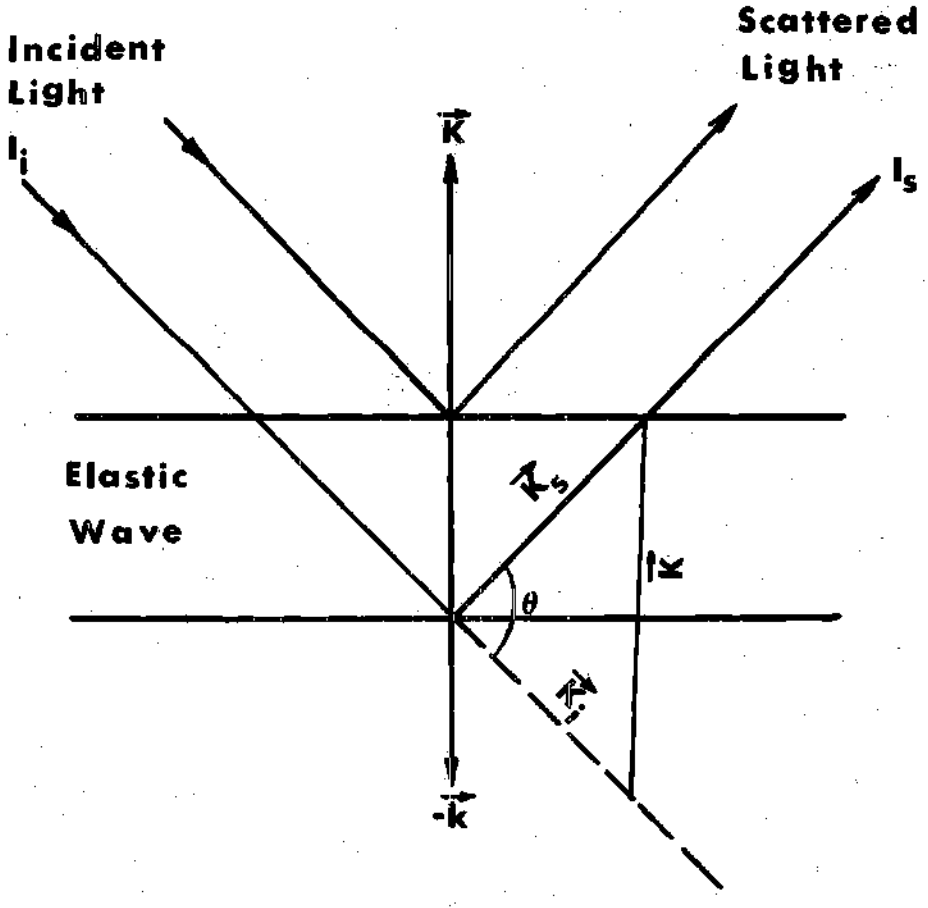

Figure 4. Bragg Condition of Light Scattered at an Angle θ Relative to the Incident Light Beam.

with respect to the original value ω_o. This effect was first predicted by Brillouin[18] as

$$\omega_B = \mp 2\omega_o\left(\frac{n_i v}{c}\right)\sin \theta/2 \qquad (10)$$

where c is the speed of light.

Rearranging and using the relation $\lambda = c/\omega_o$ we can write equation (10) as

$$V = \mp \omega_B \cdot \frac{\lambda}{2n_i \sin(\theta/2)} \qquad (11)$$

Comparing equations (9) and (11) we obtain the frequency shift, ω_B, equal to the sound frequency, Ω. For scattering angle of 90^o and incident light of wavelength of 5145^oA, the frequency shift in materials having a sound velocity of the order of 3000 m/sec. and a refractive index of 1.5 is about 12×10^9 Hz. This result shows that the Brillouin method deals with acoustical phenomena in the gigacycle region. This frequency shift represent a frequency change of less than 0.002 percent. The observation of frequency shift of this order is possible by a gas laser as a source of monochromatic light source and a Fabry-Perot interferometer as a detector. The two signs in the above equations correspond to the two opposite directions in which the sound wave may travel.

According to Landau and Placzek[19], the scattered light produced by the entropy fluctuations of $\Delta\epsilon$ does not propagate in normal liquids and these fluctuations are the source of the central unshifted component of the scattered light. The intensity of this component, I_c, is expressed as a function of the total intensity in the Brillouin doublet, $2I_B$, by

the Landau-Placzek relation[20,21]

$$\frac{I_C}{2I_B} = \gamma - 1 \tag{12}$$

where γ is the specific heat ratio.

Measurements on Brillouin spectra have been made by a number of workers such as Rank et al.[20,22], Cummins and Gammon [23], Pinnow et al.[21], and others[24,25] who observed the Brillouin effect by using He-Ne and Argon ion laser as light source. A typical frequency spectrum of lubricating oils is shown in Figure 5. The shift of the Brillouin lines from the laser frequency is of interest since it enables us to calculate the velocity of sound according to equation (11).

For a viscous medium, two types of Brillouin scattering can be observed

(i) Scattering from longitudinal sound waves which gives a measurement of the longitudinal modulus, M, as

$$M = \rho V_\ell^2 \tag{13}$$

where V_ℓ is the longitudinal velocity of sound given by

$$V_\ell = \omega_{B\ell} \frac{\lambda}{2n_i \sin \theta/2} \tag{14}$$

(ii) In highly viscous materials just as in crystals and glasses, a second set of Brillouin lines is often observed in the depolarized spectrum with a shift smaller than that of the longitudinal Brillouin lines (not shown in Figure 5). These new shifted components are

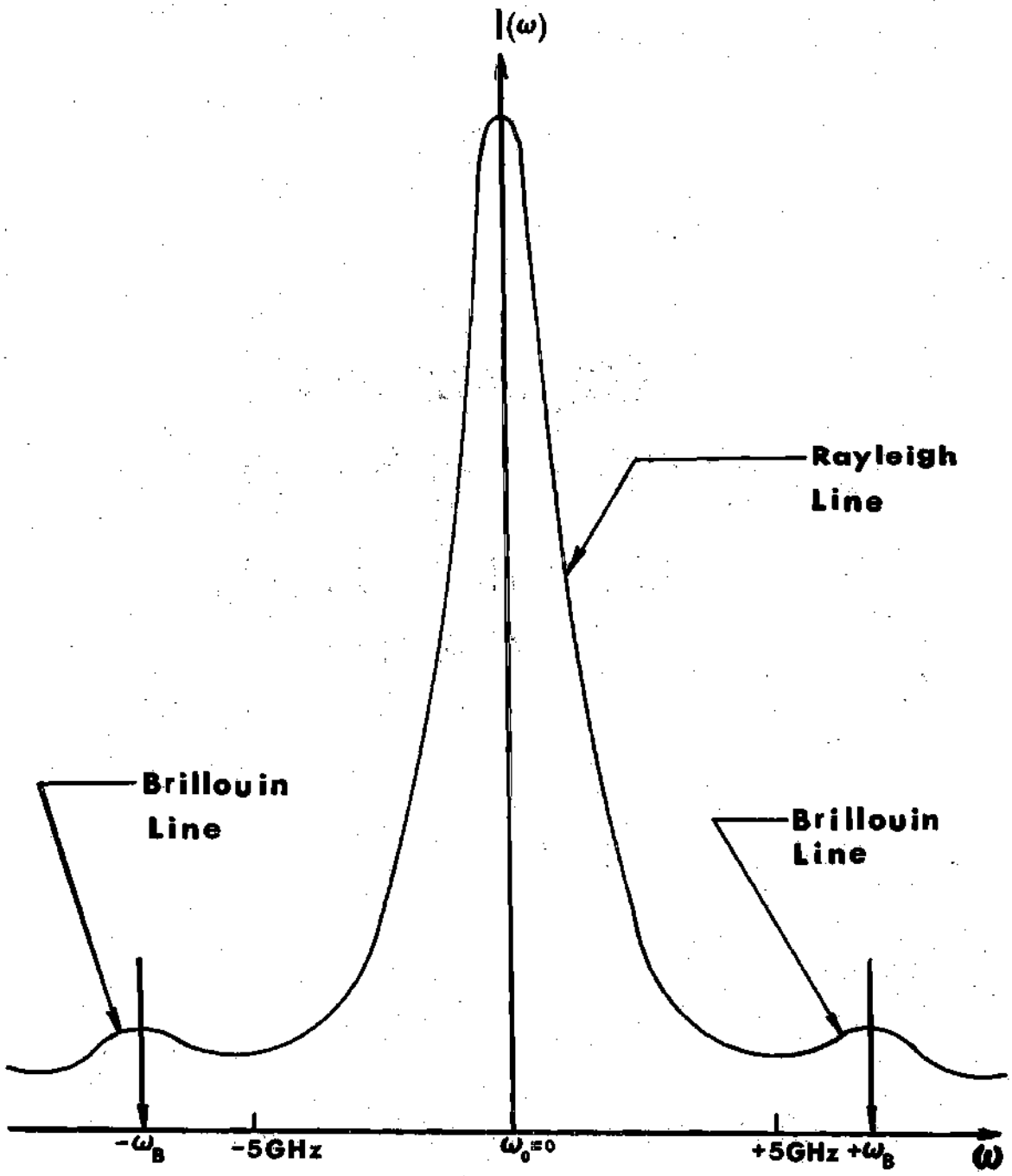

Figure 5. Frequency Spectrum of a Naphthenic Base Oil at 76F and Atmospheric Pressure.

transverse Brillouin lines due to scattering from propagating thermal transverse waves which can propagate in the medium as it becomes more viscous. Scattering from transverse waves appear in the depolarized spectrum because these waves cause anisotropic fluctuations in the local structure of the material. In lubricants at high viscosities, the material is acting in a glassy manner and the transverse Brillouin peaks may be detected. The fact that these peaks appear in the frequency spectrum is an indication that there are shear waves propagating in the sample. Scattering from transverse sound waves gives a measurement of the shear modulus, G, as

$$G = \rho V_t^2 \tag{15}$$

where V_t is the transverse velocity of sound given by

$$V_t = \omega_{Bt} \frac{\lambda}{2n_i \sin \theta/2} \tag{16}$$

In low-viscosity liquids, the transverse elastic waves are so weak that the inner Brillouin doublet, which is brought about by the diffraction and modulation of light by the transverse wave, is difficult to observe. In this research only longitudinal frequency shifts and longitudinal sound velocities will be reported.

Pressure and Temperature Coefficients of the Sound Velocity

A change in the slope of the sound velocity as a function of temperature and pressure like density or specific heat also defines the glass transition and has been observed by many workers[24,25,27,28].

It has been established that the change in the temperature coefficient of the sound velocity is a manifestation of the change in the thermal expansion coefficient that occurs at the glass transition temperature[29-31]. This allows us to detect the glass transition with gigacycle sound waves. Figure 6 shows the variation of the sound velocity and frequency shift with temperature for atactic polystyrene[25] where a change in slope is clearly observed at the glass transition temperature. This change in the temperature and pressure coefficients of the sound velocity was observed in all the lubricating oils investigated in this work.

The dependence of the velocity of sound on the density, ρ, is seen through the relation

$$V = (M/\rho)^{1/2} \qquad (17)$$

where M represents the appropriate modulus of elasticity which is a function of the density. Since the density appears explicitly in the above relation, it is clear that a change must appear in the slope of the velocity-temperature and velocity-pressure curves at the glass transition. A comparison of volume-temperature data with velocity-Temperature data taken from literature[29] is consistent with the above observation. However, the expansion coefficient of polystyrene is $2.2 \times 10^{-4}\ ^{o}C^{-1}$ for $T < Tg$ and $5 \times 10^{-4}\ ^{o}C^{-1}$ for $T > Tg$ while the velocity coefficient is $8 \times 10^{-4}\ ^{o}C^{-1}$ for $T < Tg$ and 14×10^{-4} for $T > Tg$ which shows that the dependence of velocity on density is chiefly through the strong dependence of the modulus on density and only to a lesser extent through the explicit appearance of density in equation (17).

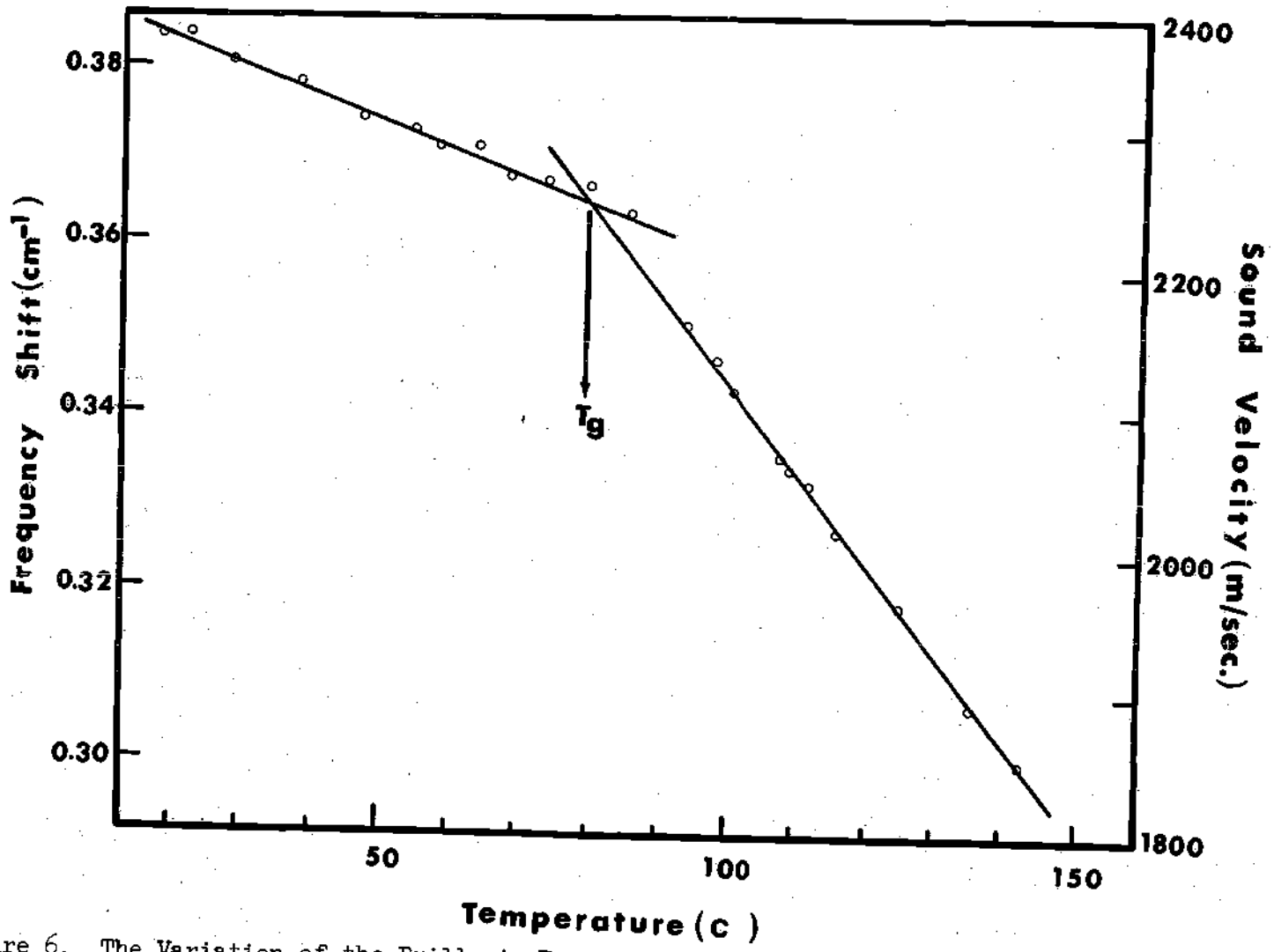

Figure 6. The Variation of the Brillouin Frequency Shift and the Sound Velocity with Temperature at Atmospheric Pressure for Atactic Polystyrene[25].

Experimental Equipment

This section will include the description of the light-scattering and high pressure equipment.

Light Scattering Equipment

The schematic arrangment of the basic components of the light-scattering experiment is shown in Figure 7 and consist of (1) a CRL Argon ion laser model 52 in single frequency operation and having a power of about 200 milliwatt at $\lambda = 5145^{\circ}A$. Single line operation is accomplished by inserting a wavelength-dispersing element (Prism) into the laser cavity, (2) a high pressure scattering cell containing the lubricant sample to be investigated, and (3) a detector which permits the spectroscopic analysis of the scattered light.

The scattered light from the lubricant sample is collected by a lens and enters a Fabry-Perot interferometer as shown in Figure 8. The output of the interferometer, consisting of polarized and depolarized scattered light, is focused on a screen which has a pinhole in front of a photomultiplier tube (PMT). The output signal from the PMT can be processed by a standard counting system and recorded with a multichannel analyser. The spectrum in the multichannel analyser is recorded on X-Y recorder and/or punched on paper tape.

The Fabry-Perot interferometer used in the light-scattering experiment consists of a pair of highly reflective mirrors separated by a specified distance, d. The mirrors can be moved and tilted to ensure exact parallism between their surfaces. At certain wavelengths[32], the amount of light transmitted through the mirrors will be many times larger than expected from the combined transmission for two highly

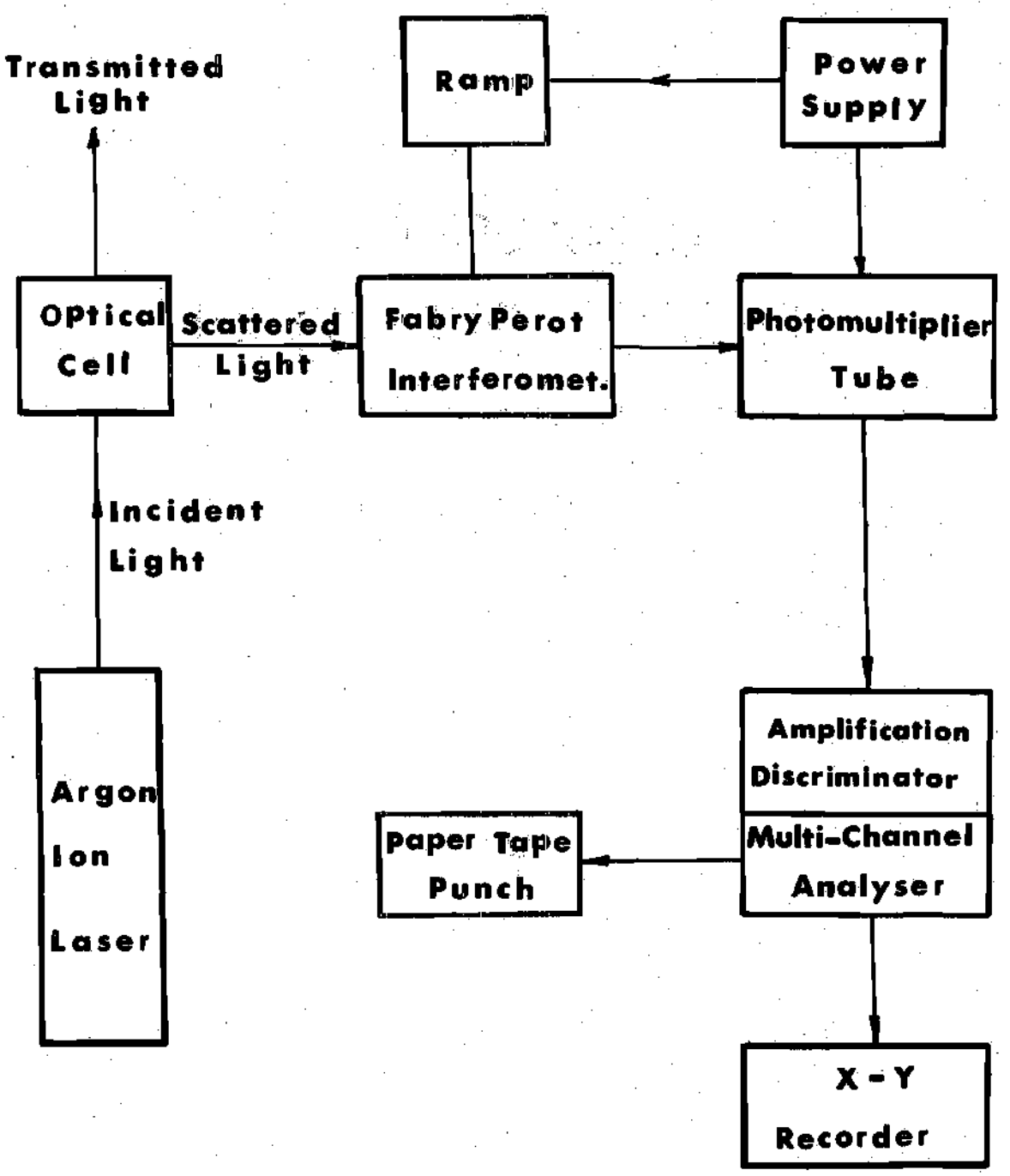

Figure 7. Schematic Arrangement of the Light-Scattering Experiment.

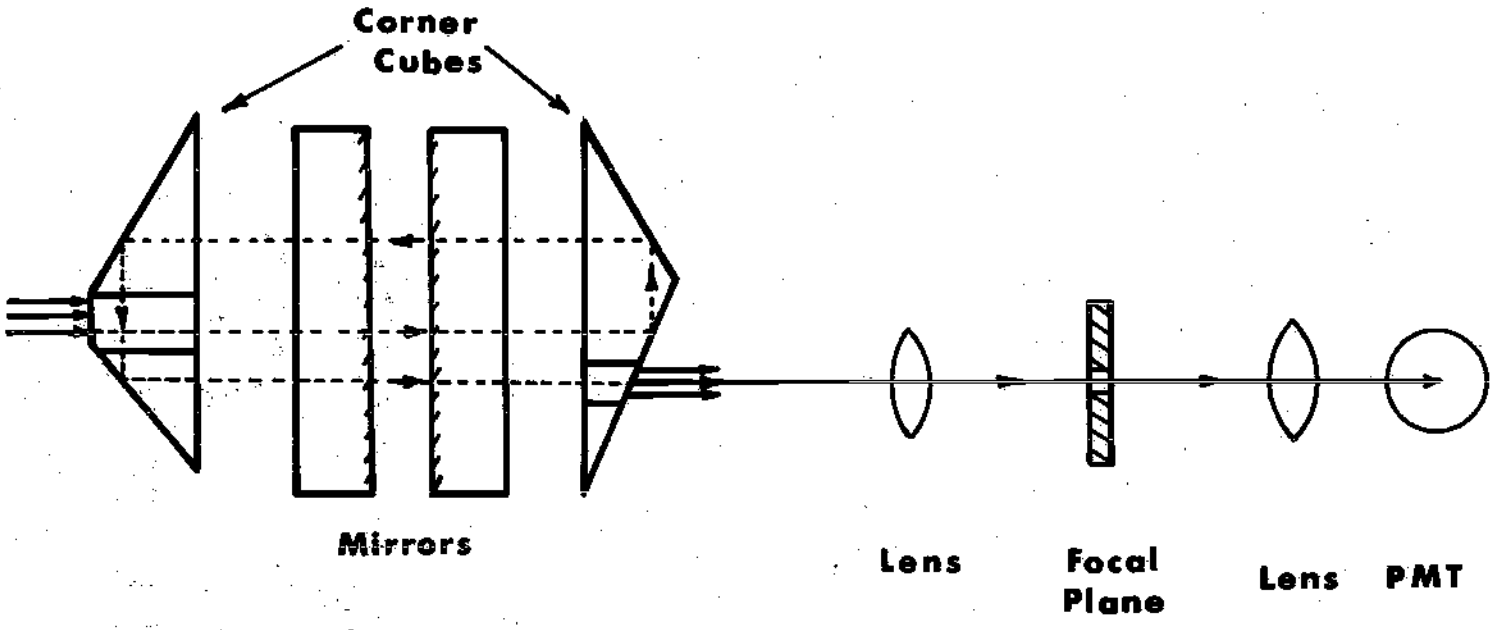

Figure 8. Schematic Arrangement of the Fabry-Perot Interferometer.

reflective mirrors. This occurs when there is constructive interference between incident light waves with those of different reflections. Only when all the waves from the multiple reflections are in phase will there be high transmission. For incident light normal to the mirror faces, the maximum transmission will occur when

$$\lambda_m = \frac{2d}{m} \tag{18}$$

where m is the order of interference (an integer). In terms of frequency, the above equation can be written as

$$\nu_m = \frac{c}{\lambda_m} = m \frac{c}{2d} \tag{19}$$

The transmitted beams are focused by a lens onto a screen where a series of concentric interference fringes are observed and only light travelling perpendicular to the plates obey the simple resonance condition. This light is focused to the center of the ring pattern. By placing a pinhole at this center, only light with frequency $\nu_m = m \frac{c}{2d}$ is allowed to pass through and be detected by a photomultiplier tube. If we plot the transmission of the interferometer as a function of frequency for a monochromatic incident light of frequency f, we would obtain a curve similar to that shown in Figure 9. These transmission characteristics enable the device to be used as a tunable filter to display the laser light and any shifted light due to Brillouin effect as a function of frequency. The frequency range which is transmitted during the Fabry-Perot scan is known as the free spectral range (FSR) which is

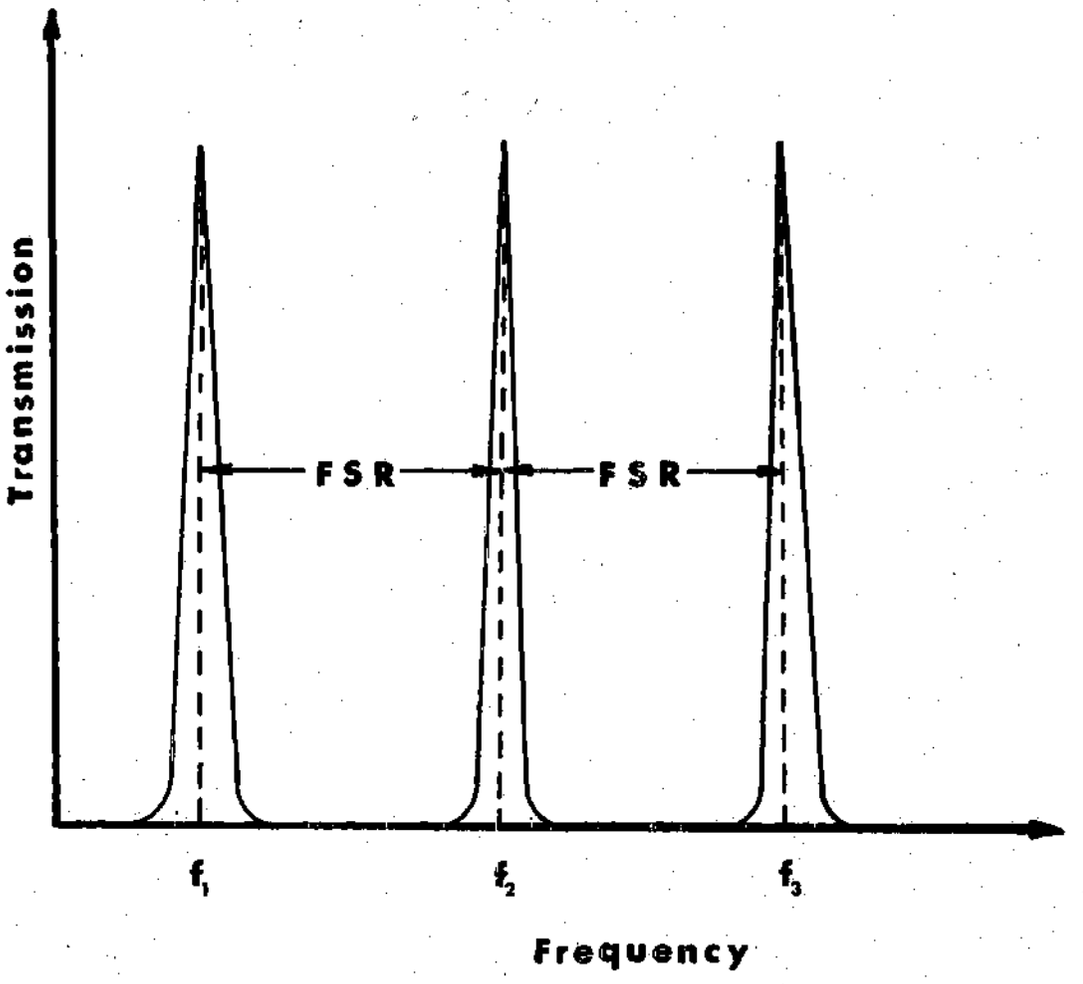

Figure 9. Transmission of the Fabry-Perot Interferometer as a Function of Light Frequency.

$$FSR = \frac{c}{2d} \tag{20}$$

Since the speed of light is approximated by 3×10^8 m/sec., the frequency units can be expressed in cm^{-1} (wave number units). A frequency of 15×10^9 Hz corresponds to 0.5 cm^{-1}. Unless otherwise specified, the frequency units will be reported in cm^{-1}.

In the scanning mode, we observe the spectral content of the scattered light by moving one mirror along the interferometer axis without disturbing the parallelism of the mirrors by applying a ramp (sawtooth) voltage to a piezoelectric transducer (PZT) attached to one of the mirrors.

The temperature inside the Fabry-Perot interferometer is controlled by a proportional controller and a thermister sensor. Two resistors (20 ohm-20 watt) are glued to each of the bottom and side panels of a plexiglass box enclosing the interferometer. The temperature is controlled to about $2\text{-}3^{\circ}$ above room temperature.

Since the Rayleigh line intensity is usually several orders of magnitude greater than that of Brillouin lines, a significant improvement of the frequency spectrums can be obtained by operating the Fabry-Perot interferometer in triple pass geometry. This is accomplished by using a pair of corner cubes (Figure 8).

In summary, the light-scattering technique enables one to determine the sound velocity at frequency ω_B if a monochromatic beam of light strikes the scattering medium and the frequency shift of the Brillouin scattered light at angle θ is measured. The location of the change in the slope of the sound velocity as a function of temperature

and pressure is a measure of the glass transition.

High Pressure Equipment

The high pressure equipment consists of a scattering cell, a strain gauge pressure transducer, a 9:1 area ratio intensifier and a hand pump.

The high pressure cell (3" x 2-3/4" x 1-3/4") is shown schematically in Figure 10. It was used to pressures of 100,000 psi. The test fluid in the cell was separated from the hand pump oil by an intensifier which was connected to the cell by high pressure tubing. The cell material is vasco max 300 CVM alloy which has the nominal composition and properties given in Table 1.

Table 2 gives the annealed properties for this alloy.

Heat treatment of the cell was necessary to raise the hardness and increase the strength properties. Aging the cell by heat treatment for six hours at 900 F followed by an air quench raised the hardness to about 52-55 Rockwell "C" and increased the yield strength to 280,000-300,000 psi according to the reference data sheet for this alloy.

The intensifier had a 9:1 piston area ratio and was mounted between the hand pump and the high pressure scattering cell. It is shown schematically in Figure 11. The test fluid is contained in the high pressure side of the intensifier cavity, the high pressure tubing and the optical cell. The high and low pressure sides of the intensifier piston were sealed with Viton O-rings which were protected by anti-extrusion rings. The intensifier material in the same as that of the optical cell and it was heat treated is the same manner.

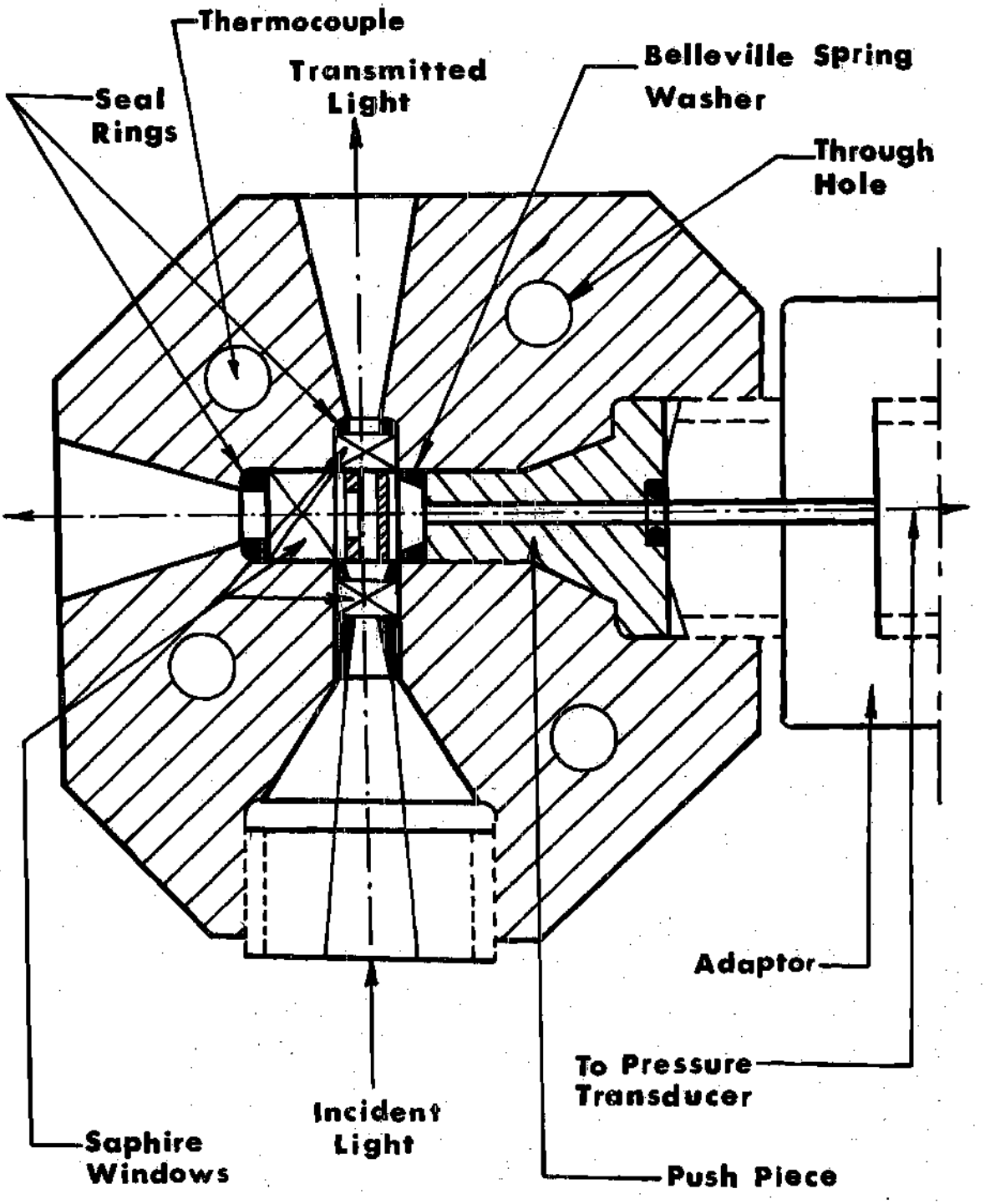

Figure 10. Schematic of Light-Scattering Cell. The Intensifier is Attached Perpendicular to the Paper Plane at the Centerline of the Cell.

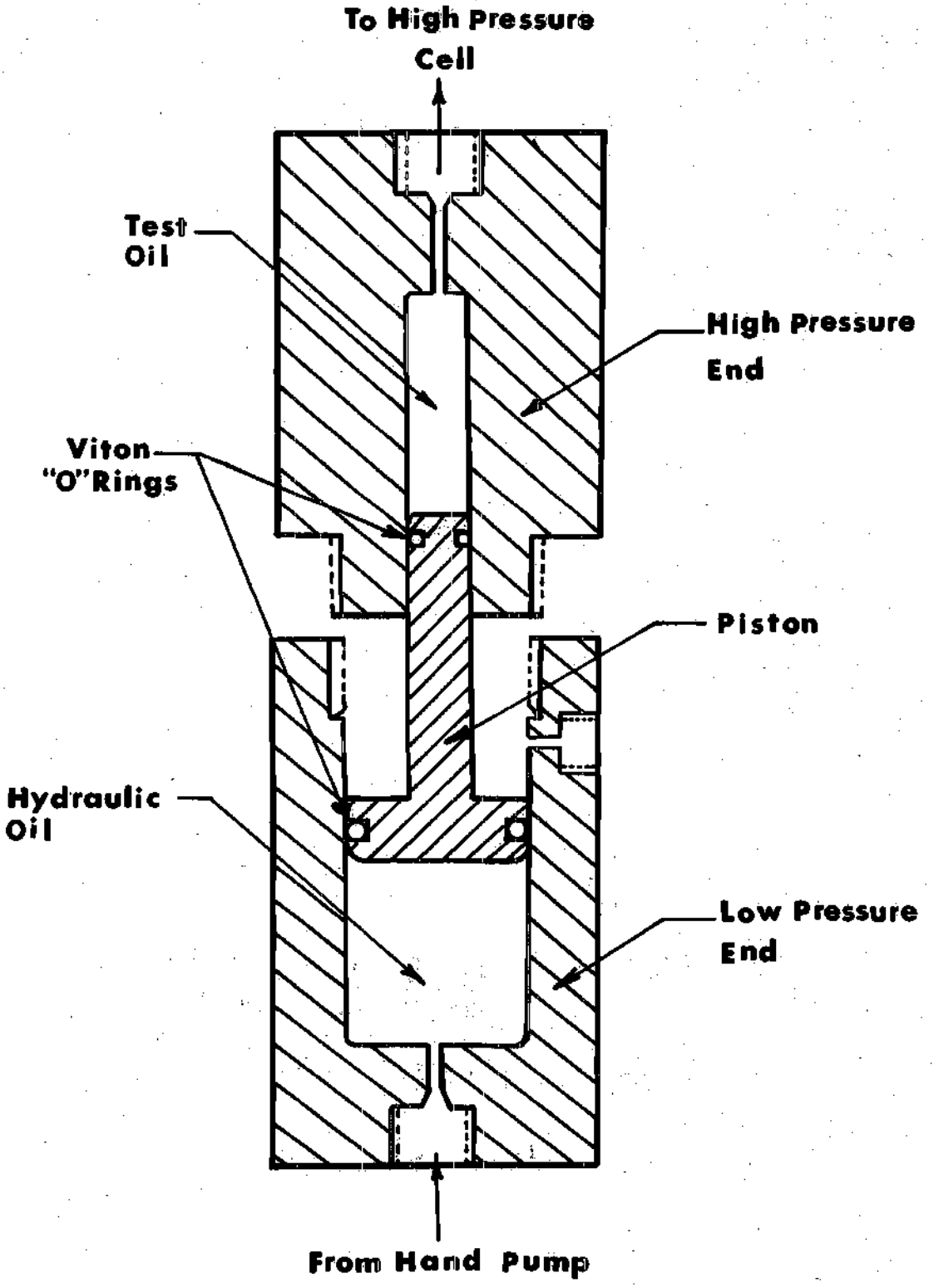

Figure 11. Schematic of Intensifier Assembly.

Table 1. Nominal Composition and Properties of the High Pressure Cell Material.

Carbon	0.031 max.
Silicon	0.03 max.
Manganese	0.10 max.
Sulfer	0.01 max.
Phosphorus	0.01 max.
Molybdenum	4.80
Nickel	18.50
Cobolt	9.0
Titanium	0.60
Aluminum	0.10
Boron	0.003
Zirconium	0.02
Average Coefficient of Thermal Expansion (70 - 900°F), in/in/°F	5.6×10^{-6}
Modulus of elasticity, psi	27.5×10^{6}
Density, lbs/cu.in.	0.289
gm/cc.	8.0
Thermal conductivity, BTU/ft^2/hr/°F/in.	
at 68°F	136
at 122°F	139
at 212°F	145

Table 2. Annealed Properties of the High Pressure Cell Material.

Hardness, Rockwell "C"	30-32
Yield Strength, kpsi	110
Ultimate Strength, kpsi	150
Elongation, %	18
Reduction of Area, %	72

The pressure of the lubricant samples contained in the optical cell was measured with a commercial strain gage pressure transducer as shown in Figure 10. The pressure transducer is a Norwood model 114 manufactured by the Advanced Technology Division of American Standard and was used in high pressure measurements[33,34] at the Tribology and Rheology Research Laboratory, School of Mechanical Engineering, Georgia Institute of Technology. It consists of a stainless steel diaphragm and strain cylinder assembly and utilizes a balanced four-arm bridge. The four arms are permanently bonded to the strain cylinder in such a manner that the deflection caused by the measured pressure results in an equivalent resistive unbalance of the bridge. The pressure to be measured is imposed upon the diaphragm. As the pressure increases, the strain cylinder decreases in length while increasing in diameter. These dimensional changes decrease the resistance of the longitudinal winding while that of the circumferential winding increase. The unbalance in resistance of these windings create an electrical millivolt output directly proportional to the measured pressure. This electrical unbalance was measured with a potentiometer in the same manner as described in the calibration procedure. Recommended excitation, mounting torque, arm resistance and other details are given in the technical data sheet supplied by the manufacturer and listed in Appendix C. The calibration procedure is also presented in Appendix C.

One of the important features of using the pressure transducer is that the lubricant sample pressure is measured directly in the optical cell and thus the influence of intensifier seal friction on pressure measurements is eliminated.

Experimental Fluids

The four lubricants investigated in this work are listed in Table 3 and a detailed description of each fluid is found in Appendix B. These oils were selected because of their relatively low glass transition pressures (less than 100,000 psi) at moderate temperatures of the range 76 to 200 F and because of the large amount of the data on elasto-hydrodynamic and pressure-viscosity behavior available in our laboratory and elsewhere[5,33,34,41,42]. In addition, these oils are representative of typical commercially available lubricants and research materials of current interest in the field of EHD lubrication.

Table 3. List of the Experimental Fluids

5P4E	Polyphenyl Ether
MCS-1218	Cycloalphatic Hydrocarbon
N1	Naphthenic Base oil, R-620-15
N2	N1 + 2.2% Polybutane LF-5346

The list of lubricants includes a naphthenic base oil blended with polymeric viscosity-index improver (N2) which will enable several trends and behaviors to be compared.

CHAPTER III

EXPERIMENTAL PROCEDURE AND DATA REDUCTION

This chapter is divided into three sections: the glass formation history, the data reduction technique, and the error analysis and estimate of the confidence limits of Tg and Pg.

Glass Formation History

Because of the dependence of the glass properties on formation history, two standard procedures were adopted to form the glass of the materials investigated. In one formation history (history A), the pressure was increased from atmospheric to a reference pressure in the liquid region. At the same time, the sample temperature was increased at a rate of 40 F per hour to about 30 F above its assumed glass transition temperature. At this point the pressure and temperature were kept constant for about 30 minutes. The sample was then cooled at constant pressure and frequency spectra were taken at 5 F intervals. Twenty minutes were allowed for the temperature to reach equilibrium before each spectrum was recorded. In this way, experimental measurements started in the liquid state and the glassy state was reached by decreasing the temperature at constant pressure as shown in Figure 12. This procedure was repeated at different constant pressures and, therefore, the structure of the glass formed varies with the formation pressure. In the second formation history (history B), the glass was formed by pressurizing the samples at room temperature from atmospheric

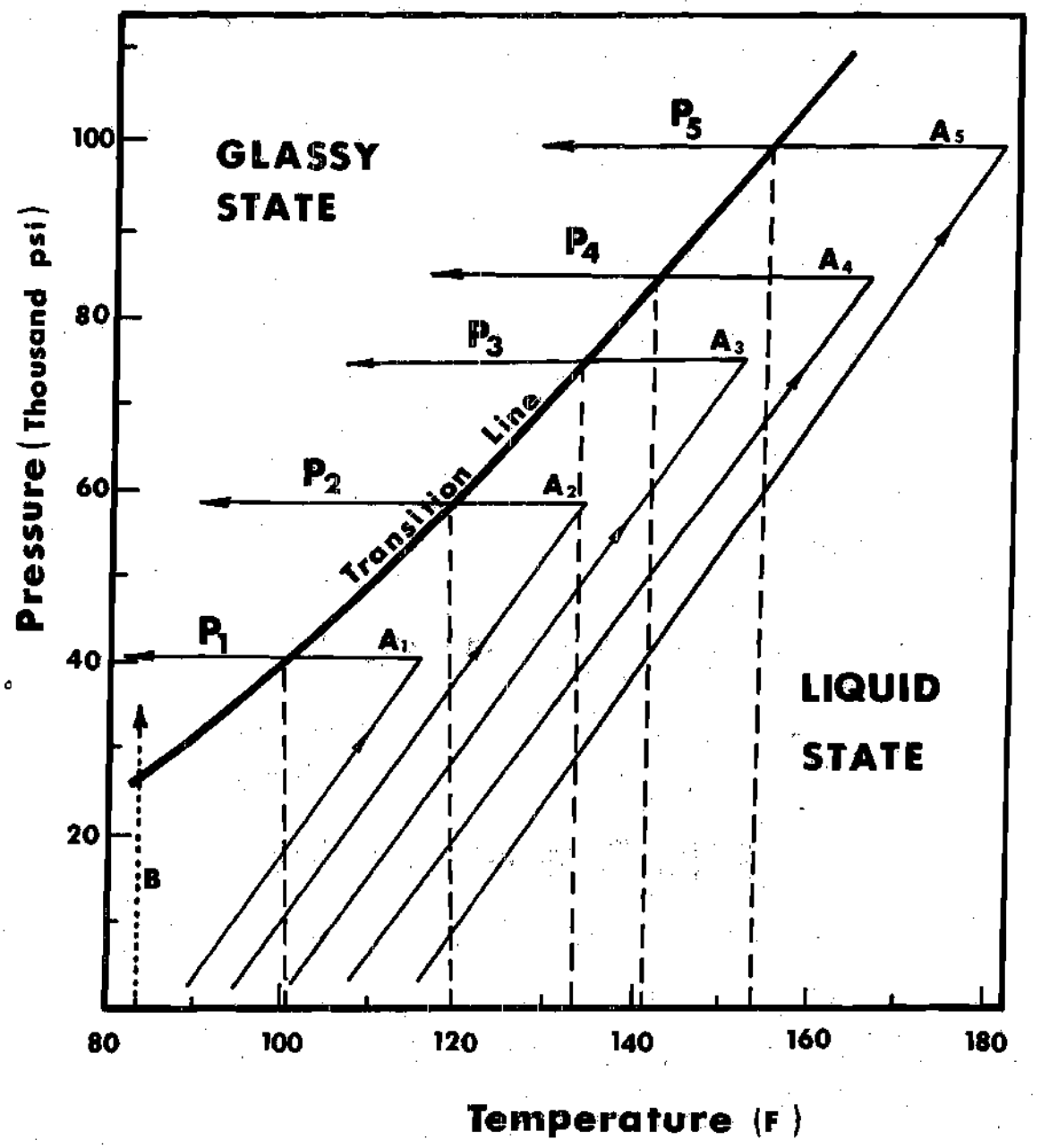

Figure 12. Schematic of Formation Histories Used to Form the Glass. A_i and B Represent Constant Formation Histories at Pressure P_i and Room Temperature Respectively.

pressure until the glassy state was reached. Frequency spectra for this case were taken at pressure intervals of about 3000 to 4000 psi. Again up to twenty minutes was allowed for the sample to reach equilibrium before the spectra were recorded. The ranges of temperature and pressure covered for each fluid are shown in Table 4 .

In history A, the sample temperature was changed by controlling the voltage input to an electric tape (30 ohms and 110 volts) wrapped around the intensifier-cell assembly which was enclosed in a Bakalite oven. The oven has three windows to allow for the incident light to be transmitted and the scattered light to be detected. The large thermal capacity of intensifier-cell assembly aided in the stability of the cell temperature. By controlling the input voltage to the electric heater, the cell temperature was controlled to better than $\pm$ 0.2 F. The temperature was measured with a copper-constantan thermocouple in conjunction with a direct reading Omega digital thermometer* model 2809. The thermocouple was in a brass well fitted into a hole in the cell body (Figure 10).

Data Reduction Technique

All frequency spectra of scattered light were obtained at a fixed scattering angle of 90°. The free spectral range for each case investigated was kept constant. This procedure was adopted to minimize the errors in measuring the separation distance of the Fabry-Perot interferometer which in turn minimized the error in the calculated frequency shift. Using the scattering angle of $\theta = 90^{\circ}$ in equation (9) and (11), one obtains

*See Appendix for specifications.

Table 4. Temperature and Pressure Ranges of the Experimental Fluids Investigated.

Experimental		Pressure	Temperature, F
Fluid	History	Range, kpsi	Range, F
5P4E	History A	30.5	119 - 80
		36.0	121 - 80
		40.0	136 - 90
		46.5	155 - 110
		51.5	161 - 115
		59.0	180 - 130
	History B	0 - 31.5	76
MCS-1218	History A	31.0	119 - 75
		37.0	139 - 90
		45.0	155 - 105
		50.0	170 - 115
		61.0	197 - 140
		67.0	210 - 155
	History B	0 - 31.0	76
N1	History A	80.0	120 - 70
		86.0	130 - 80
		92.0	135 - 80
		100.0	150 - 90
	History B	0 - 76.0	76

(Continued)

Table 4. Temperature and Pressure Ranges of the Experimental Fluids Investigated. (Continued)

Experimental		Pressure	Temperature, F
Fluid	History	Range, kpsi	Range, F
N2	History A	76.0	125 - 70
		80.0	130 - 75
		86.5	145 - 85
		91.0	155 - 95
		100.0	165 - 90
	History B	17.0 - 77.0	76

$$\Lambda = \frac{\lambda}{\sqrt{2}\, n_i} \tag{21}$$

and

$$V = \omega_B \frac{\lambda}{\sqrt{2}\, n_i} \tag{22}$$

The recorded spectra were used to measure the frequency shift and to calculate the sound velocity by employing equation (22).

Frequency spectra of polyphenyl ether were selected to explain the data reduction technique. Spectra of other experimental fluids investigated were analyzed in a similar manner. The results for all fluids will be presented in Chapter IV.

The frequency spectrum of 5P4E recorded at 28,200 psi and 76 F (formation history B) is shown in Figure 13. It contains two successive orders of the interference., The center of the four Brillouin peaks were located at some height where the Brillouin components appeared to be symmetrical. The separation distance, d, of the Fabry-Perot interformeter was 0.50 cm corresponding to a free spectral range of 30 GHZ $\left(\frac{c}{2d}\right)$. The frequency shift obtained from this spectrum is equal to

$$\omega_{B,k} = \frac{\ell}{2L_k} \cdot \frac{c}{2d} \tag{23}$$

where k = 1,2. Two values of ω_B can be calculated, each corresponding to the order of interference. These are (see Figure 13)

$$\omega_{B,1} = \frac{\ell}{2L_1} \cdot \frac{c}{2d} = \frac{6.85}{16.50} \times \frac{3 \times 10^{10}}{2 \times 0.50} = 12.45 \text{ GHZ}$$

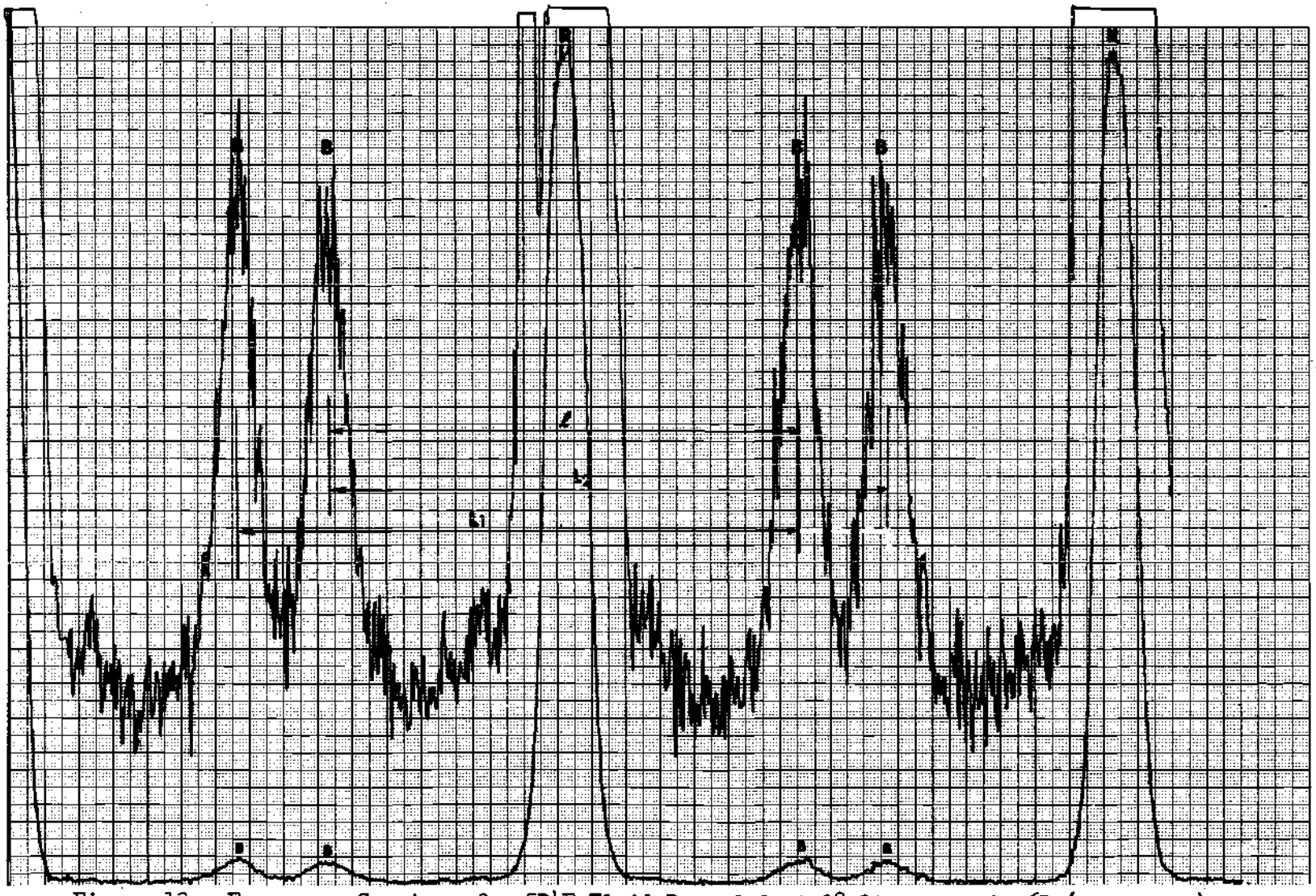

Figure 13. Frequency Spectrum for 5P4E Fluid Recorded at 28,200 psi and 76F (History B). B and R represent the Brillouin and Rayleigh Components Respectively.

and

$$\omega_{B,2} = \frac{\ell}{2L_2} \cdot \frac{c}{2d} = \frac{6.85}{16.40} \times \frac{3 \times 10^{10}}{2 \times 0.50} = 12.53 \text{ GHZ}$$

Each value of ω_B together with the values of n_i(1.6873) and λ(5145 Å) is used in equation (22) to determine the velocity of sound at the indicated pressure and temperature as follow

$$V_1 = \frac{\lambda\omega_{B,1}}{\sqrt{2}\, n_i} = 12.45 \times 10^9 \times \frac{5145 \times 10^{-10}}{1.6873\sqrt{2}} = 2685 \text{ m/sec.}$$

and

$$V_2 = \frac{\lambda\omega_{B,2}}{\sqrt{2}\, n_i} = 12.53 \times 10^9 \times \frac{5145 \times 10^{-10}}{1.6873\sqrt{2}} = 2702 \text{ m/sec.}$$

The average values of $\omega_{B,k}$ and V are reported. Frequency shifts and sound velocities at other pressures and temperatures are calculated in the same manner. The results of these calculations for 5P4E at 76F (history B) are shown in Table 5 and plotted in Figure 14. From this figure, it is seen that the sound velocity and the frequency shift increase with increasing pressure and a change in the slope is apparent at 24,700 psi corresponding to a velocity of sound of 2658 m/sec. This change of slope represent the glass transition. The velocities on each side of the transition region can be represented by linear functions of pressure. The two sections of Figure 14 were each fit by least squares regression to a linear expression of the form

Table 5. Frequency Shift and Velocity of Sound as Function of Pressure for 5P4E at 76F (History B).

Date: December 26, 1975
Separation Distance = 0.50 cm
Resulting Pg = 24,700 psi

Spectrum Number	Pressure kpsi	Frequency Shift cm^{-1}	Frequency Shift GHZ	Refractive Index	Velocity of Sound, m/sec
1	4.78	0.33194	10.00	1.6405	2208
2	7.2	0.34034	10.21	1.6453	2258
3	10,460	0.35364	10.61	1.6518	2337
4	14,250	0.36805	11.04	1.6594	2421
5	16,800	0.37819	11.35	1.6645	2480
6	20,840	0.39429	11.83	1.6726	2573
7	23,125	0.40259	12.08	1.6772	2620
8	26,050	0.41204	12.36	1.6829	2672
9	28,200	0.41642	12.49	1.6873	2695
10	29,950	0.42067	12.62	1.6909	2715
11	31,500	0.42347	12.70	1.6939	2729

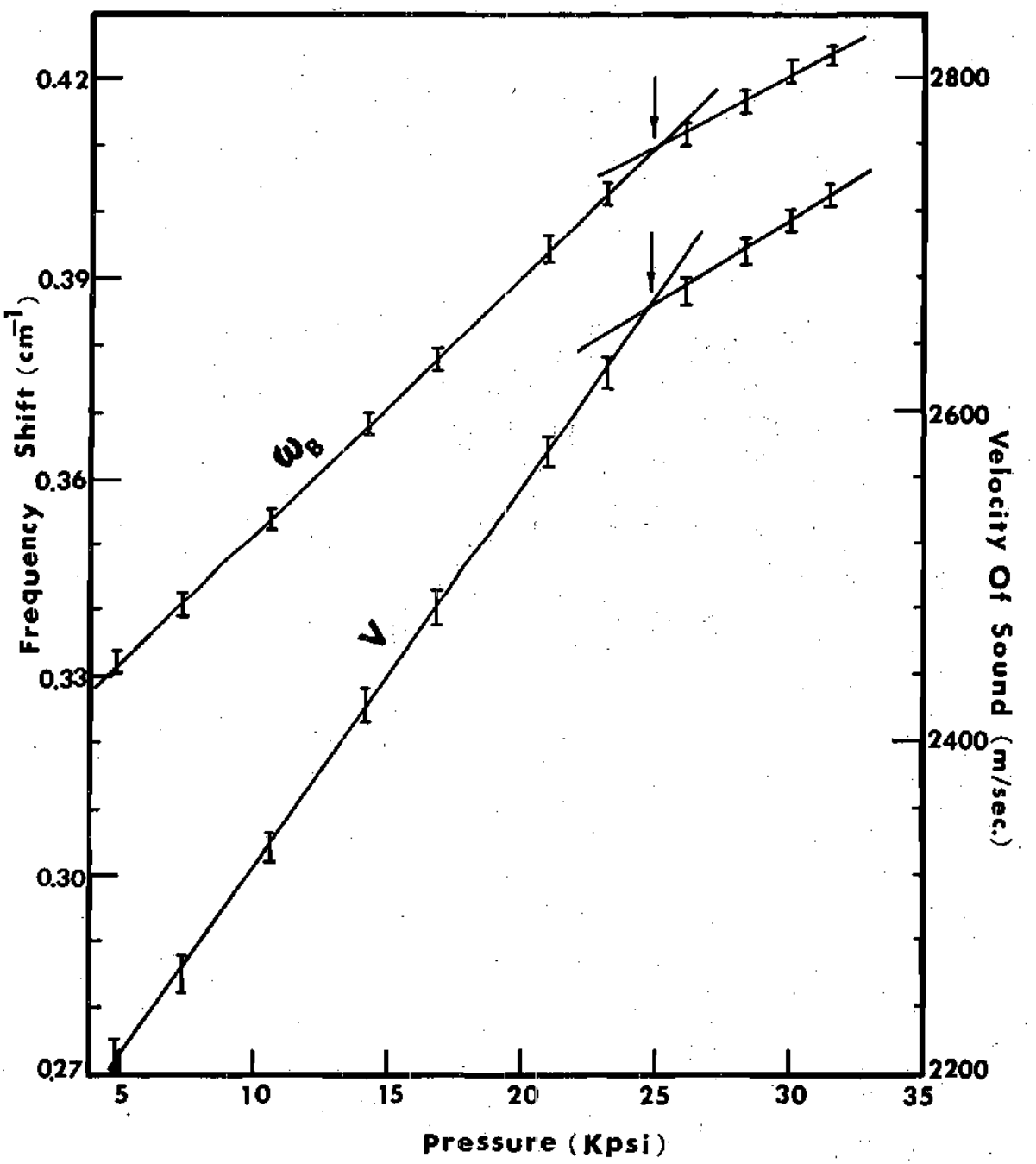

Figure 14. Variation of Frequency Shift and Velocity of Sound with Pressure at 76 F for 5P4E Fluid (History B). Arrows Indicate Glass Transition.

$$V = A + B\,P \qquad (24)$$

where V is in m/sec. and P in kpsi. The intersection of these lines is interpreted[24,25,27-31] as occurring at the glass transition pressure. The least square expression obtained for each section of the velocity-pressure curve shown in Figure 14 is

$$V_L = 2098 + 22.67P$$

and

$$V_g = 2397 + 10.57P$$

Solving these two equations for their intersection, one obtains

$P_g = 24{,}700$ psi and $V = 2658$ m/sec.

Frequency spectrum of 5P4E obtained by formation history A (at 59,000 psi) and recorded at 148F is reproduced in Figure 15. It is typical in general appearance of all frequency spectra obtained. The separation distance, d, was 0.725 cm corresponding to FSR of 20.7 GHZ. The frequency shifts and the sound velocities were calculated from the position of the Brillouin peaks as discussed above. The result of these calculations are shown in Table 6 and are plotted in Figure 16. The sound velocity increases as the temperature is decreased. At the transition region the dependence of sound velocity on temperature changes to that of a solid. This change of slope of the temperature coefficient of the sound velocity was observed at all formation pressures. Once again, the two portions of the sound velocity curves were fit by least

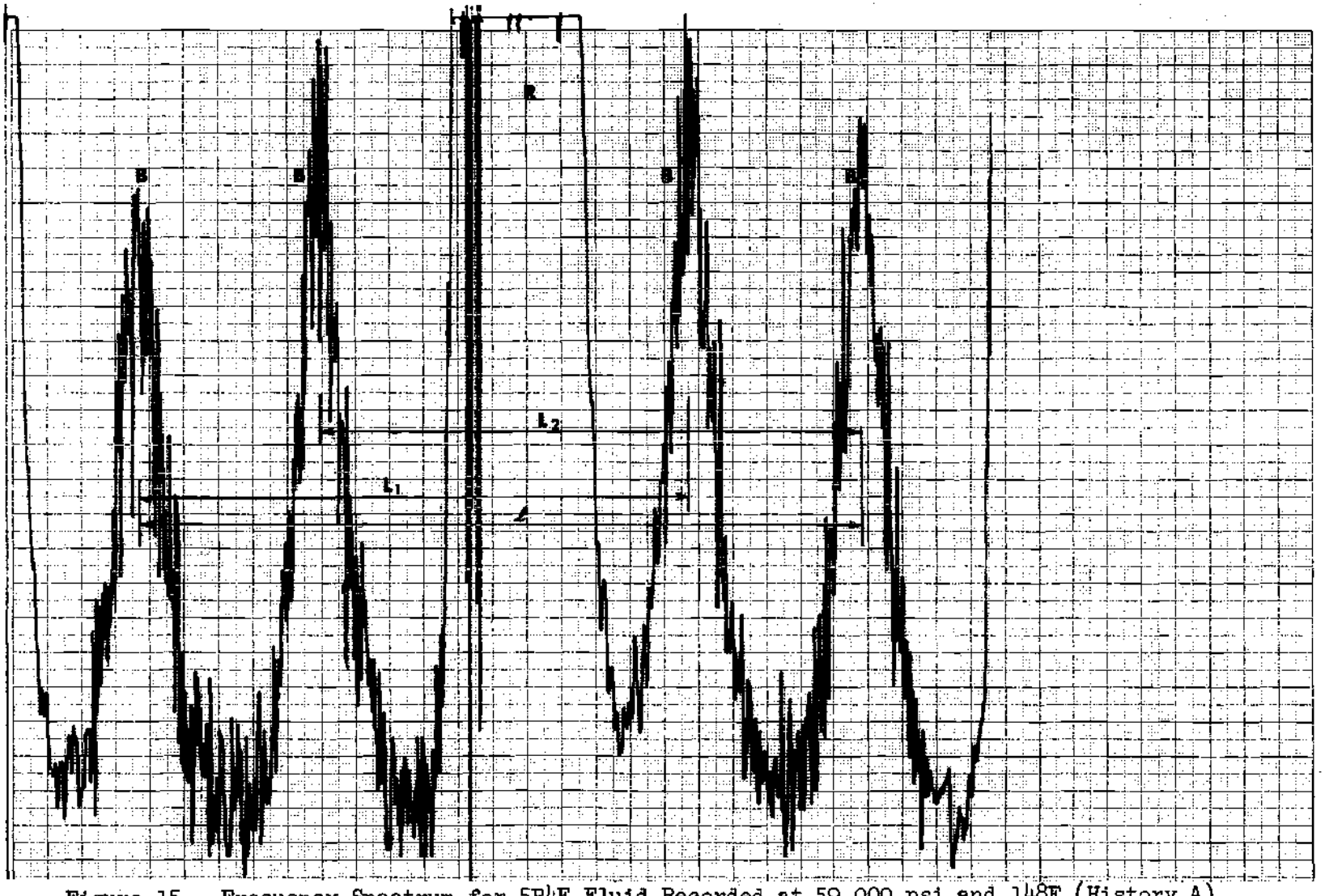

Figure 15. Frequency Spectrum for 5P[4]E Fluid Recorded at 59,000 psi and 148F (History A). B and R Represent the Brillouin and Rayleigh Components Respectively.

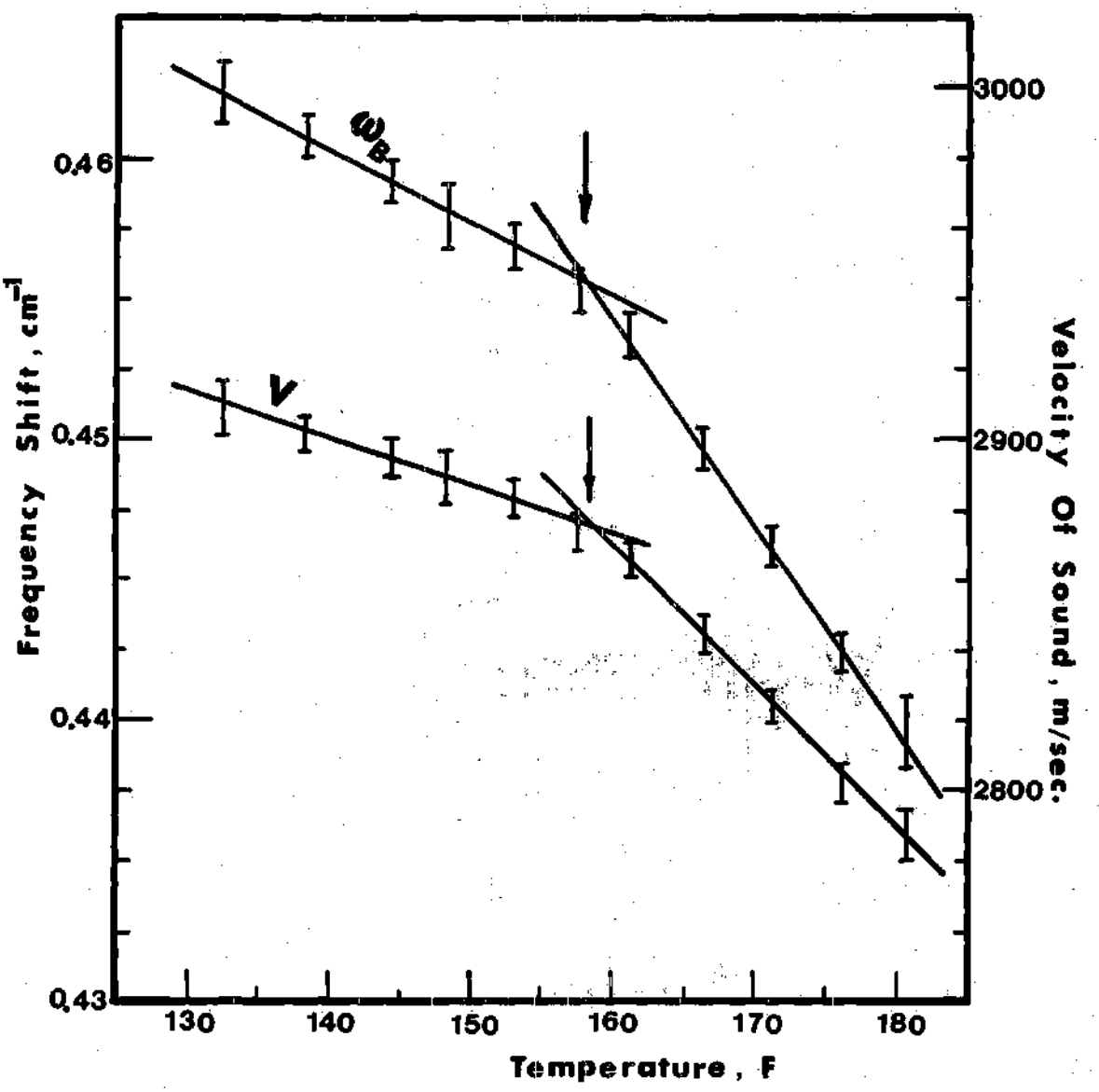

Figure 16. Variation of Frequency Shift and Velocity of Sound with Temperature at 59,000 psi for 5P4E (History A). Arrows Indicate Glass Transition.

Table 6. Frequency Shift and Velocity of Sound as a Function of Temperature at 59,000 psi for 5P4E Oil (History A).

Date: March 2, 1976
Separation Distance = 0.725 cm
Resulting: Tg = 158.5 F

Spectrum Number	Temperature F	Frequency Shift cm^{-1}	Frequency Shift GHZ	Refractive Index	Velocity of Sound m/sec
64	180.3	0.43966	13.19	1.7222	2787
65	175.8	0.44236	13.27	1.7233	2801
66	170.8	0.44618	13.39	1.7246	2823
67	166.2	0.44973	13.49	1.7258	2844
68	161.0	0.65369	13.61	1.7271	2867
69	157.5	0.45511	13.65	1.7280	2875
70	152.9	0.45691	13.71	1.7292	2883
71	148.3	0.45789	13.74	1.7303	2888
72	144.5	0.45910	13.77	1.7313	2894
73	138.3	0.46064	13.82	1.7328	2901
74	132.5	0.46216	13.86	1.7343	2908

square regression to straight lines of the form

$$V = a + b\,T \qquad (25)$$

where V in m/sec. and T in F.

These least square expressions for both portions of the Velocity-Temperature curves were solved for their intersection to determine the glass transition temperature at each formation pressure. These glass formation temperature-pressure combinations result in the phase diagram shown in Figure 17. The glass transition temperatures and pressures were least square fit with a straight line. The expression obtained is given by

$$Tg = 2.27\,Pg + 23.46$$

where Tg in F and Pg in thousand psi. The glass transition temperature at 76F by history B was excluded from the fit due to the different history by which the glass was formed. However, in general, the transition obtained by History B fall on or near the line obtained by History A.

The frequency shift as function of pressure and temperature was also least square fit with straight lines and the expressions obtained were solved for their intersection to locate the glass transition. The results obtained from the frequency shift did not differ from those obtained from the sound velocity by more than 200 psi for the glass transition pressure (History B, at 76F) nor more than 2F transition temperature at any formation pressure for History A. Therefore the glass transition data were obtained from the sound velocity only.

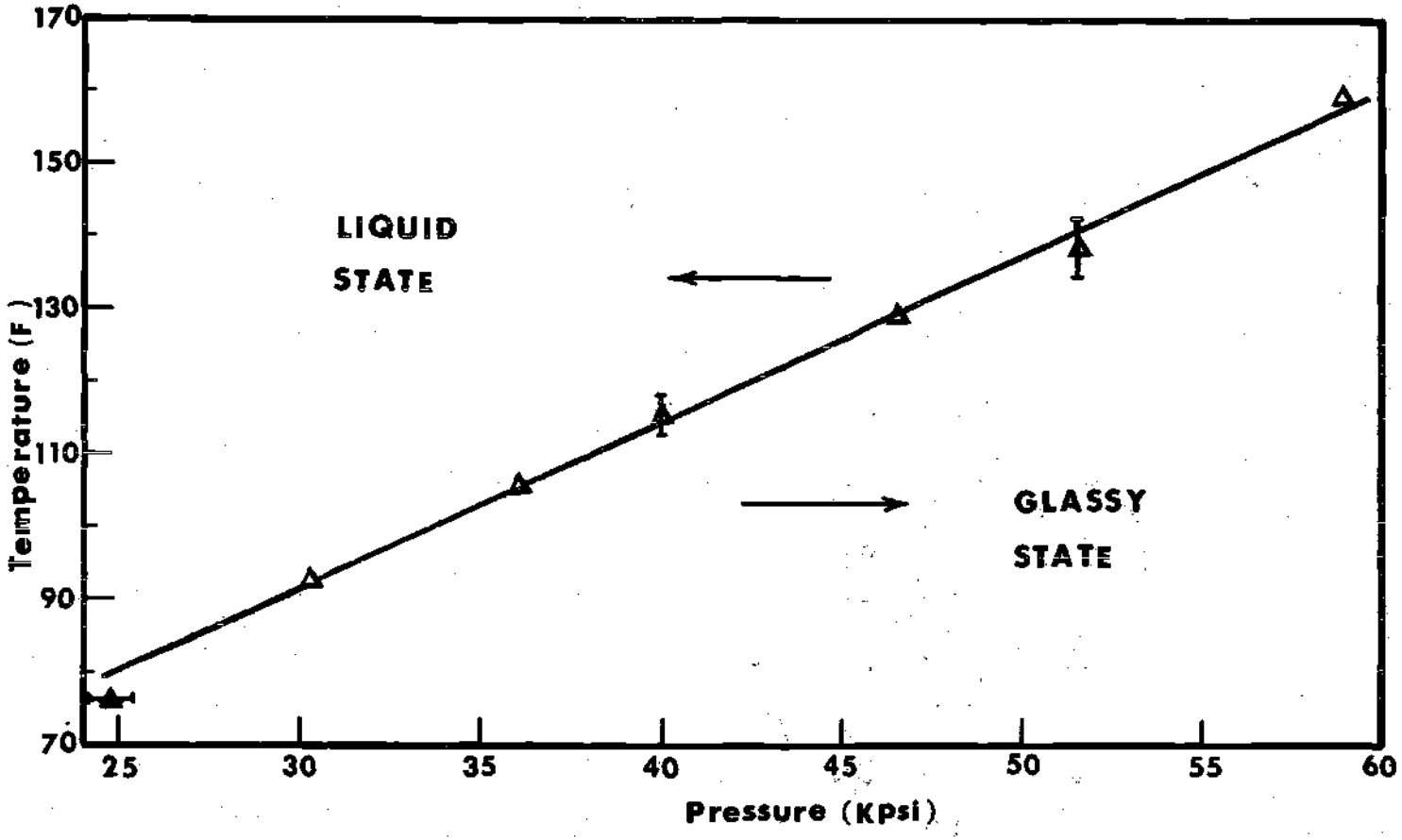

Figure 17. Phase Diagram for 5P4E Fluid. $\frac{dTg}{dP}$ = 2.27F Per kpsi. ▲ History A, ▲ History B, ⊢ and I indicate the Confidence Bands on Pg and Tg Respectively.

The above procedure was repeated for all experimental fluids investigated and the results are presented in more detail in Chapter IV.

Error Analysis

The relative error in the determination of the sound velocity is the sum of the errors involved in the measurements of the quantities[44] occurring in equation (11)

$$\Delta V = \frac{\partial V}{\partial \omega_B} \Delta\omega_B + \frac{\partial V}{\partial n_i} \Delta n_i + \frac{\partial V}{\partial \theta} \Delta\theta + \frac{\partial V}{\partial \lambda} \Delta\lambda \qquad (26)$$

Evaluating the partial derivatives of V from equation (11), one obtains

$$\frac{\Delta V}{V} = \frac{\Delta\omega_B}{\omega_B} - \frac{\Delta n_i}{n_i} - \frac{1}{2} \cot(\theta/2) \cdot \Delta\theta + \frac{\Delta\lambda}{\lambda} \qquad (27)$$

Since the incident wavelength was constant at 5145 $\mathring{A}$, the last term in the above equation does not contribute to the error in V. The error in the measurement of the refractive index as a function of temperature was estimated in the following manner: an averaging technique was used which involves three measurements of n_i at each temperature and the average value of these measurements was taken as the refractive index at the selected temperature. The error in measuring n_i by this method was estimated to be $\pm$ 0.03 percent. The error in determining n_i as function of pressure was estimated to be $\pm$ 0.02 percent. It is evident from equation 27 that the error in determining the sound velocity depends primarily on the precision with which the frequency shift ω_B and the scattering angle θ were measured. As seen from equation 23

the error in measuring ω_B depends on the precision by which the chart distance and the Fabry-Perot separation distance are measured. This error was estimated to be $\pm$ 0.8 percent. This error can be reduced by increasing the number of measurement of the frequency shift. For the sample MCS-1218, two spectra at the same temperature and pressure were recorded and four values of the frequency shift were calculated. The value of ω_B obtained did not differ by more than 0.03 percent from that obtained by using two interference orders of each spectrum. All Brillouin shift measurements were made at a scattering angle of 90°. An estimate on the error in θ is thought to be $\pm 1^\circ$ which will result in an error of $\pm$ 1/2 percent in V.

From the above discussion, an estimated error of $\pm$ 1.5 percent at most can be expected in the measurements of V. However, the uncertainties in the absolute value of the sound velocity which arise from the uncertainties in the scattering angle θ, the frequency shift ω_B and the refractive index n_i are not of great concern in the present work as the absolute value of the sound velocity is not our main concern. The quantity of interest is the intersection of the sound velocity versus temperature or pressure curves in the liquid and glassy regions which represents the glass transition for the material. This quantity is not strongly influenced by any of the above uncertainties. In obtaining all frequency spectra for each experimental fluid at different constant formation pressures, the position of the scattering cell remained fixed and a single separation distance of the Fabry-Perot mirrors was chosen to cover the expected frequency range of the calculated velocities. This arrangement ensured that the error in the calculated velocities

due to the uncertainties discussed above for each constant formation pressure run is the same for all other runs. The influence of the above errors on our measurements is to shift the velocity-temperature or the velocity-pressure curves to higher or lower velocities without changing the location of the glass transition temperature or pressure.

The error in the location of Tg and Pg is one of the most important uncertainty in this work. A statistical method giving the confidence limits of the abscissca of the intersection of two linear regressions is described in Reference [43]. This method can be used to determine the confidence limits on Tg using the liquid and the glassy linear regressions of the form

$$V = a + b\,T$$

The data required to apply this method consist of liquid-glass linear regression pairs of the following quantities: n, the number of experimental points; a, the least-square intercept; b, the least-square slope; T_{av}, the average temperature; s, the standard deviation of the residuals of V and the quantity S_p defined as

$$S_p^2 = \sum_{i=1}^{n} (T_i - T_{av})^2 \qquad (28)$$

Using the equal varience assumption, the confidence limit, ΔTg, is equal to the difference of the two roots of the following quadratic equation

$$A\,T_g^2 + B\,Tg + C = 0 \quad . \qquad (29)$$

The coefficients A, B, and C are given in Reference [43] as

$$A = (b_1 - b_2)^2 - s_p^2 G_t^2 \left[\frac{1}{S_{P1}^2} + \frac{1}{S_{P2}^2}\right] \tag{30}$$

$$B = 2(a_1 - a_2)(b_1 - b_2) + 2 s_p^2 G_t^2 \left[\frac{T_{av,1}}{S_{P1}^2} + \frac{T_{av,2}}{S_{P2}^2}\right] \tag{31}$$

$$C = (a_1 - a_2)^2 - s_p^2 G_t^2 \left[\frac{1}{n_1} + \frac{1}{n_2} + \frac{T_{av,1}^2}{S_{P1}^2} + \frac{T_{av,2}^2}{S_{P2}^2}\right] \tag{32}$$

where G_t is the 97.5 percent point of the t-distribution with $n_1 + n_2 - 4$ degrees of freedom[45] and s_p^2 is the pooled variance defined as

$$s_p^2 = [s_1^2(n_1 - 2) + s_2^2(n_2 - 2)]/(n_1 + n_2 - 4) \tag{33}$$

and subscripts 1 and 2 in the above expressions refer to the liquid and glassy regions respectively. This analysis was also used to calculate the confidence band for the glass transition pressure for History B transitions.

The above analysis applied to 5P4E resulted in confidence bands ranged from 1.35 to 6.6F for history A and 1.2 kpsi for that of history B and are shown in Figure 17. The confidence bands for the other experimental fluids will be presented in Chapter IV.

CHAPTER IV

EXPERIMENTAL RESULTS

The figures presented in this chapter were obtained by the data reduction technique presented in Chapter III. The frequency shift and pressure-velocity curves obtained by formation history B for all fluids examined are presented in Figures 18 A-D. Frequency shift results obtained by formation history A are shown in Figures 19 A-D and sound velocity results in Figures 20 A-D (at constant formation pressures as indicated in the figures). The resulting phase diagrams are shown in Figures 21A-B. Figure 22 contains the phase diagrams of all experimental fluids.

Least-square expressions for the sound velocity in the liquid and glassy region for history A, the resulting glass transition temperatures and the sound velocities at transition are summarized in Table 7 A-D. Similar results obtained during formation history B are summarized in Table 8 . Least square expressions for transition temperature as a function of pressure for each fluid based on formation history A are given in Table 9 . They show the rate at which the glass transition temperature increases with formation pressure. Tables of the detailed experimental data from which the above figures and tables were obtained are listed in Appendix A .

It should be noted that the velocity of sound of all four fluids exhibited a non-linear dependence on pressure at low pressures. For N1

and N2 the non-linear range extended up to about 35,000 psi as shown in Figure 23 (only N1 is shown). For 5P4E and MCS-1218 the non-linear behavior ended at a much lower pressure (about 5000 psi). This non-linear behavior is the result of the non-linear dependence of the bulk modulus on pressure at low pressure.

Figure 24 and 25 show the effect of the viscosity-index improver blended with the naphthenic base oil on the glass transition behavior of the blend relative to the base oil. Figure 24 shows that the glass transition pressure for the blend occurred at 63.5 kpsi compared with 68.8 kpsi obtained for the base oil. Also, the sound velocity of blend descreased relative to that of the base oil. In the glassy region, the larger decrease in the sound velocity is due to the fact that the glass transition of the blend occurred at lower pressure. Figure 25 shows that the glass transition temperature for N2 fluid occurred at 10 to 15F higher than that of N1 at 80.0 and 100.0 kpsi respectively. This result is not surprising since the glass transition in polymers occurs at low pressures and high temperatures compared to those of lubricating oils. In the liquid region of Figure 25, the sound velocity of N2 oil is slightly higher than that of N1. This is due to the different temperature dependence of the compressibility of each oil at high temperatures.

The 95 percent confidence limits were calculated for the glass transition following the technique of Chapter III. The results of this analysis for three pressures from formation history A are shown in Table 10 A-D. Similar results for history B are shown in Table 11. It is seen from these tables that the confidence bands ranged from 1.32 to

6.6 F for the glass transition temperature and from 1.20 to 2.65 kpsi for the glass transition pressure. These confidence bands, centered about Tg and Pg, are shown on the phase diagrams of each experimental fluid (Figure 21A-B). The confidence band of history B for N1 fluid was not calculated due to the small number of data points in the glassy region.

Table 7A. Least-Square Expressions for Sound Velocity, Temperatures and Sound Velocity at Transition for Different Constant Pressures: 5P4E history A. (T in F and V in m/sec)

Formation Pressure, kpsi	Range of Measurements F	Least-Square Expression for Sound Velocity	Glass Transition Temperature (Tg) F	Sound Velocity at Tg, m/sec
30.5	119 - 80	$V_L = 3103 - 4.44T$ $V_g = 2854 - 1.75T$	92.6	2692
36.0	121 - 80	$V_L = 3176 - 4.16T$ $V_g = 2907 - 1.60T$	105.0	2739
40.0	136 - 90	$V_L = 3279 - 4.41T$ $V_g = 2954 - 1.60T$	115.6	2769
46.5	155 - 110	$V_L = 3294 - 3.77T$ $V_g = 2985 - 1.35T$	127.9	2812
51.5	161 - 115	$V_L = 3383 - 3.86T$ $V_g = 3059 - 1.38T$	138.7	2848
59.0	180 - 130	$V_L = 3545 - 4.22T$ $V_g = 3072 - 1.24T$	158.5	2875

Table 7 B. Least-Square Expressions for Sound Velocity, Temperature and Sound Velocity at Transition for Different Constant Pressures: MCS-1218 history A. (T in F and V in m/sec)

Formation Pressure, kpsi	Range of Measurements F	Least-Square Expression for Sound Velocity	Glass Transition Temperature (Tg) F	Sound Velocity at Tg, m/sec
31.0	119 - 75	$V_L = 3654 - 5.27T$ $V_g = 3299 - 1.67T$	98.6	3135
37.0	139 - 90	$V_L = 3794 - 5.11T$ $V_g = 3387 - 1.61T$	116.3	3200
45.0	155 - 105	$V_L = 3824 - 3.86T$ $V_g = 3467 - 1.18T$	133.2	3310
50.0	170 - 115	$V_L = 3954 - 4.27T$ $V_g = 3463 - 0.89T$	145.3	3334
61.0	197 - 140	$V_L = 4063 - 3.76T$ $V_g = 3542 - 0.71T$	170.8	3421
67.0	210 - 155	$V_L = 4171 - 3.85T$ $V_g = 3618 - 0.93T$	189.4	3442

Table 7 C. Least-Square Expressions for Sound Velocity, Temperature and Sound Velocity at Transition for Different Constant Pressures: N1 history A. (T in F and V in m/sec)

Formation Pressure, kpsi	Range of Measurements F	Least-Square Expression for Sound Velocity	Glass Transition Temperature (Tg) F	Sound Velocity at Tg, m/sec
80.0	120 - 70	$V_L = 3782 - 4.81T$ $V_g = 3462 - 1.37T$	93.0	3335
86.0	130 - 80	$V_L = 3812 - 4.56T$ $V_g = 3499 - 1.51T$	102.6	3344
92.0	135 - 80	$V_L = 3868 - 4.59T$ $V_g = 3522 - 1.48T$	113.3	3357
100.0	150 - 90	$V_L = 3911 - 4.36T$ $V_g = 3524 - 1.22T$	123.2	3374

Table 7D. Least-Square Expressions for Sound Velocity, Temperature and Sound Velocity at Transition for Different Constant Pressures: N2 history A. (T in F and V in m/sec)

Formation Pressure, kpsi	Range of Measurements F	Least-Square Expression for Sound Velocity	Glass Transition Temperature (Tg) F	Sound Velocity at Tg, m/sec
76.0	125 - 70	$V_L = 3596 - 3.36T$ $V_g = 3393 - 1.34T$	100.5	3258
80.0	130 - 75	$V_L = 3622 - 3.35T$ $V_g = 3434 - 1.56T$	105.0	3270
86.5	145 - 85	$V_L = 3630 - 2.99T$ $V_g = 3422 - 1.20T$	116.2	3283
91.0	155 - 95	$V_L = 3659 - 3.00T$ $V_g = 3432 - 1.17T$	124.0	3287
100.0	165 - 90	$V_L = 3723 - 2.99T$ $V_g = 3463 - 1.13T$	139.7	3305

Table 8. Least-Square Expressions for Sound Velocity, Pressure and Sound Velocity at Transition at 76F (History B) for all Experimental Fluids. (P in kpsi and V in m/sec)

Experimental Fluids	Range of Measurements kpsi	Least-Square Expression for Sound Velocity	Glass Transition Pressure (Pg), kpsi	Sound Velocity at Pg, m/sec
5P4E	5 - 32	$V_L = 2098 + 22.67P$ $V_g = 2397 + 10.57P$	24.7	2658
MCS-1218	7 - 31	$V_L = 2446 + 27.44P$ $V_g = 2844 + 10.63P$	23.7	3096
N1	36 - 76	$V_L = 2301 + 14.19P$ $V_g = 2821 + 6.63P$	68.8	3278
N2	36 - 77	$V_L = 2217 + 15.00P$ $V_g = 2656 + 8.08P$	63.5	3169

Table 9 . Least-Square Expressions for the Glass Transition Temperature as Function of Pressure for all Experimental Fluids Based on Formation history A. (Tg in F and Pg in kpsi)

Experimental Fluids	Range of Measurements kpsi	Least-Square Fit
5P4E	24 - 59	Tg = 23.46 + 2.27 Pg
MCS-1218	23 - 67	Tg = 23.62 + 2.45 Pg
N1	68 - 100	Tg = - 27.03 + 1.50 Pg
N2	63 - 100	Tg = - 28.12 + 1.67 Pg

Table 10A. Confidence Bands on Tg (history A) for 5P4E.

Formation Pressure, kpsi	30.5	40.0	51.5
a_1	3103	3279	3383
a_2	2854	2954	3039
b_1	-4.44	-4.41	-3.86
b_2	-1.75	-1.60	-1.38
n_1	5	5	5
n_2	4	5	4
$T_{av,1}$, F	108.0	126.66	150.58
$T_{av,2}$, F	87.9	101.26	125.83
S^2_{p1}	295.56	208.4	256.3
S^2_{p2}	67.95	303.1	182.1
s^2_p	3.41	7.07	2.39
Confidence Band ΔTg,F	1.35	4.77	6.6

Table 10B. Confidence Bands on Tg (history A) for MCS-1218.

Constant Formation History kpsi	37.0	45.0	61.0
a_1	3794	3824	4063
a_2	3387	3467	3542
b_1	-5.11	-3.86	-3.76
b_2	-1.61	-1.18	-0.71
n_1	5	5	5
n_2	5	5	5
$T_{av,1}$, F	129.18	144.94	187.14
$T_{av,2}$, F	103.14	120.36	154.50
s^2_{p1}	2272	223.2	259.6
s^2_{p2}	285.7	314.9	301.9
s^2_p	2.45	1.205	5.24
Confidence Band ΔTg,F	2.88	2.66	4.47

Table 10C. Confidence Bands on Tg (history A) for N1.

Constant Formation History kpsi	80.0	92.0	100.0
a_1	3782	3868	3911
a_2	3462	3522	3524
b_1	-4.81	-4.59	-4.36
b_2	-1.37	-1.48	-1.22
n_1	6	5	5
n_2	5	5	5
$T_{av,1}$, F	108.1	124.56	136.00
$T_{av,2}$, F	81.06	96.24	107.24
S^2_{p1}	406.6	268.0	250.2
S^2_{p2}	302.1	447.8	465.5
s^2_p	1.03	0.81	1.93
Confidence Band ΔTg,F	1.99	1.47	1.32

Table 10D. Confidence Bands on Tg (history A) for N2.

Constant Formation History kpsi	76.0	80.0	100.0
a_1	3596	3622	3723
a_2	3393	3434	3463
b_1	-3.36	-3.35	-2.99
b_2	-1.34	-1.56	-1.13
n_1	6	5	6
n_2	6	6	9
$T_{av,1}$, F	111.53	116.82	153.4
$T_{av,2}$, F	87.4	89.65	116.1
S^2_{p1}	337.4	230.7	292.0
S^2_{p2}	483.0	440.0	1797.9
s^2_p	1.85	2.92	1.79
Confidence Band ΔTg,F	3.64	3.36	5.66

Table 11. Confidence Bands on Pg at 76F (history B) for 5P4E, MCS-1218 and N2.

Experimental Fluid	5P4E	MCS-1218	N2
a_1	2098	2446	2217
a_2	2397	2844	2656
b_1	22.67	27.44	15.00
b_2	10.57	10.63	8.08
n_1	7	7	7
n_2	4	4	5
$P_{av,1}$,kpsi	13.92	15.44	50.40
$P_{av,2}$,kpsi	28.93	27.44	72.16
S_{p1}^2	281.7	184.9	341.2
S_{p2}^2	16.47	23.6	62.2
s_p^2	4.66	65.3	4.7
Confidence Band ΔPg,kpsi	1.20	2.65	1.22

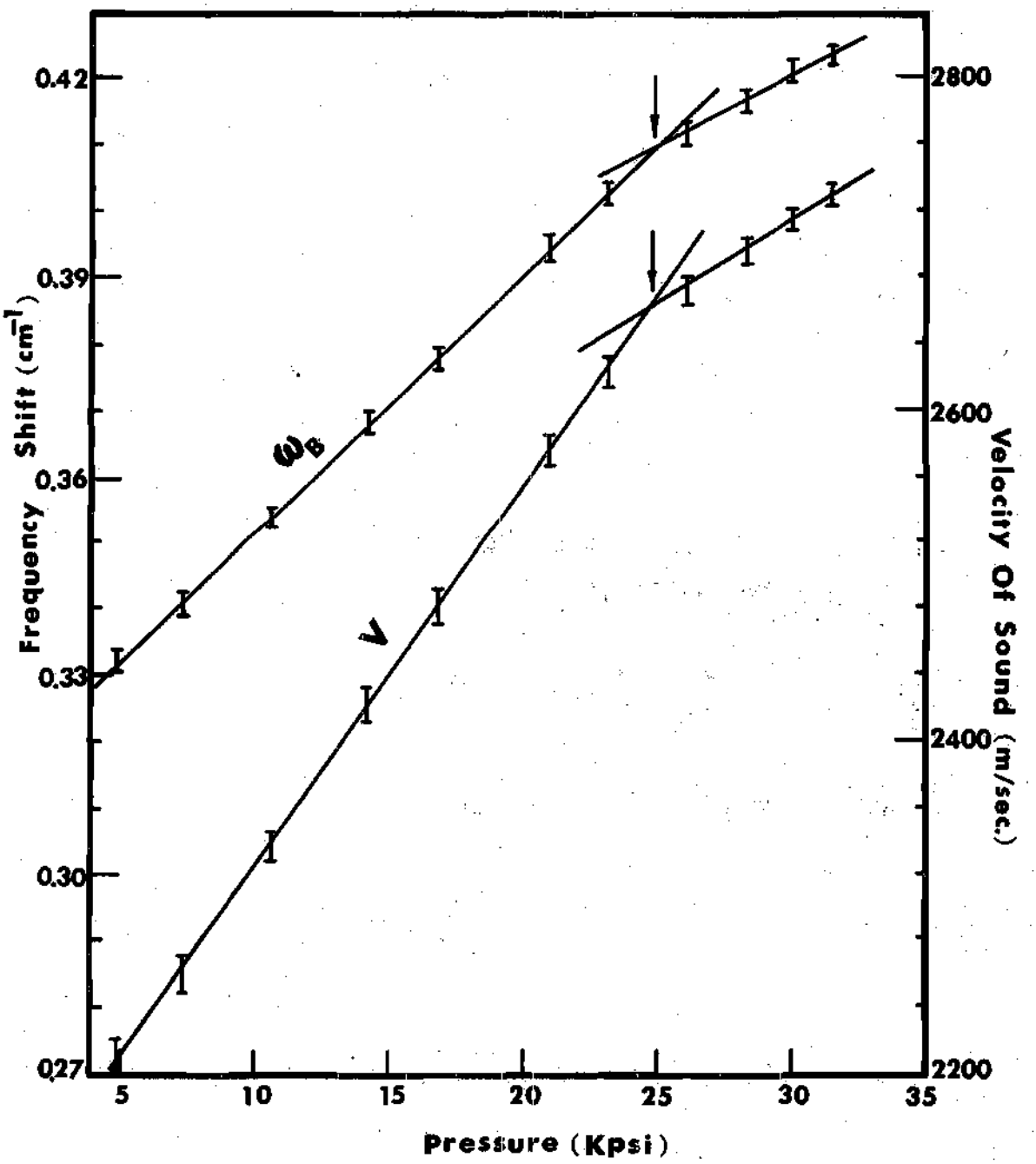

Figure 18-A. Variation of Frequency Shift and Sound Velocity with Pressure at 76F for 5P4E Fluid (History B). Arrows Indicate Pg.

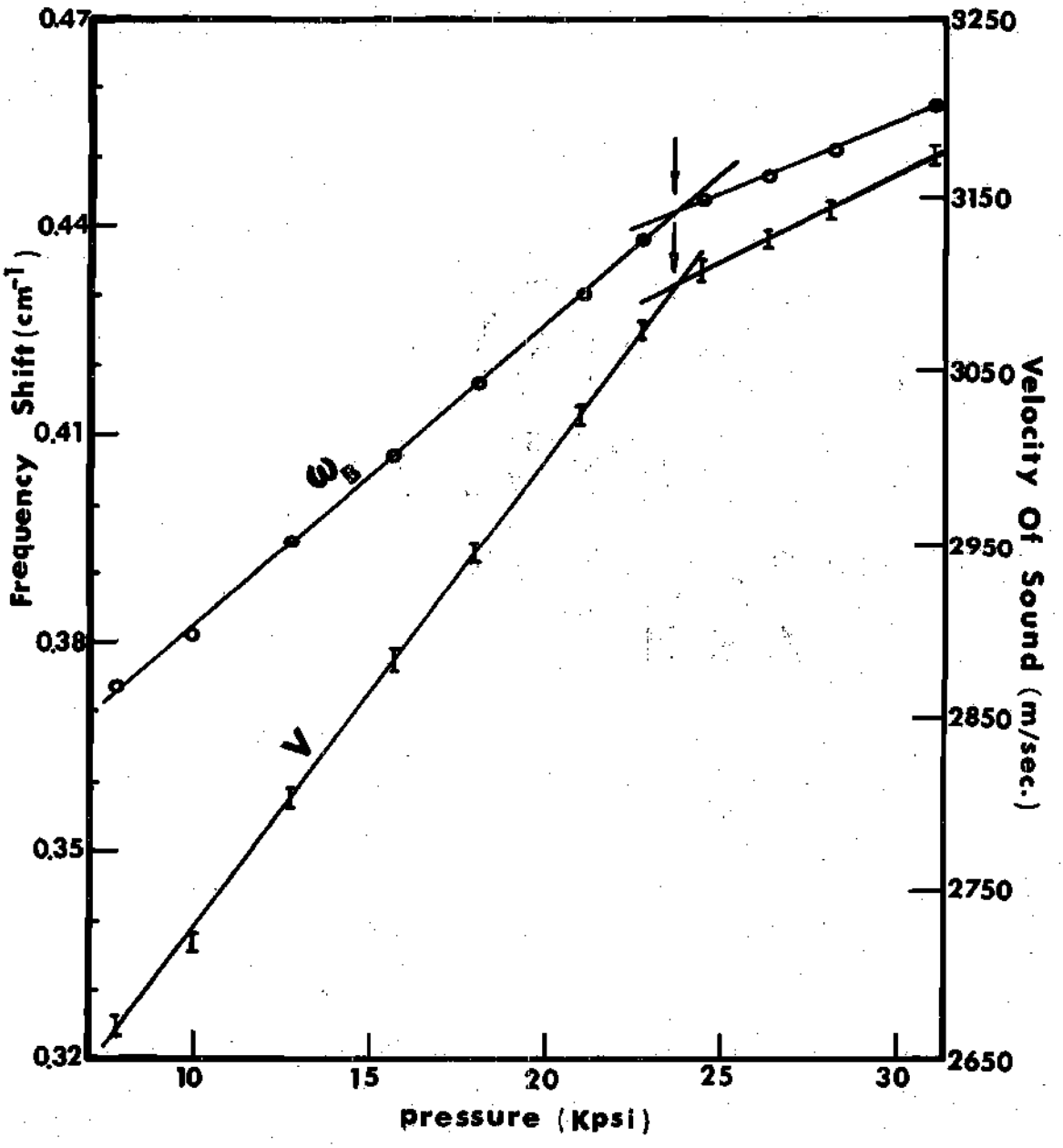

Figure 18-B. Variation of Frequency Shift and Sound Velocity with Pressure at 76F for MCS-1218 Fluid (History B). Arrows Indicate Pg.

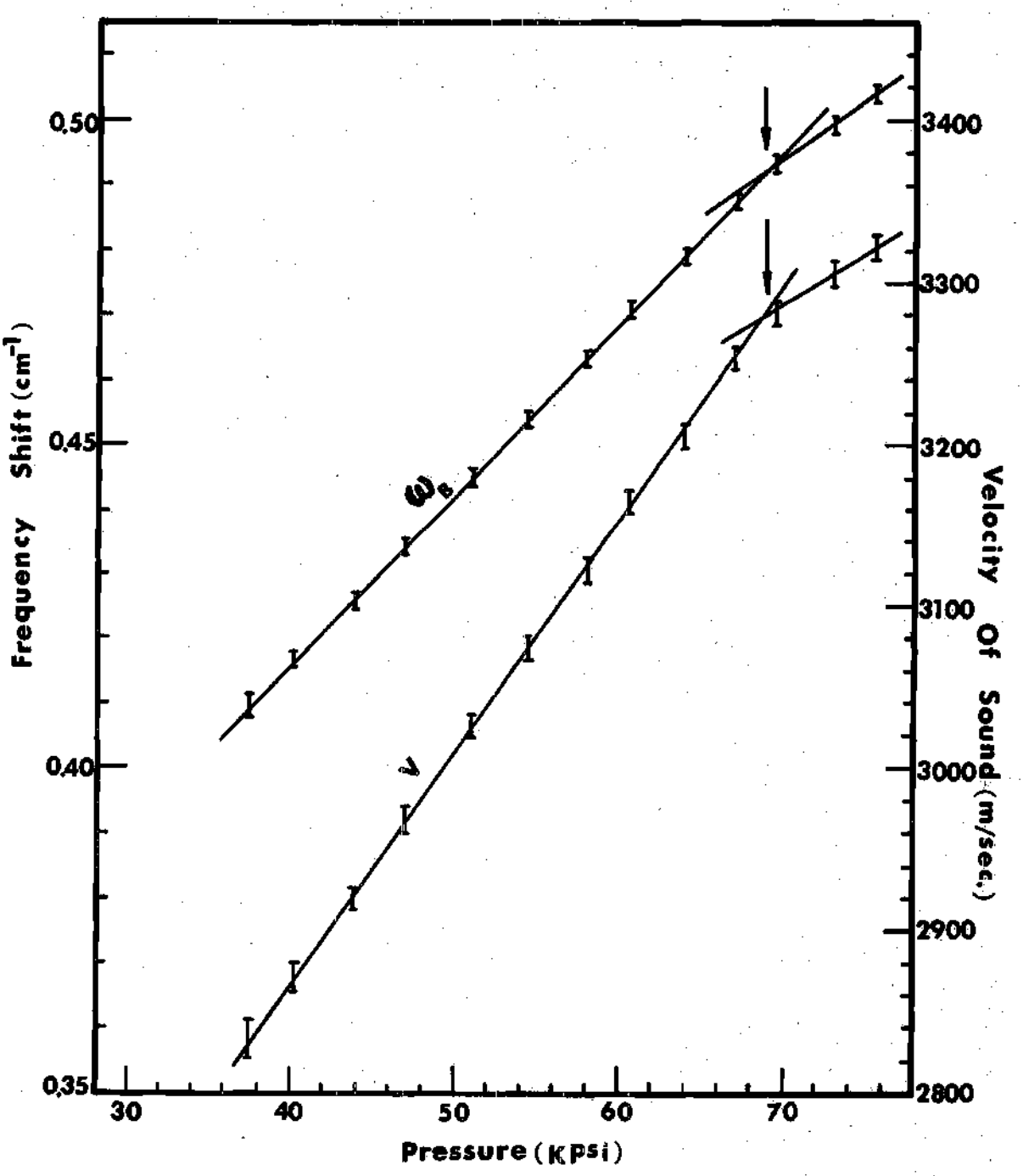

Figure 18-C. Variation of Frequency Shift and Sound Velocity with Pressure at 76F for N1 Fluid (History B). Arrows Indicate Pg.

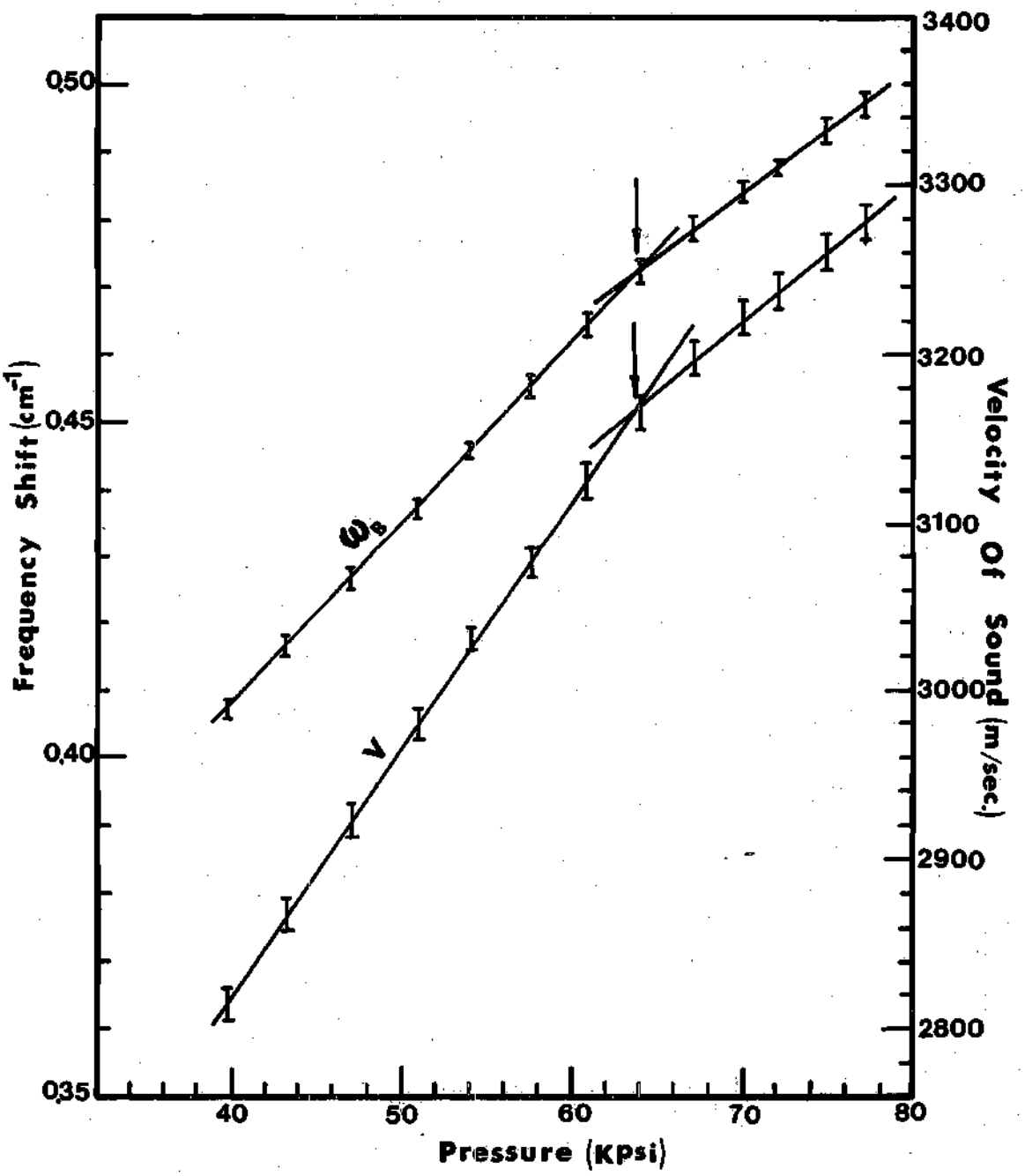

Figure 18-D. Variation of Frequency Shift and Sound Velocity with Pressure at 76F for N2 (History B). Arrows Indicate Pg.

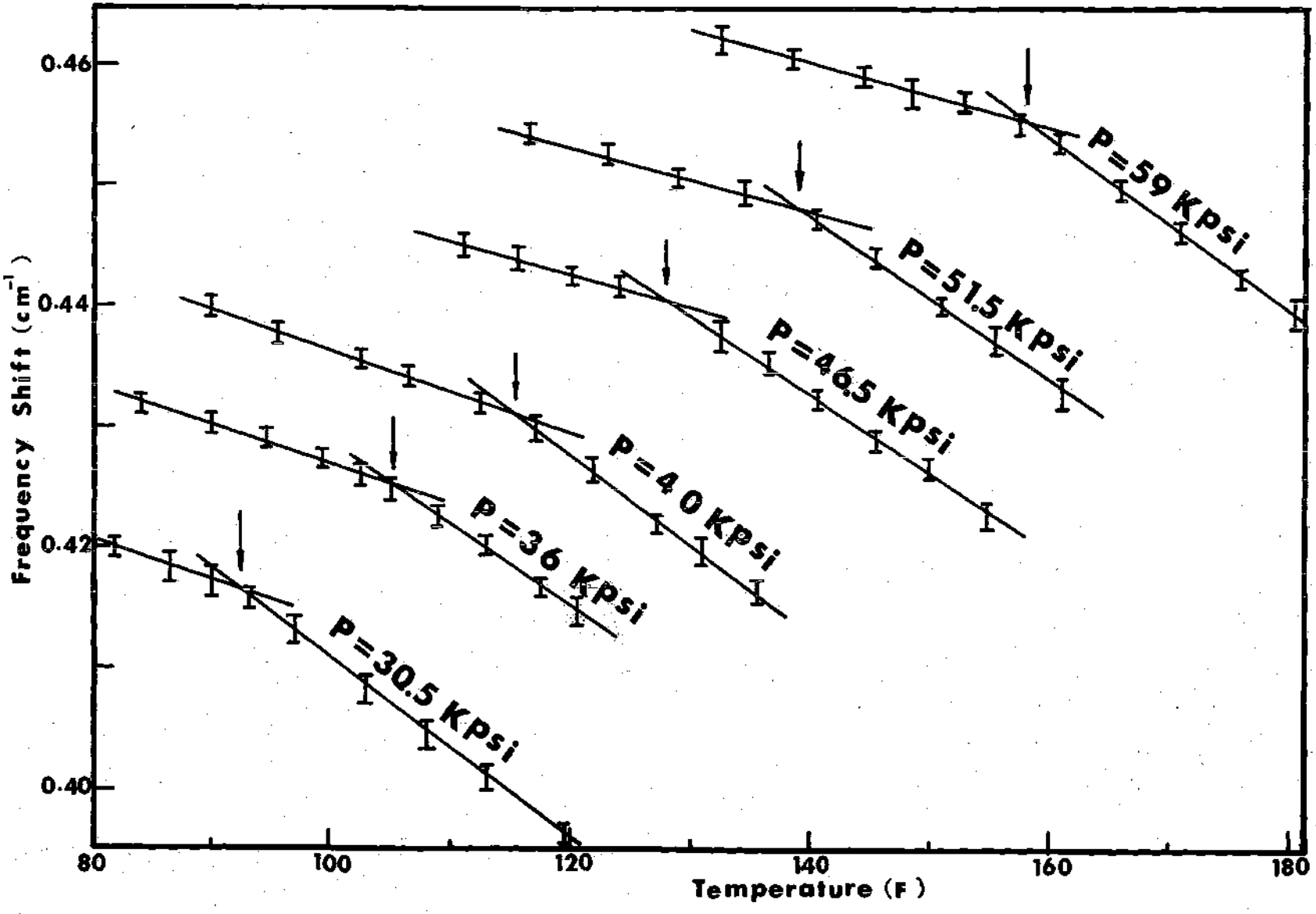

Figure 19-A. Frequency Shift Dependence on Temperature at Different Constant Pressures for 5P4E Fluid (History A). Arrows Indicate Tg.

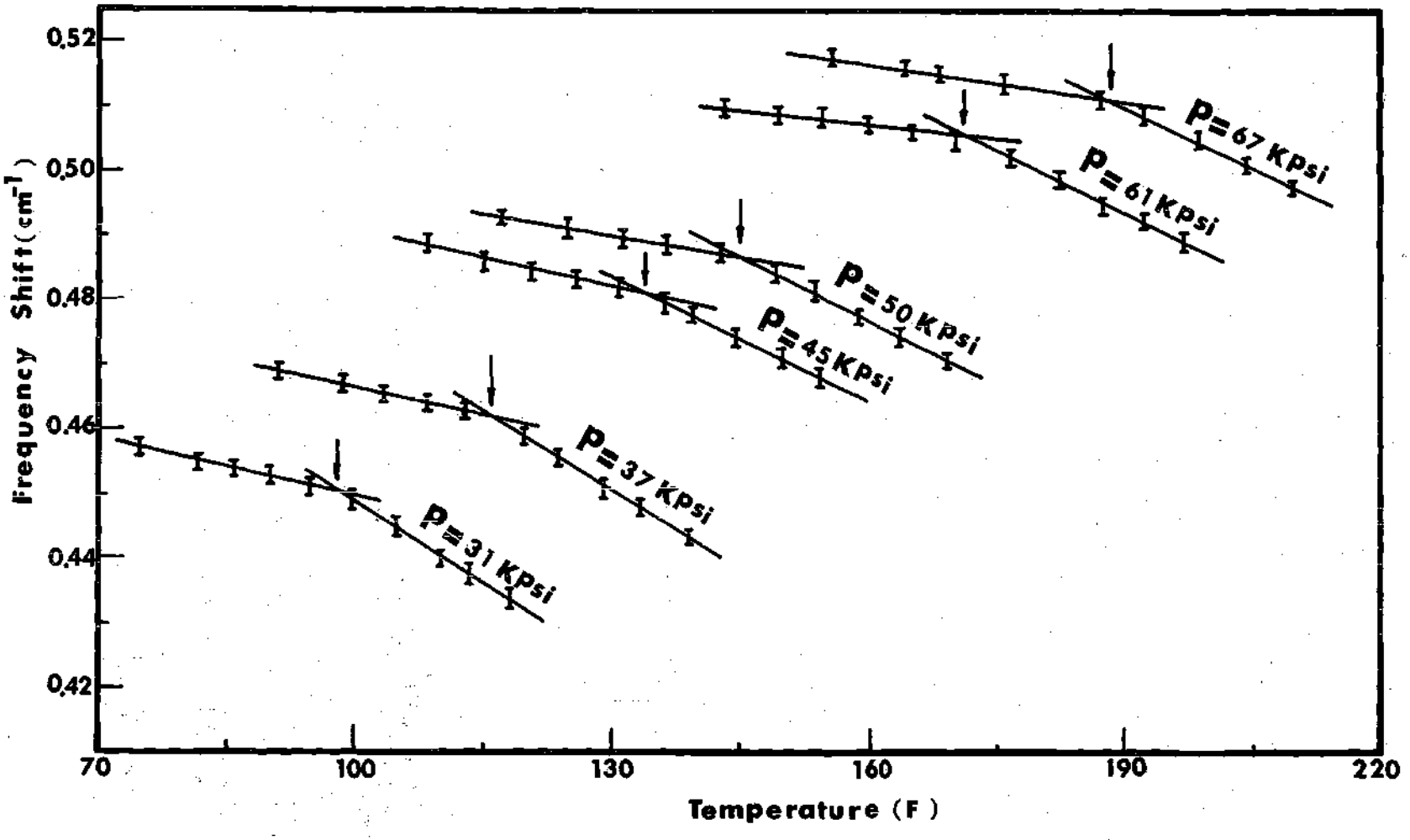

Figure 19-B. Temperature Variation of the Frequency Shift at Different Constant Pressures for MCS-1218 Fluid (History A). Arrows Indicate Tg.

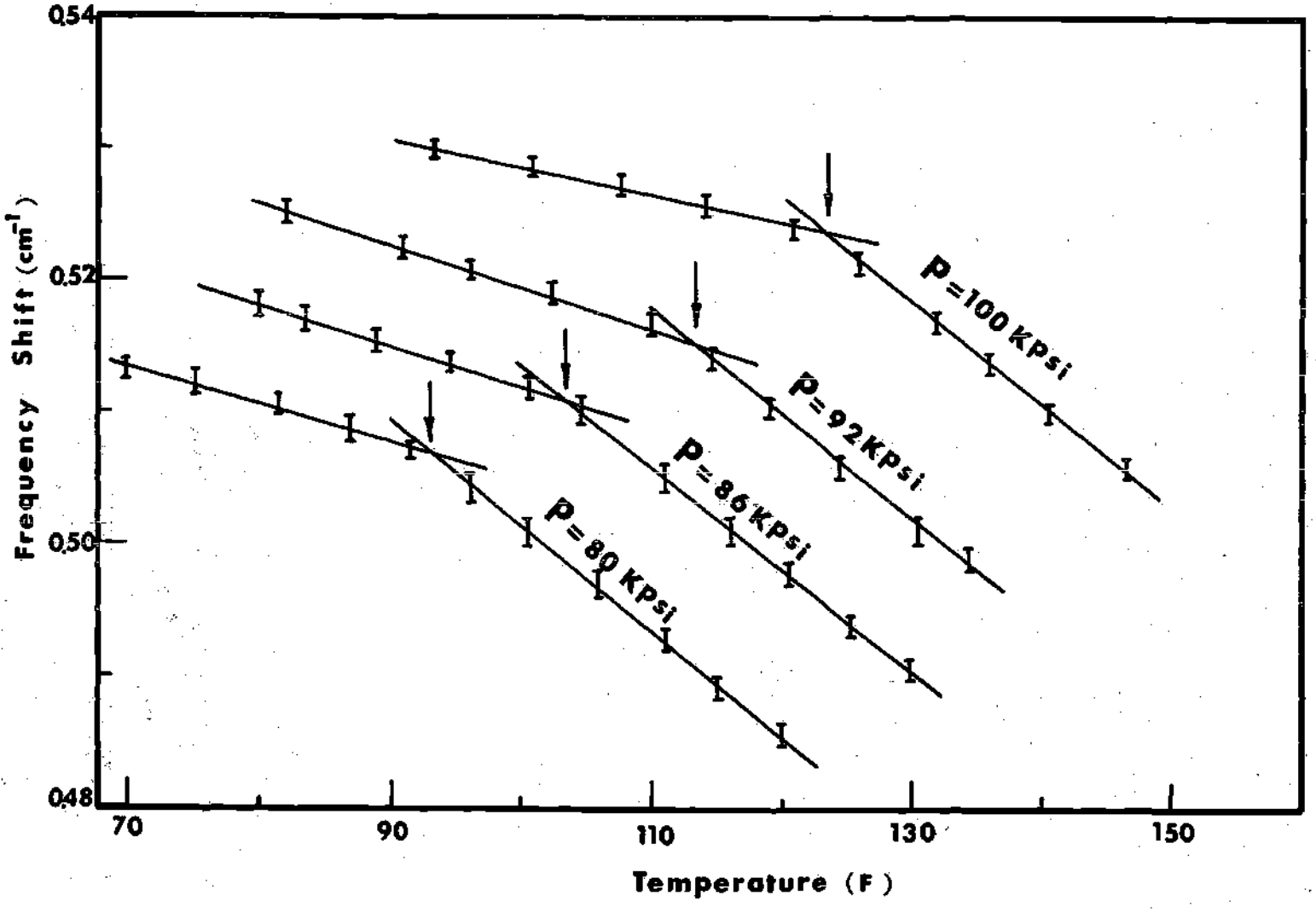

Figure 19-C. Frequency Shift Dependence on Temperature at Different Constant Pressures for N1 Fluid (History A). Arrows Indicate Tg.

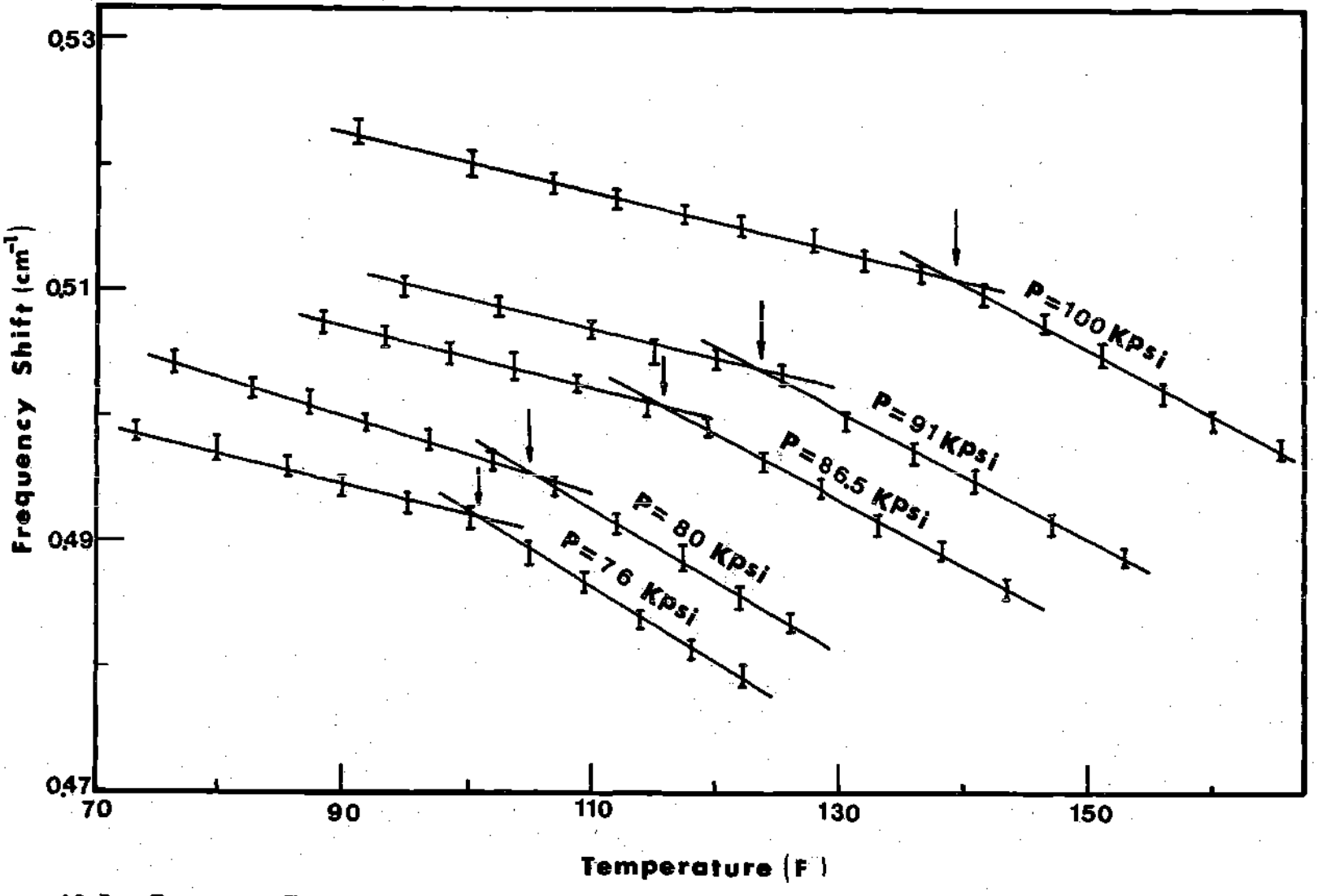

Figure 19-D. Frequency Shift Dependence on Temperature at Different Constant Pressures for N2 Fluid (History A). Arrows Indicate Tg.

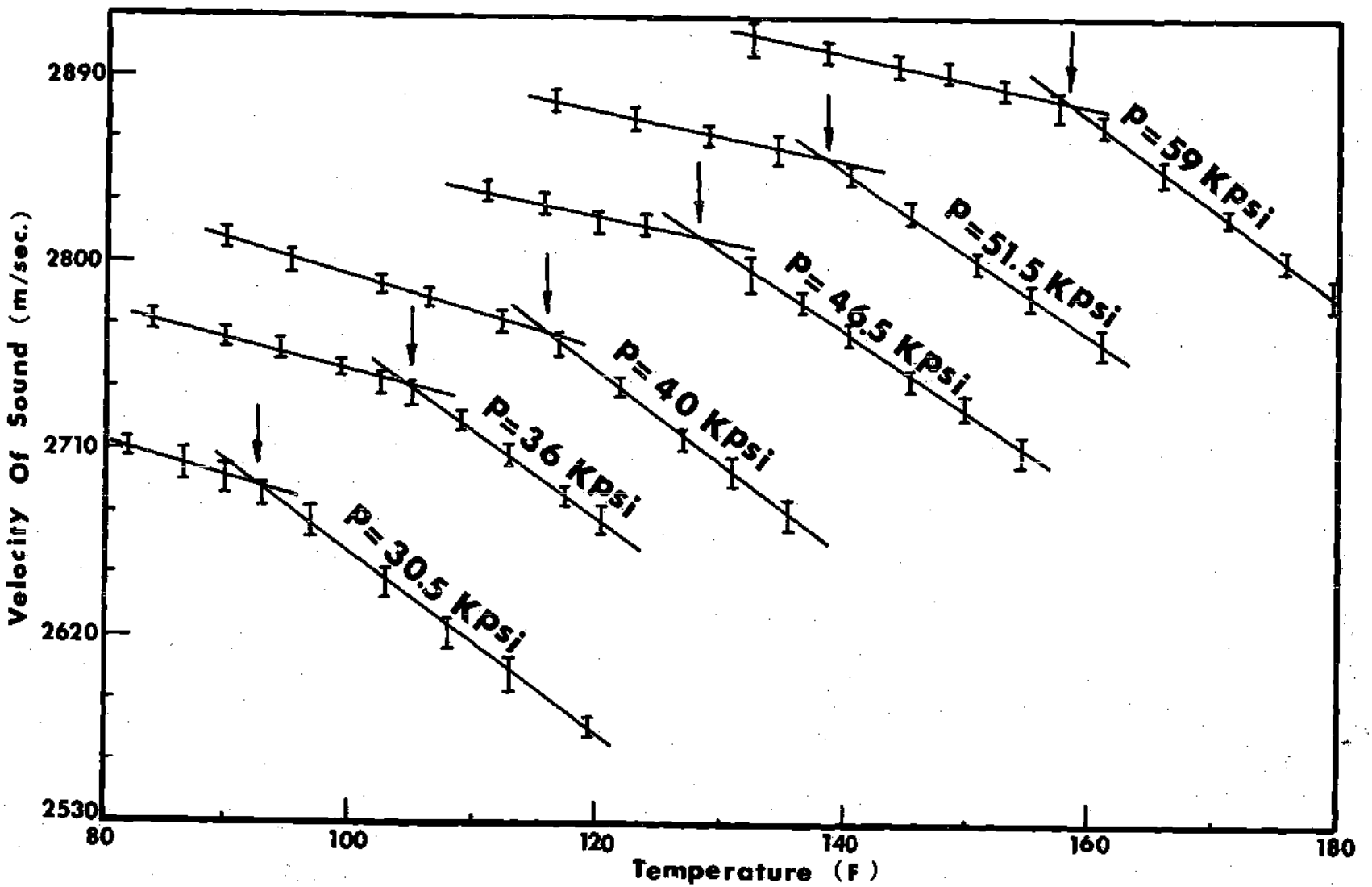

Figure 20-A. Velocity of Sound Dependence on Temperature at Different Constant Pressures for 5P4E Fluid (History A). Arrows Indicate Tg.

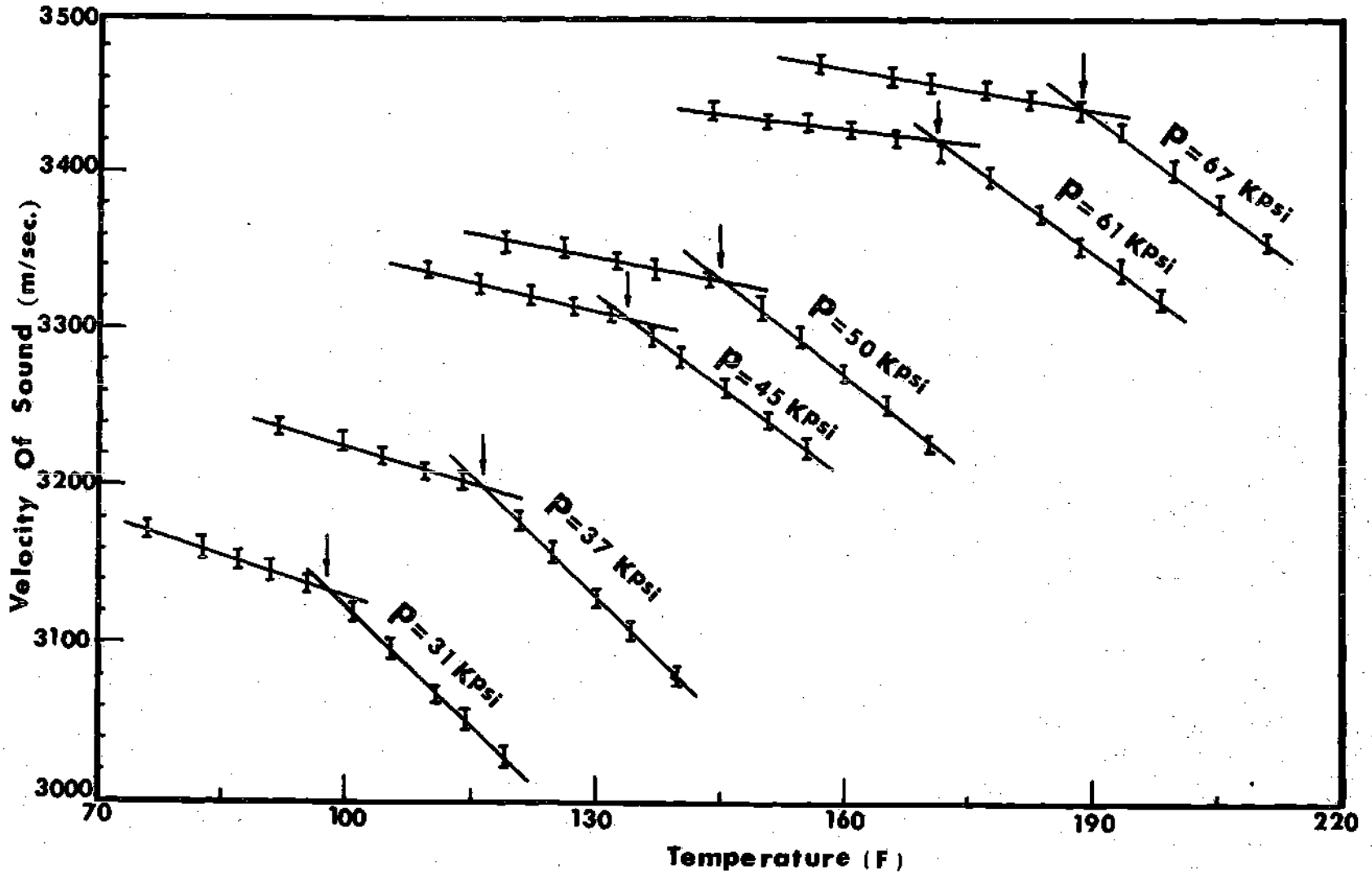

Figure 20-B. Temperature Variation of the Sound Velocity at Different Constant Pressures for MCS-1218 Fluid (History A). Arrows Indicate Tg.

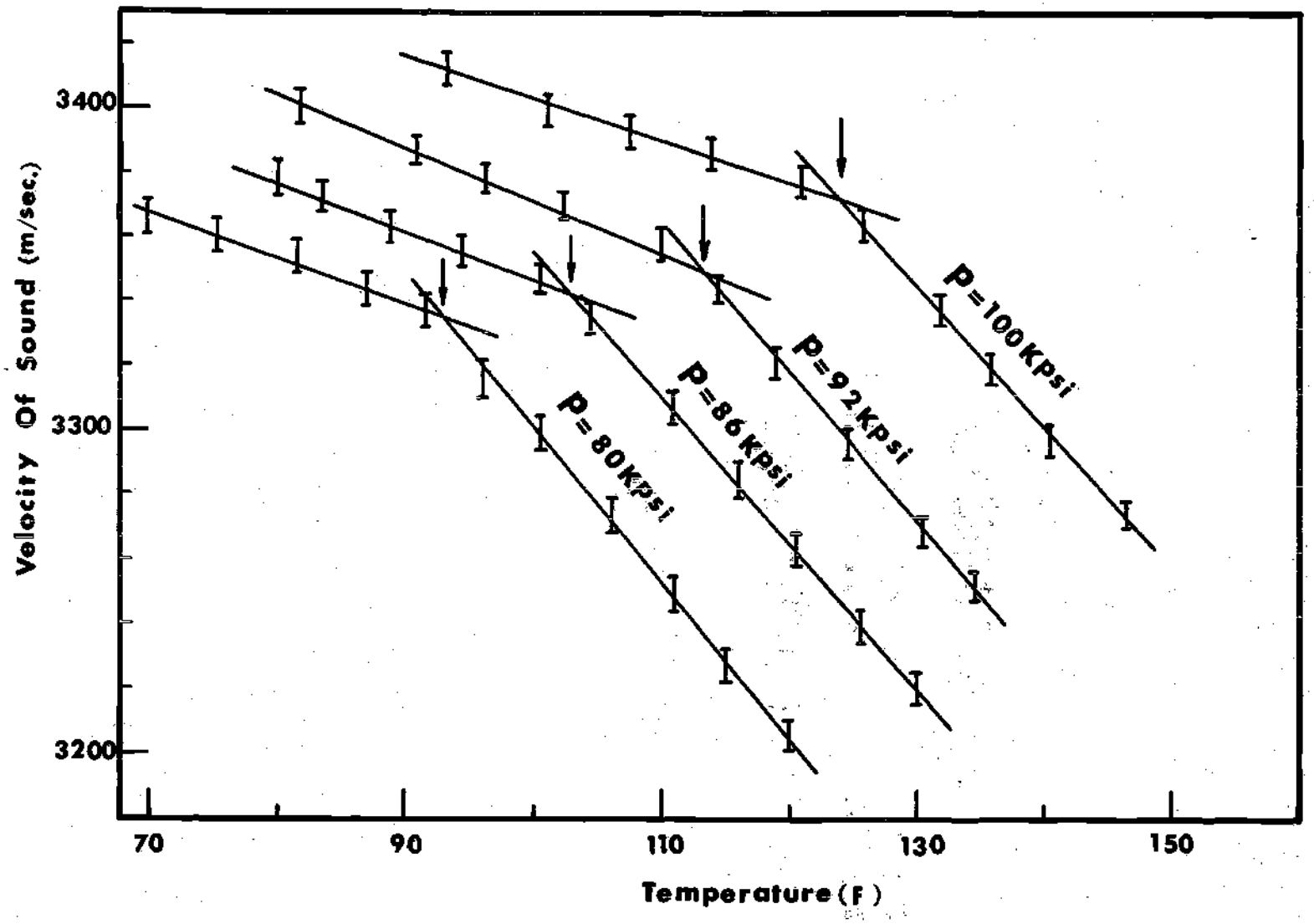

Figure 20-C. Velocity of Sound Dependence on Temperature at Different Constant Pressures for N1 Fluid (History A). Arrows Indicate Tg.

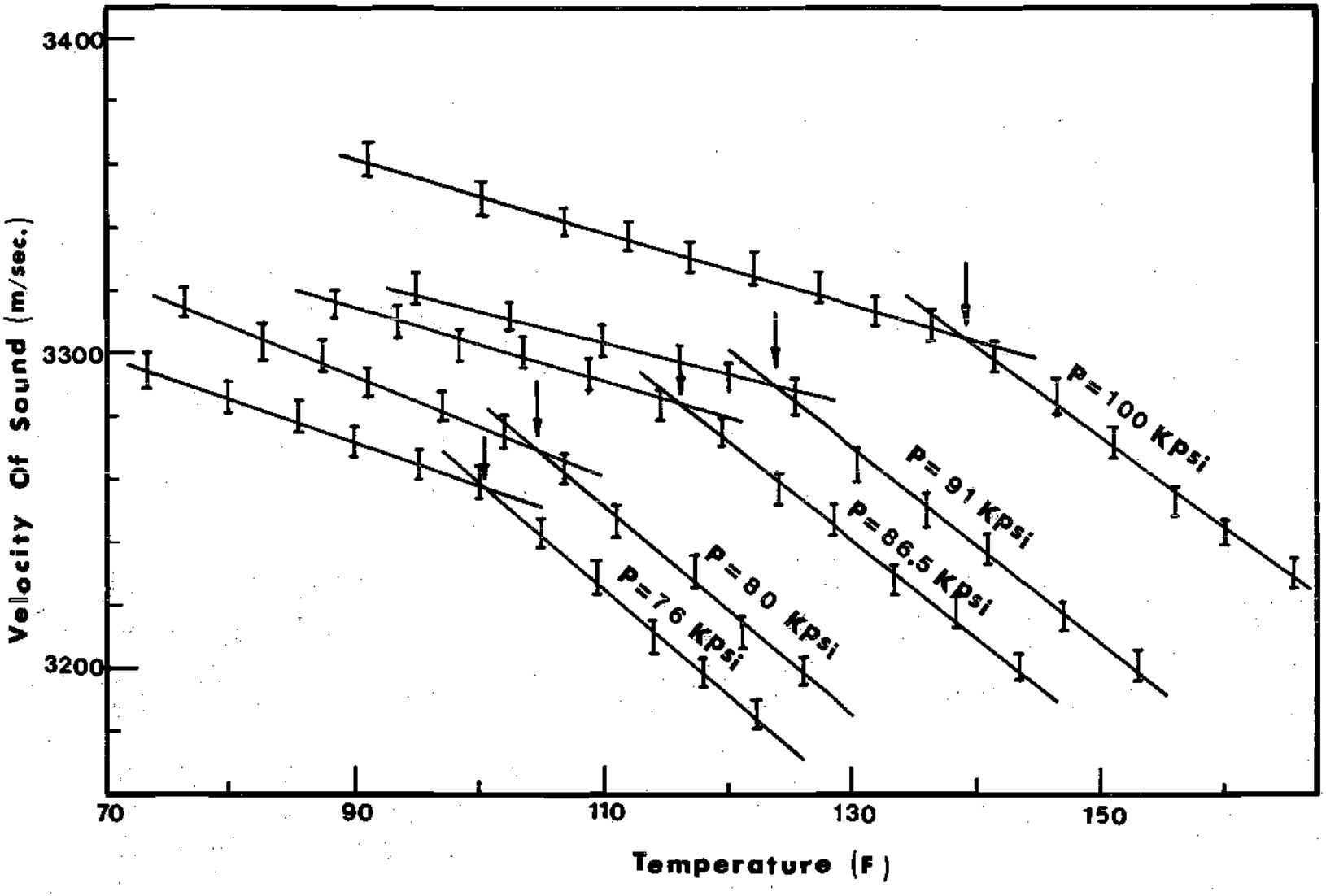

Figure 20-D. Velocity of Sound Dependence on Temperature at Different Constant Pressures for N2 Fluid (History A). Arrows Indicate Tg.

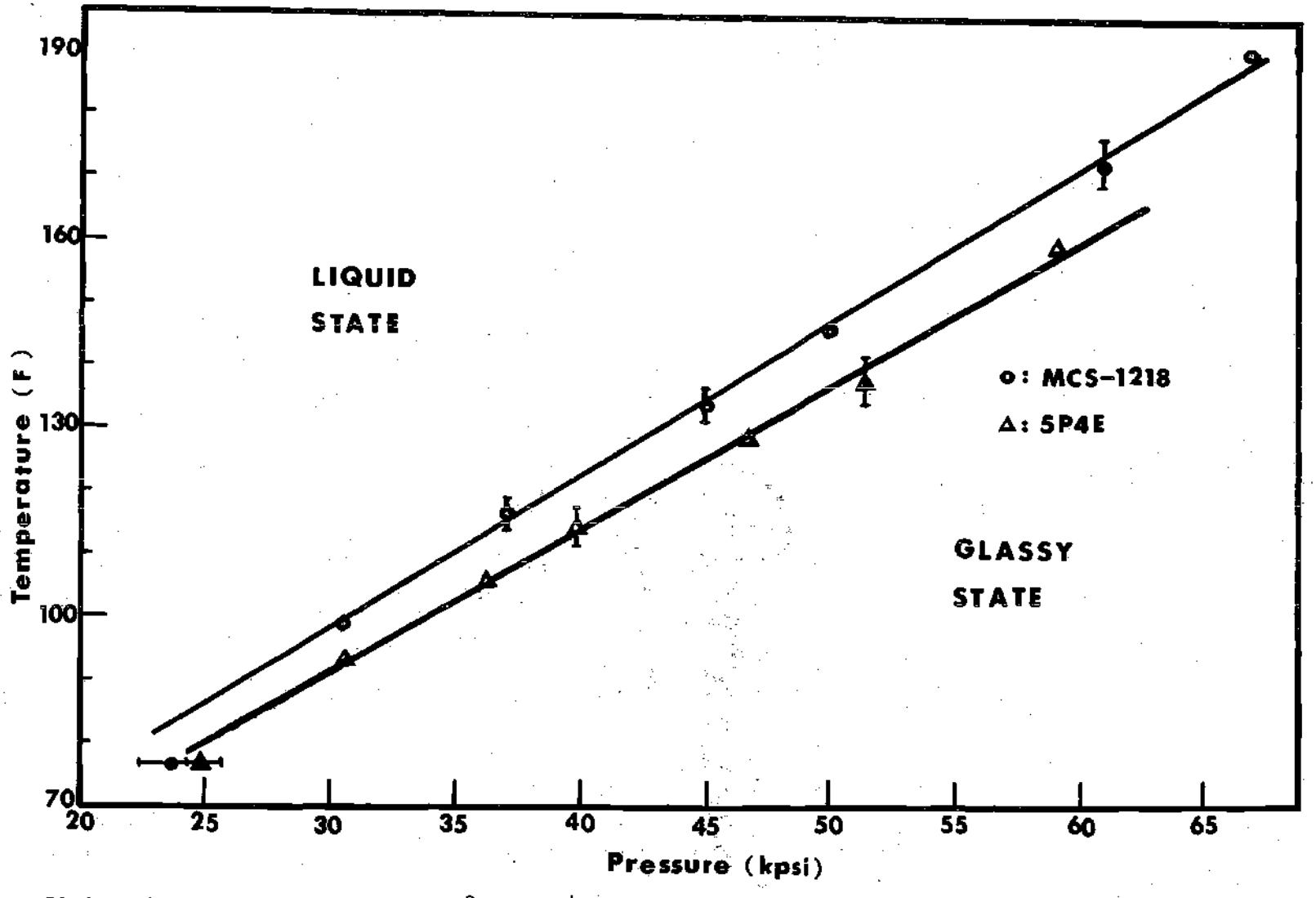

Figure 21-A. Phase Diagram for MCS-1218 and 5P4E Fluids. Open and Solid Symbols Represent Histories A and B Respectively. ⟷ and I Indicate the Confidence Bands on Pg and Tg Respectively.

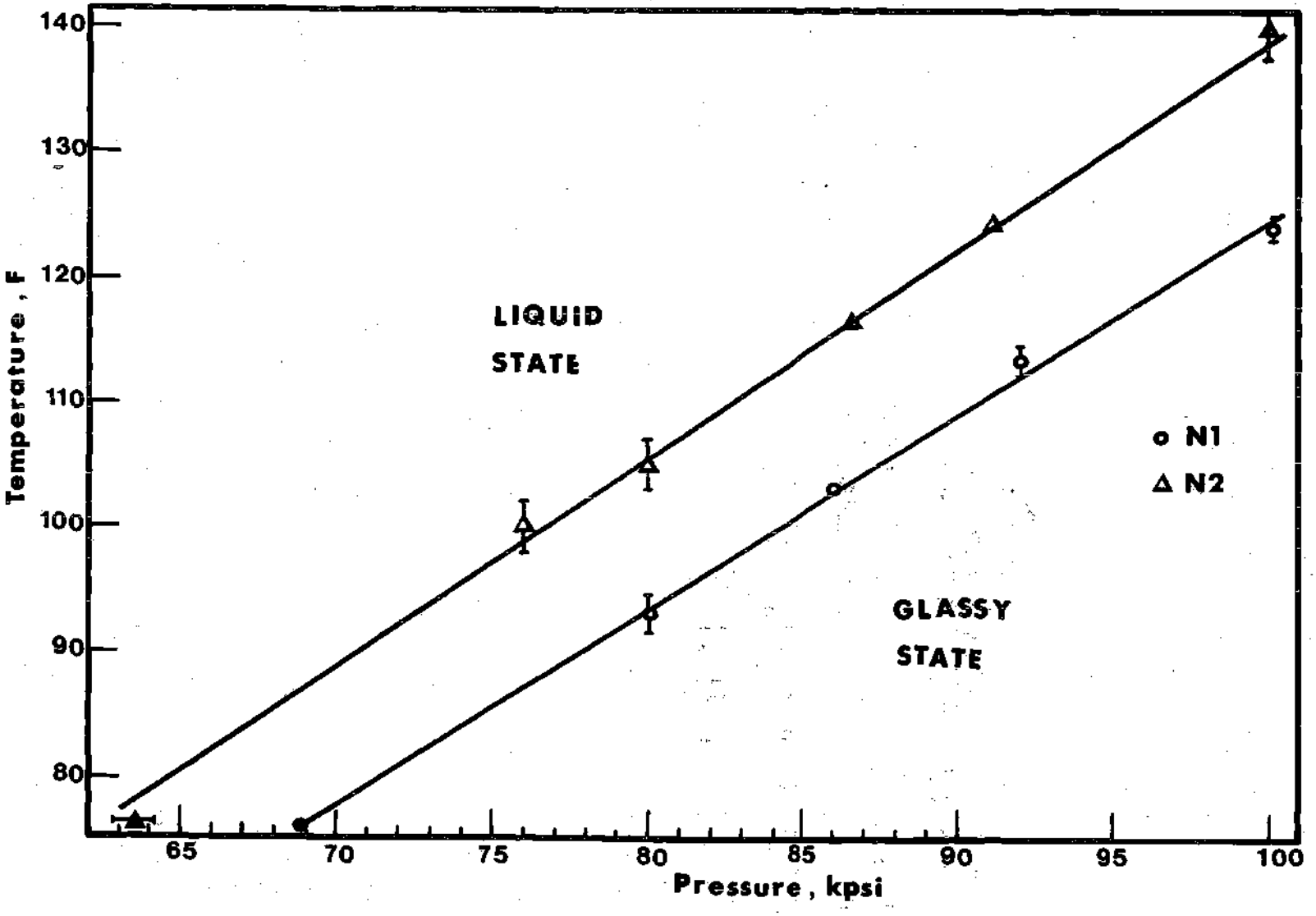

Figure 21-B. Phase Diagram for N1 and N2 Fluids. Open and Solid Symbols Represent Histories A and B Respectively. ⟷ and I Indicate the Confidence Bands on Pg and Tg Respectively.

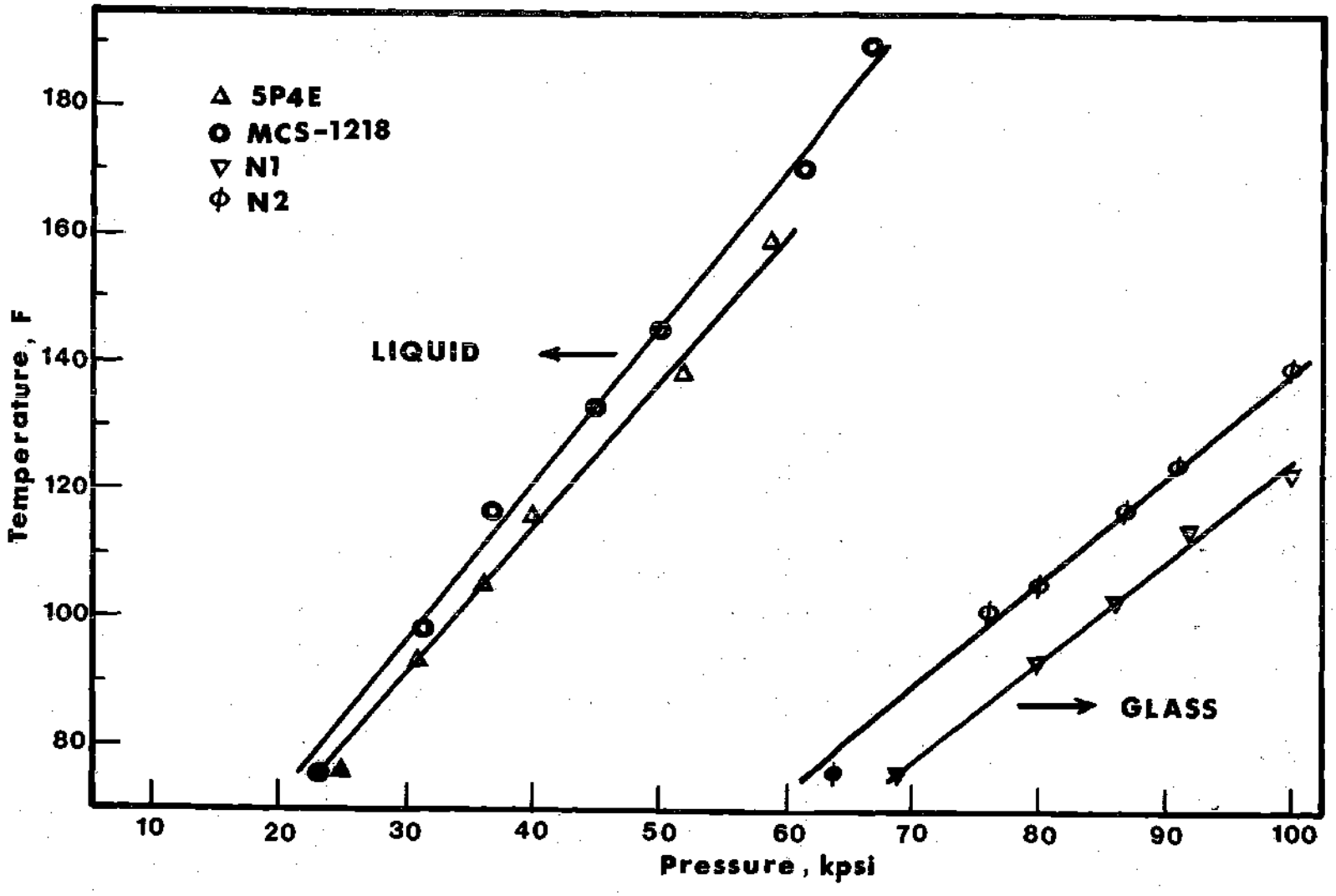

Figure 22. Phase Diagram for all Experimental Fluids. Open and Close Symbols are for Histories A and B Respectively. Glassy State is to Right and Below Transition Lines and Liquid State is to Left and Above Transition Lines.

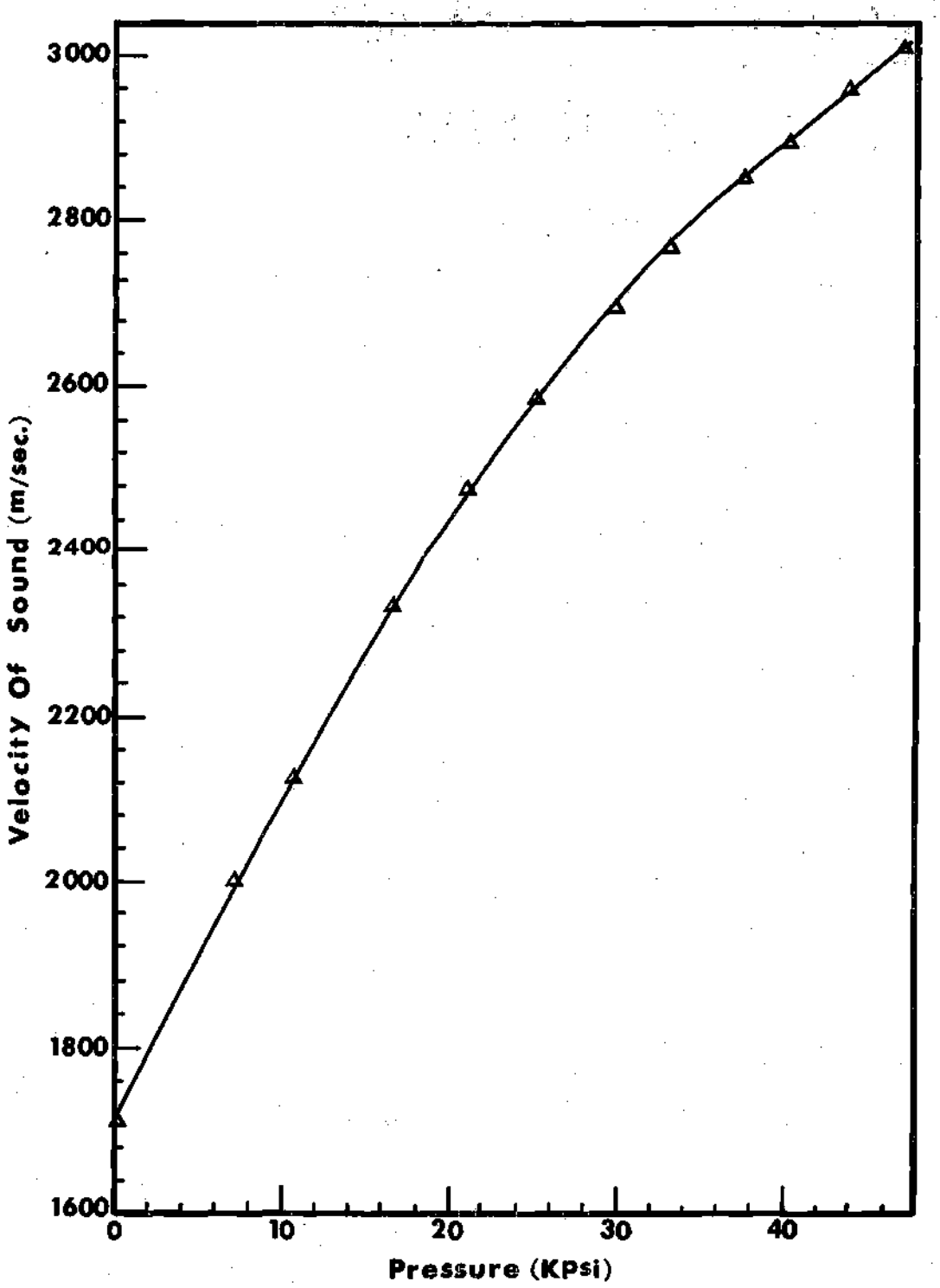

Figure 23. The Non-Linear Dependence of Sound Velocity on Pressure for N1 Fluid.

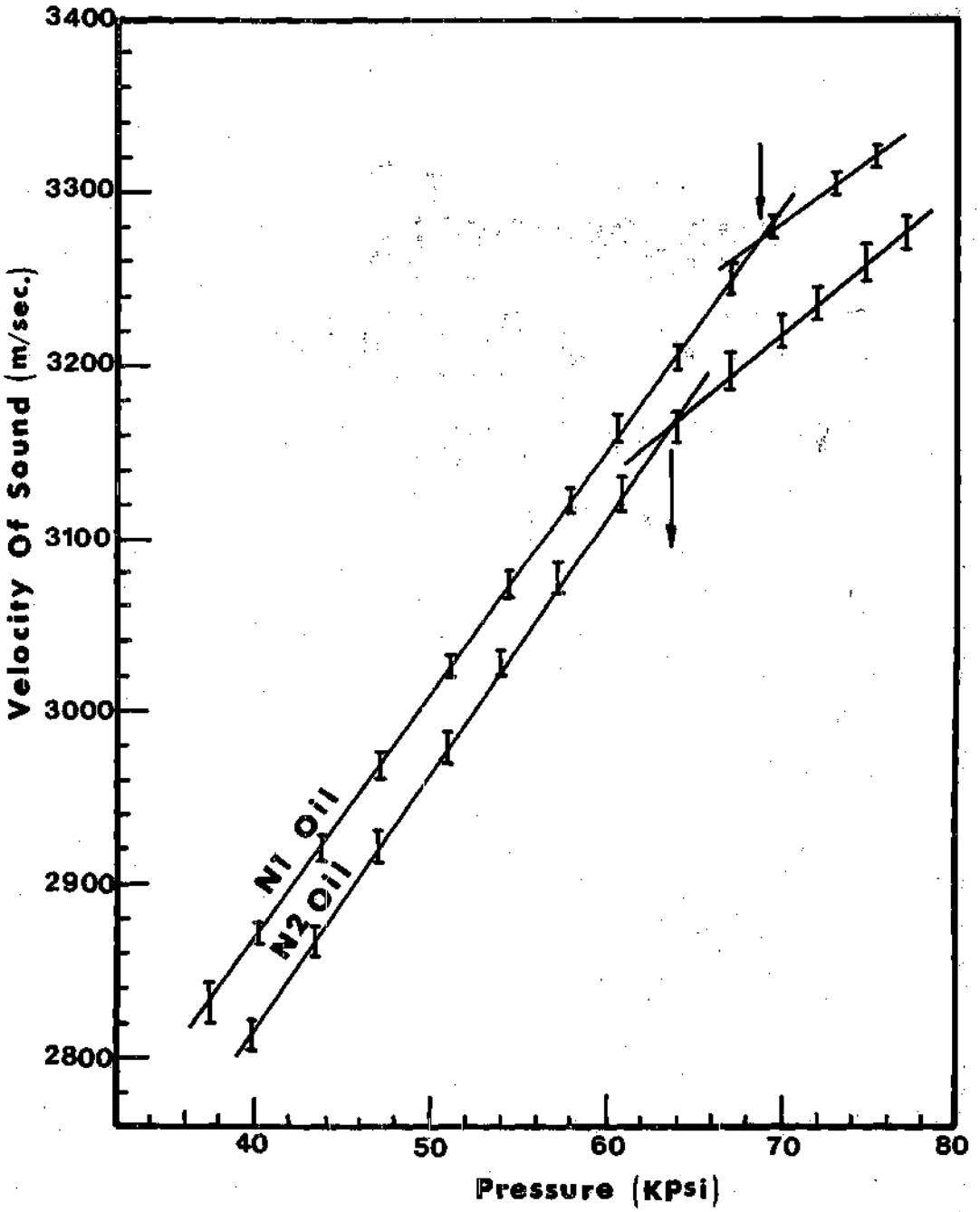

Figure 24. Variation of Sound Velocity with Pressure for N1 and N2 Fluids. Arrows Indicate Pg.

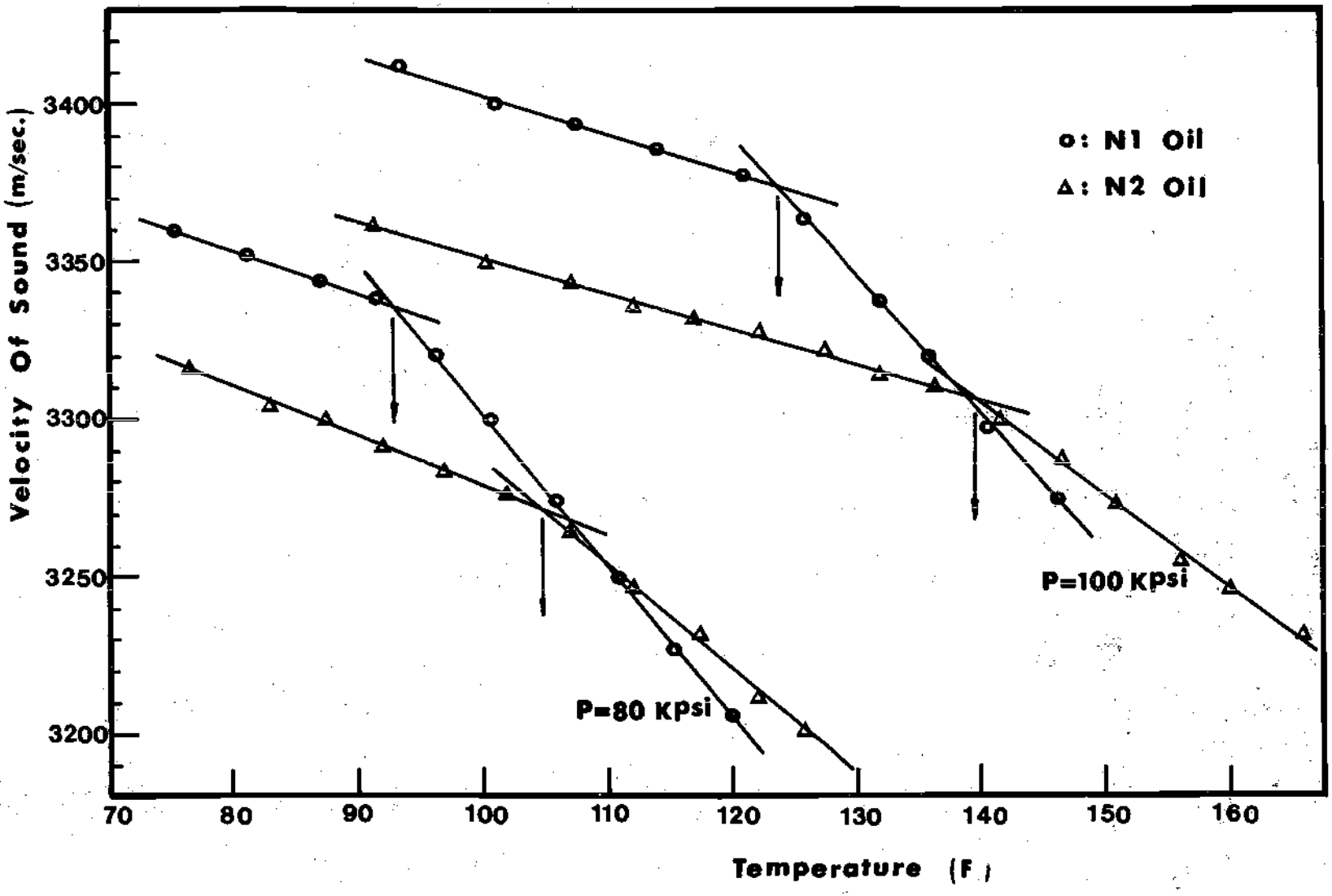

Figure 25. Variation of the Sound Velocity with Temperature at 80,000 and 100,000 psi for N1 and N2 Fluids. Arrows Indicate Tg.

CHAPTER V

DISCUSSION OF RESULTS

The discussion of results will be divided into three parts: a) The glass transition behavior of the experimental fluids examined in this work, b) The glass transition data obtained compared to glass transition data obtained by Volume-Temperature measurements at different constant pressures, and c) The relation between the glass transition data and lubricant behavior in EHD contacts.

Glass Transition Behavior of the Experimental Fluids

The figures presented in Chapter IV show the following general behavior:

1. The sound velocity and the frequency shift increased as the operating temperature was decreased or as the pressure was increased.

2. The velocity of sound in the temperature and pressure ranges investigated was 2200 to 2900 m/sec for 5P4E, 2600 to 3500 m/sec for MCS-1218 and 2300 to 3400 m/sec for both N1 and N2 fluids. This data can be used to determine the secant bulk modulus from the relation:

$$\text{sound velocity} = (\text{modulus/density})^{\frac{1}{2}} .$$

3. There is a definite change in the temperature and pressure coefficients of the sound-velocity and frequency shift at the glass transition.

4. The transition temperature shifted to higher values as the

formation pressure was increased.

5. In the glassy region, the pressure and temperature coefficients of the sound velocity is similar to that of a solid.

6. The measured sound velocities in the liquid and the glassy state and the resulting glass transition data were adequately represented by linear function of pressure or temperature in the range examined.

A comparison between the glass transition behavior of the experimental fluids indicates the following trends:

1. The glass transition pressures at 76 F (history B) for 5P4E and MCS-1218 have relatively low values (24.7 and 23.7 kpsi respectively) compared to those of N1 and N2 fluids (68.8 and 63.5 kpsi respectively).

2. The rate of increase of Tg with pressure for N1 has the lowest value (1.5 F per kpsi) while that of MCS-1218 has the largest value (2.45 F per kpsi).

The viscosity-index improver blended with the naphthenic base oil resulted in the following effects on the glass transition behavior of the blend relative to the base oil:

1. The glass transition pressure decreased by about 5000 psi at 76F.

2. The glass transition temperature was higher for all constant formation pressures. Tg increased by 1.0F at 80,000 psi and by 1.5F at 100,000 psi.

3. The rate of increase of Tg with pressure increased about 10 percent from 1.50 to 1.67 F per kpsi.

Relation of the Glass Transition Data to Volumetric Measurements

Glass transition temperature as a function of pressure for N1 fluid

was also determined by volumetric measurements. An apparatus has been constructed to permit measurements of the glass transition temperature in the range of up to 160 kpsi and temperatures to 250 F[46].

Volumetric measurements were obtained by history A at different formation pressures. Figure 26 shows the volume-temperature relation at 51.6 kpsi. The glass transition temperature was obtained by the intersection of the extrapolated curves from the liquid and glassy states. The resulting glass transition temperature at each formation pressure is summarized in Table 12 and shown in Figure 27.

At low formation pressures (up to about 65 kpsi), the transition temperature is a linear function of pressure with a slope of 2.35 F per kpsi. Above 65 kpsi, the slope decreased gradually and the glass transition relation became linear again above 80 kpsi with a slope of 1.25 F/kpsi. Figure 27 also includes the light scattering transition data obtained by history A for fluid N1 (slope = 1.50 F/kpsi). The glass transition temperatures of the light scattering technique are seen to be higher (by about 30F) than the volumetric temperatures at all pressures. This increase in Tg is the result of the glass transition dependence on frequency. For elastic frequencies of 10 GHZ, the transition from liquid to glassy state occur at higher temperatures than under low rate (essentially static) measurements due to the relaxation process of the material. The equivalent rate of the volumetric measurement was approximately 10^{-5} sec^{-1}. Therefore, as can be seen from Figure 27, the glass transition temperature shift is approximately 3.0 F per decade of increase in frequency. This is consistent with information drawn from the literature[9].

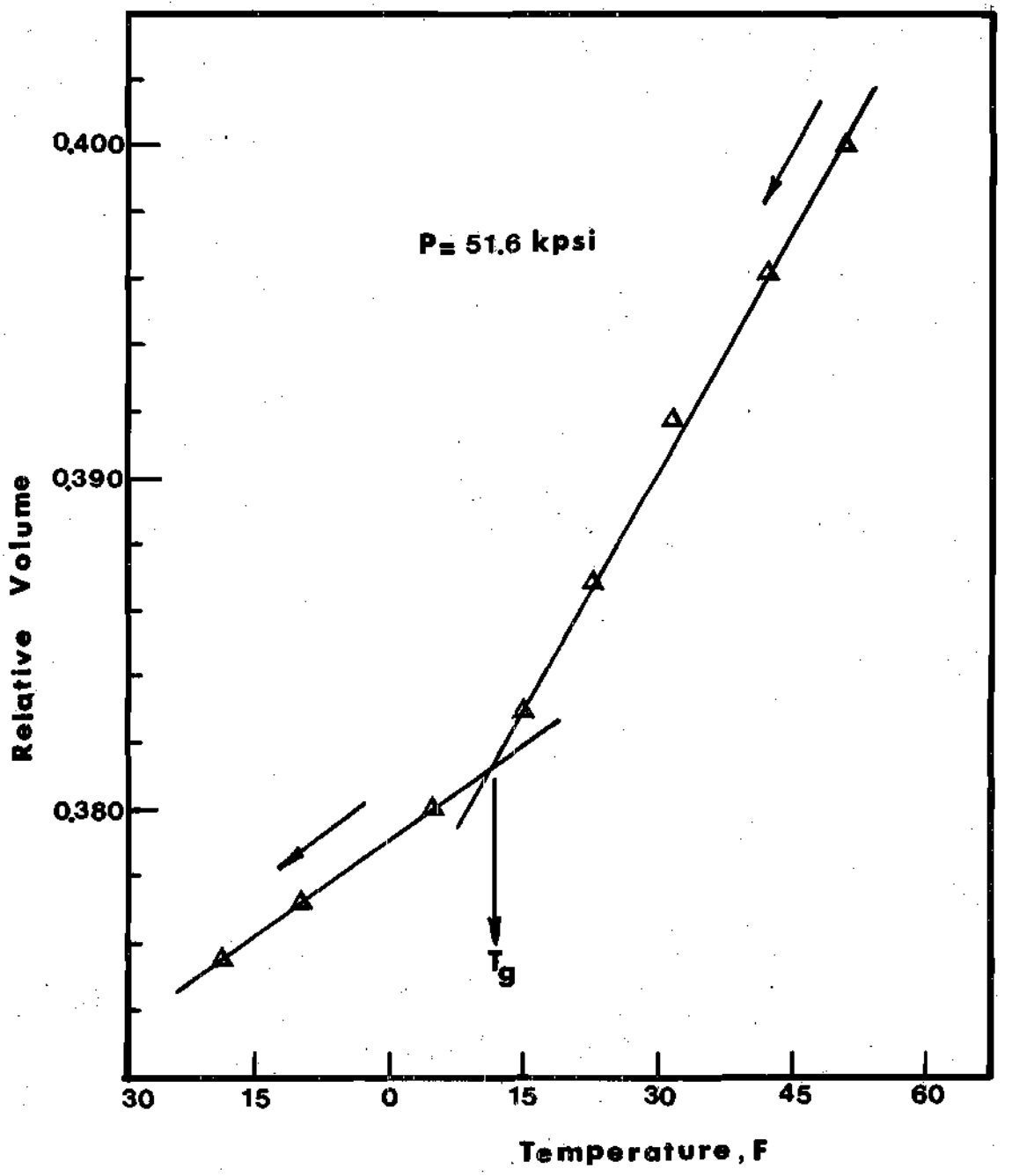

Figure 26. Relative Volume Contraction as a Function of Temperature for N1 Fluid at 51.6 kpsi (History A).

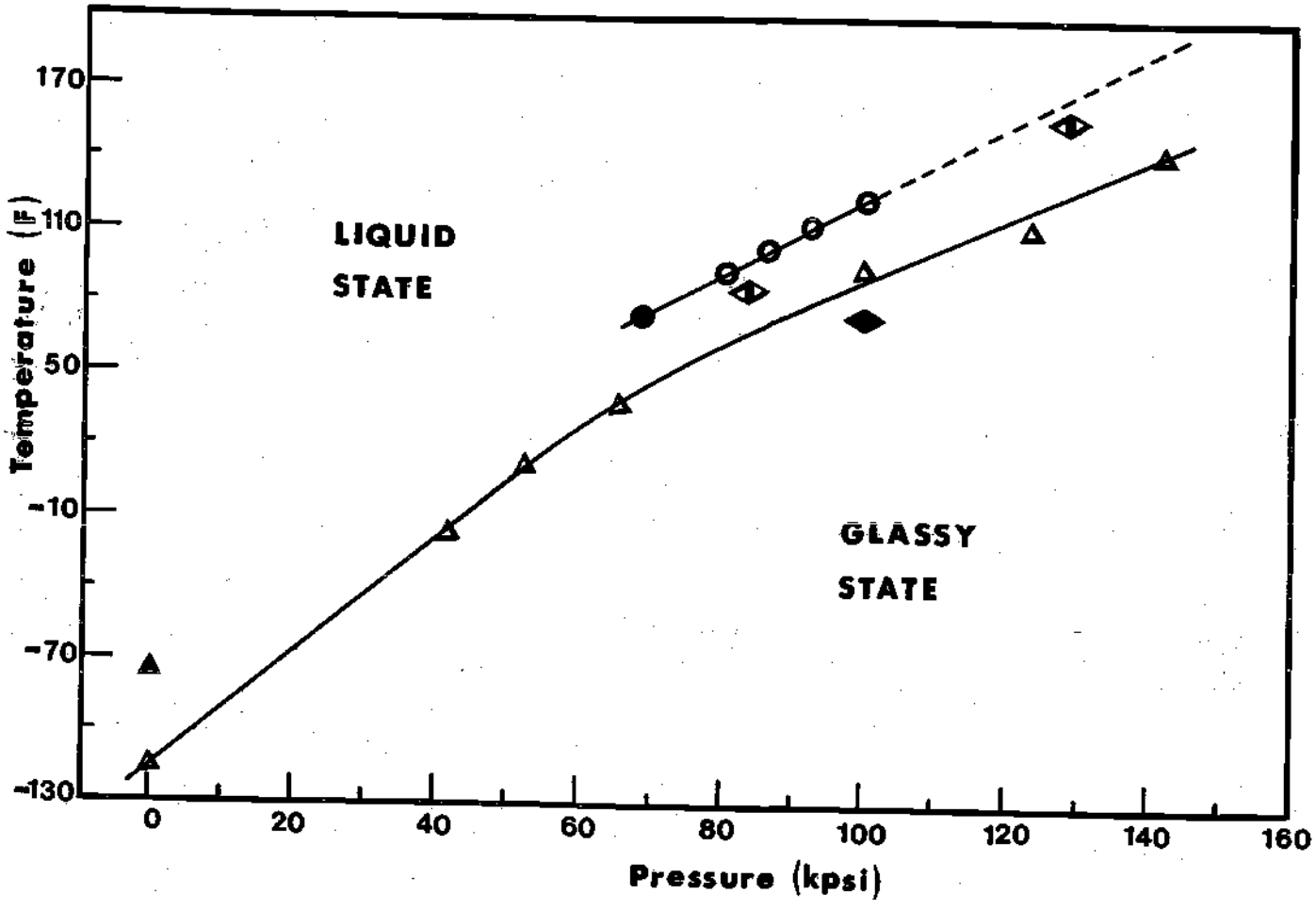

Figure 27. Phase Diagram for N1 Fluid Obtained by: ○ and ● Light Scattering Technique (Histories A and B Respectively) and △: Volume Measurements (History A). ▲DSC data, ◇ Reference [3] data, ◆ Reference [2] data.

Table 12. Volumetric Glass Transition Temperatures at Different Formation Pressures.

Formation Pressure, kpsi	0	41.4	51.6	65.0	100	132.2	141.6
Glass Transition Temperature, F	-113.8	-16.6	11.6	38.3	95.0	107.6	147.2

The glass transition temperature at atmospheric pressure was also determined by the volumetric measurements and has a value of -113.8 F. This value is lower than that obtained by the DSC measurements* by about 40 F. The decrease in Tg is due to the different cooling rates (50 F/hr for the volumetric measurements and 2200 F/hr for the DSC measurements) and the different formation history used in each technique.

From the above discussion, the glass transition determined from the light scattering technique is in agreement with glass transition measurements obtained with other techniques on the same fluid.

Relation to EHD Temperature-Pressure Measurements

Johnson and Cameron[3] measured the traction transmitted by elasto-hydrodynamic film in a rolling contact at low sliding speeds under isothermal conditions. From the traction measurements, the variation in apparent viscosity of their oil** with pressure and temperature is

*See Appendix D .

**Shell Turbo 33 oil similar to N1 but of higher viscosity.

shown in Figure 28. The variation of the apparent viscosity with pressure shows a marked change above 10^4 Poise. The authors[3] remarked that it is tempting to suppose that this change indicates a change in physical properties of the oil at high pressure. To test their remarks, the linear sections of Figure 28 were extrapolated to obtain an intersection. Pressures of about 83 and 128 kpsi were obtained at 86 and 158 F respectively. These intersection points fall near the glass transition line of N1 fluid as shown in Figure 27. The fact that the intersection points correspond to the measured glass transition points supports the authors[3] remark.

Johnson and Roberts[2] devised a rolling-contact experiment with a small amount of twist. Because of certain kinematic characteristics of their contact, no side thrust will be transmitted if the lubricant behavior is that of a liquid. If the material behaves like a solid, some side thrust will be observed. Figure 29 is a plot of the relative side thrust as a function of contact pressure. This transition in behavior of their oil* is similar to that of specific heat or expansion coefficient of a material passing through a glass transition as discussed in Chapter I. This observation raises the question of whether the behavior shown in Figure 29 is a glass transition or not. To answer this question, the technique for determining the glass transition temperature for such a behavior was used and a glass transition pressure of about 100 kpsi was obtained (at 74F). This value of pressure is seen to fall in the glassy region of Figure 27. This result agrees with the

*Shell Vitra 76 similar to N1 but of higher viscosity.

authors[2] conclusion that a transition from viscous to solid behavior occurred above a contact pressure of about 75 kpsi.

Fluid and ball surface temperatures distributions in a sliding and rolling contacts were obtained from Reference [47] for N1 fluid at different loads and speeds. Figure 30 is a plot of the ball surface temperature at the contact center versus maximum Hertz pressure at three sliding speed. Figure 31 shows the ball surface temperature versus sliding speed at different Hertz pressures. Both figures include the glass transition lines obtained by the light-scattering and the volumetric measurement techniques. As shown in these figures, the lubricant near the ball surface is in the glassy state at sliding speed of 0.2 m/sec. At higher sliding speeds, the glassy state exist only at high pressures. Temperature and pressure combinations in the contact area at some specified speeds are shown in Figure 32. This figure also includes the glass transition lines. Again, the lubricant is in the glassy state at low sliding speeds and high pressures. This result was expected since a sliding contact generates frictional heat and thus the temperature levels in the contact are relatively high.

The above discussion indicates the existence of the glassy state in sliding EHD contacts at relatively low speeds or sufficiently high pressures.

Ball surface temperature distributions for fluid N1 at different slide-to-roll ratio $\left(\Sigma = 2\,\frac{(u_2 - u_1)}{(u_2 + u_1)}\right)$ were obtained from Reference [47] and are shown in Figure 33. The speed ratio, Σ, ranged from zero (pure rolling) to 2.0 (pure sliding) at a constant Hertzian pressure of 148 kpsi

and at constantrrolling speed of 0.75 m/sec.

Temperature and pressure combinations in the contact area at different speed ratios are shown in Figure 34. The pressures are based on an assumed Hertzian pressure distribution. Figure 34 also include the glass transition lines obtained by the light scattering and volumetric techniques. As shown in this figure, the lubricant near the ball surface is in the glassy state for all speed ratios except that of $\Sigma = 2.0$. Using the light scattering and the volumetric transition data, the portions of the contact over which the glassy state exists are shown in Figure 33. At sufficiently low speed ratios, the glassy state occupies all the contact area. This result shows that the lubricant N1 is in the glassy state in a rolling/sliding contact and the glass can occupy all the contact area at low slide-to-roll speed ratios.

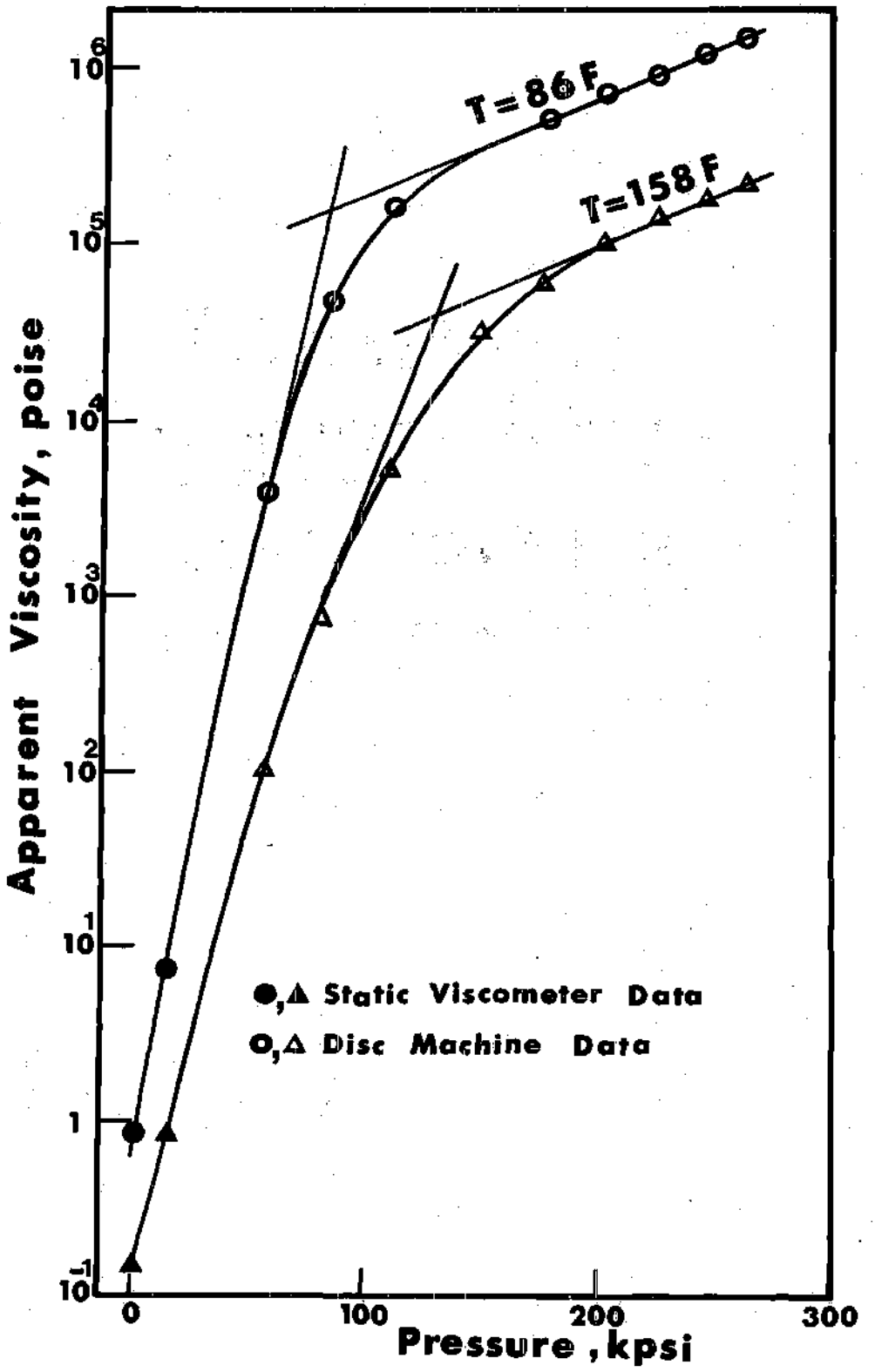

Figure 28. The Variation of Apparent Viscosity with Pressure and Temperature.(3)

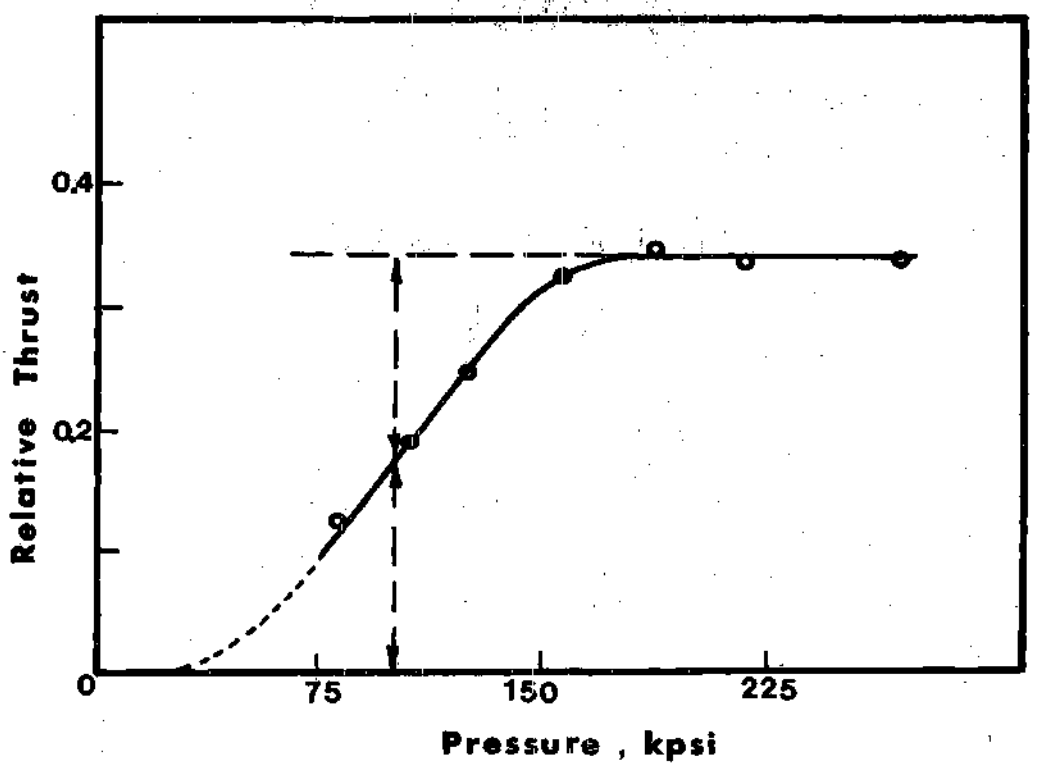

Figure 29. Variation of the Relative Side Thrust with Contact Pressure at 74.4F and 0.1 m/sec.(2)

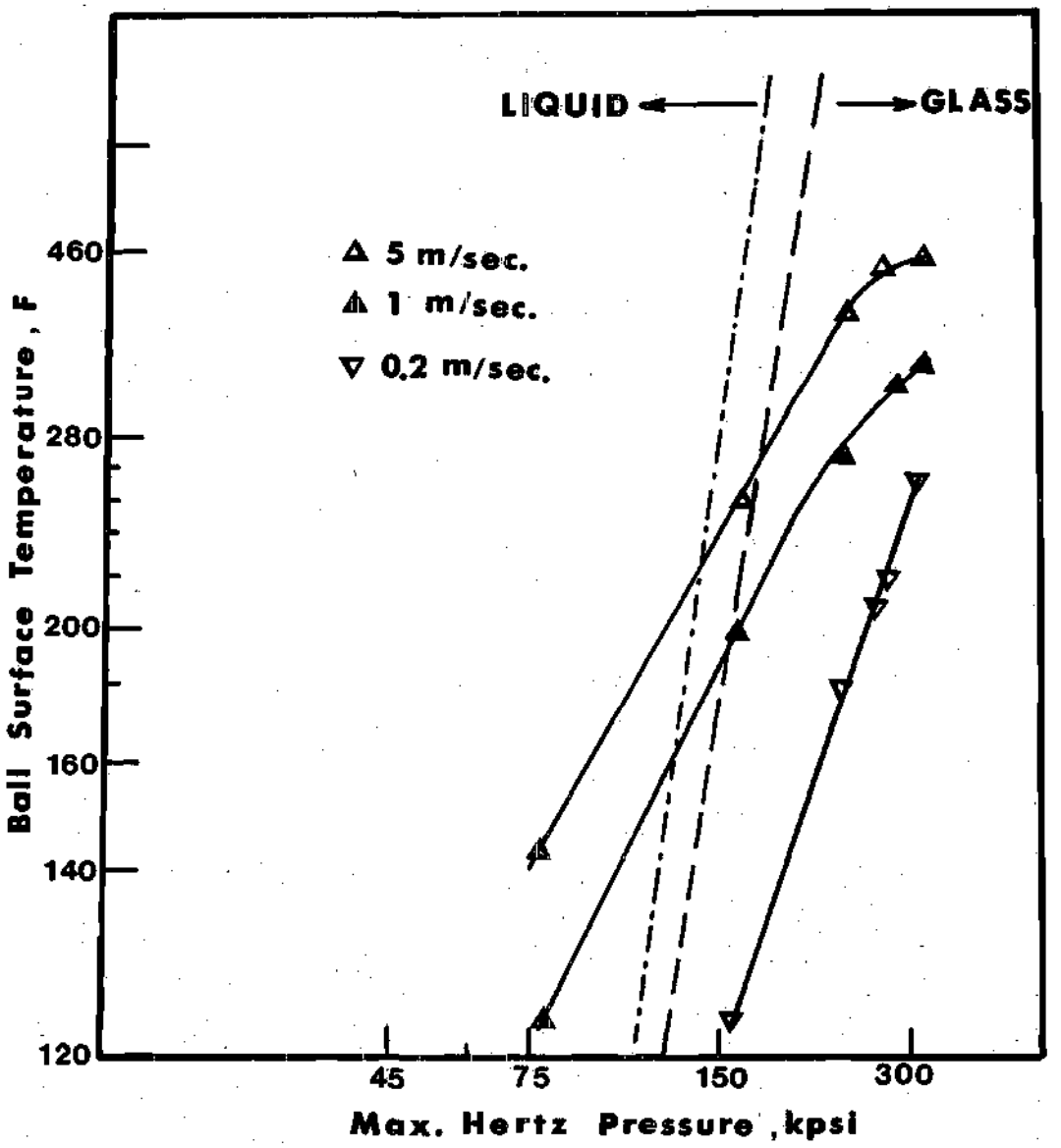

Figure 30. The Physical State of N1 Lubricant in the Center of a Sliding Contact at Various Speeds and Hertz Pressures (Reference 47) · ——— · ——— and ——— ——— Represent the Light-Scattering and the Volumetric Glass Transition Lines Respectively.

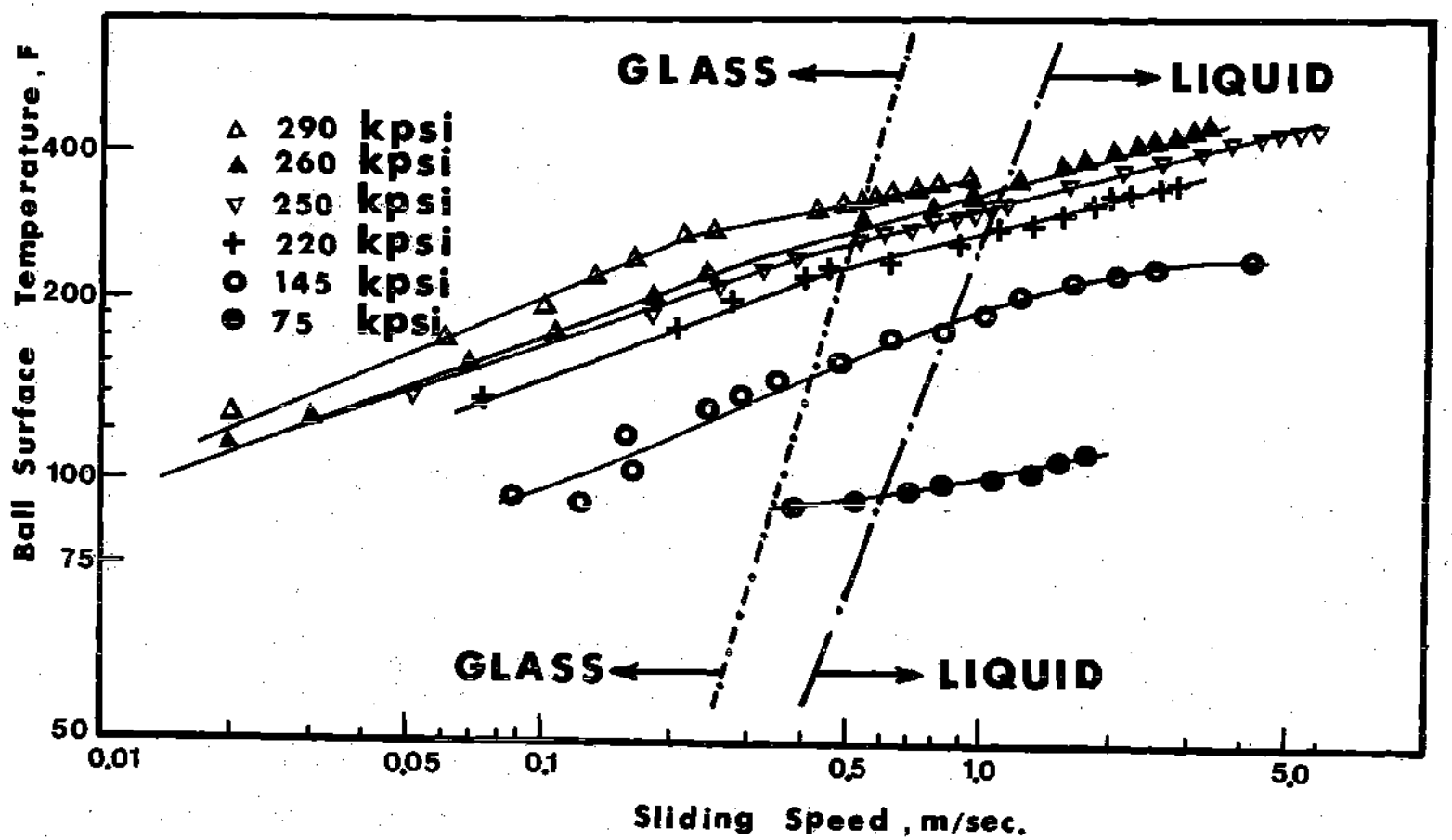

Figure 31. The Physical State of N1 Lubricant in the Center of a Sliding Contact at Various Speeds and Hertz Pressures (Reference 47) —·— and ···-·· Represent the Light-Scattering and the Volumetric Glass Transition Lines Respectively.

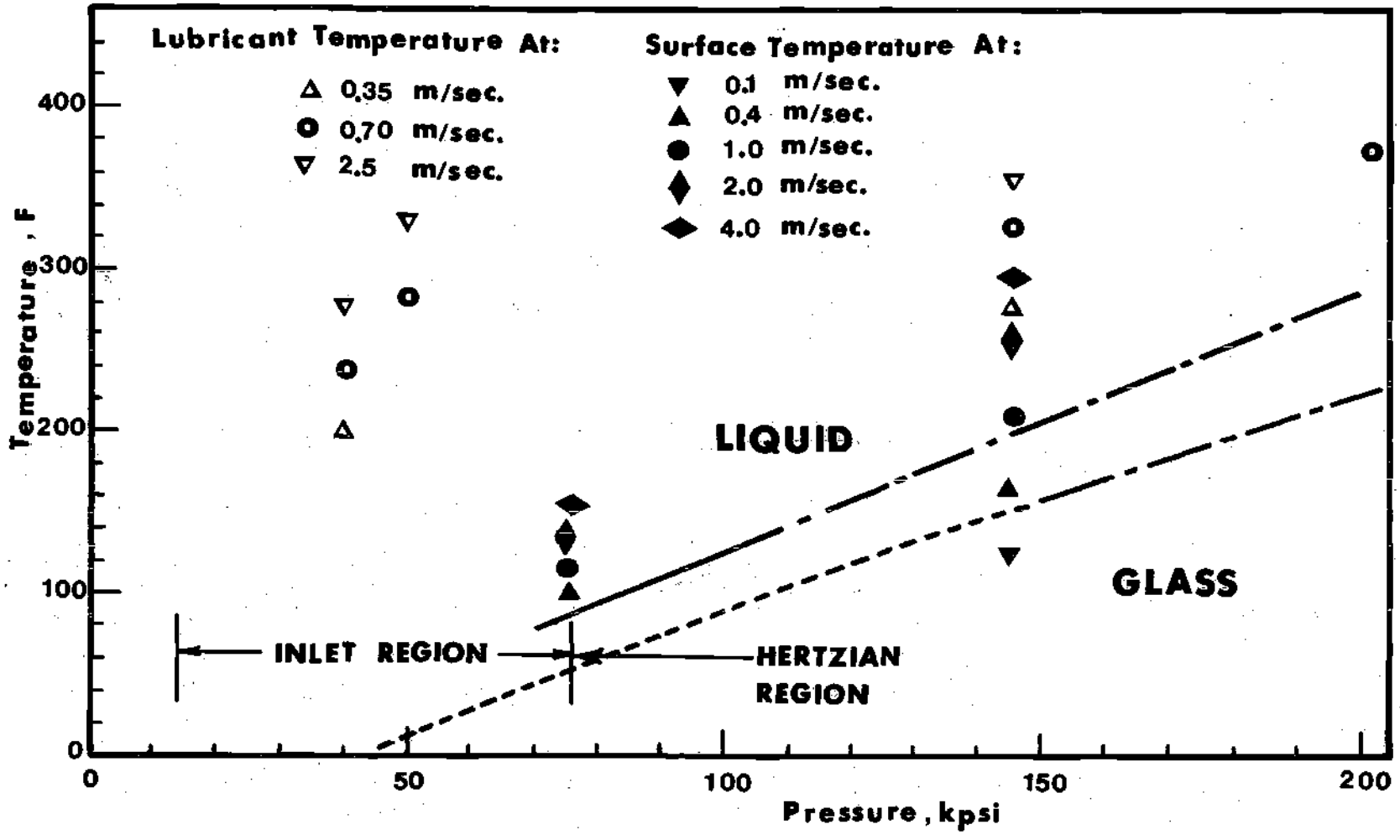

Figure 32. The Physical State of N1 Lubricant in a Sliding Contact at Various Speeds and Locations in the Contact. ——— and ------- Indicates Light Scattering and Volumetric Transition Lines Respectively. ——— - ——— Indicate Extrapolated Transition Lines. (Reference 47)

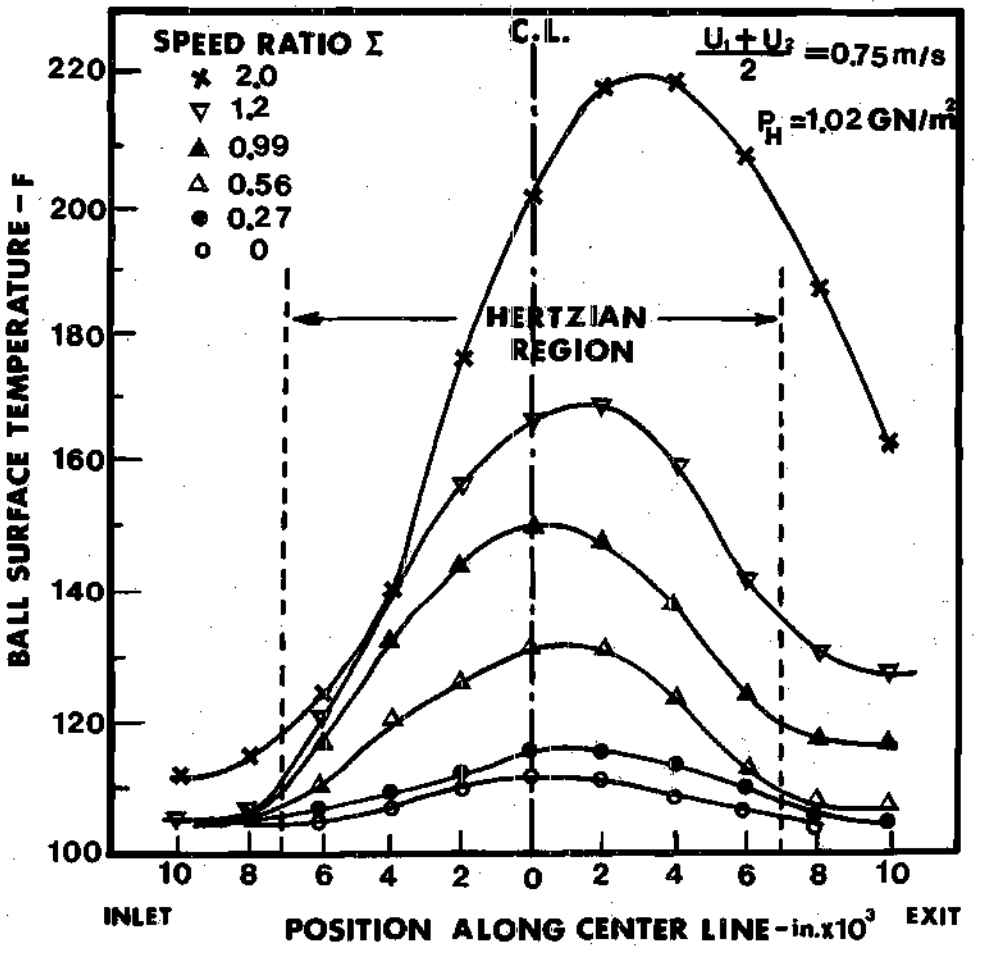

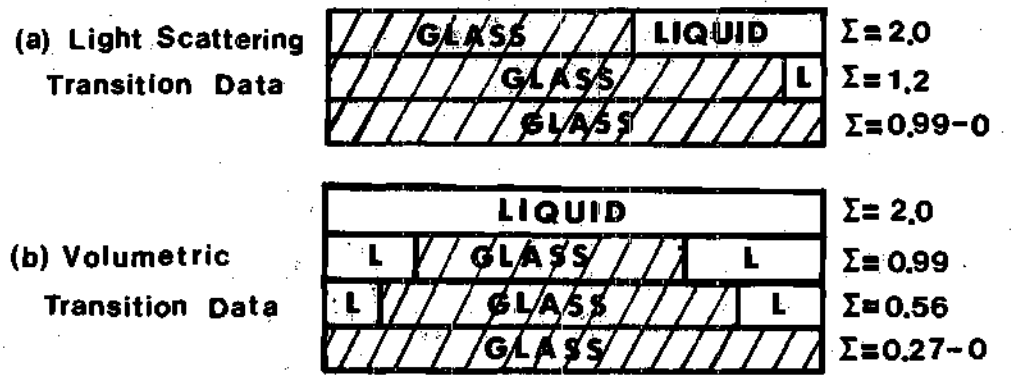

Figure 33. Ball Surface Temperature Distribution Along the Contact Centerline at Constant Hertzian Pressure of 148 kpsi and Constant Rolling Speed of 0.75 m/sec. (a) and (b) Represent the Physical State of the Lubricant in the Contact Area as Determined by the Light Scattering Volumetric Transition Data Respectively.

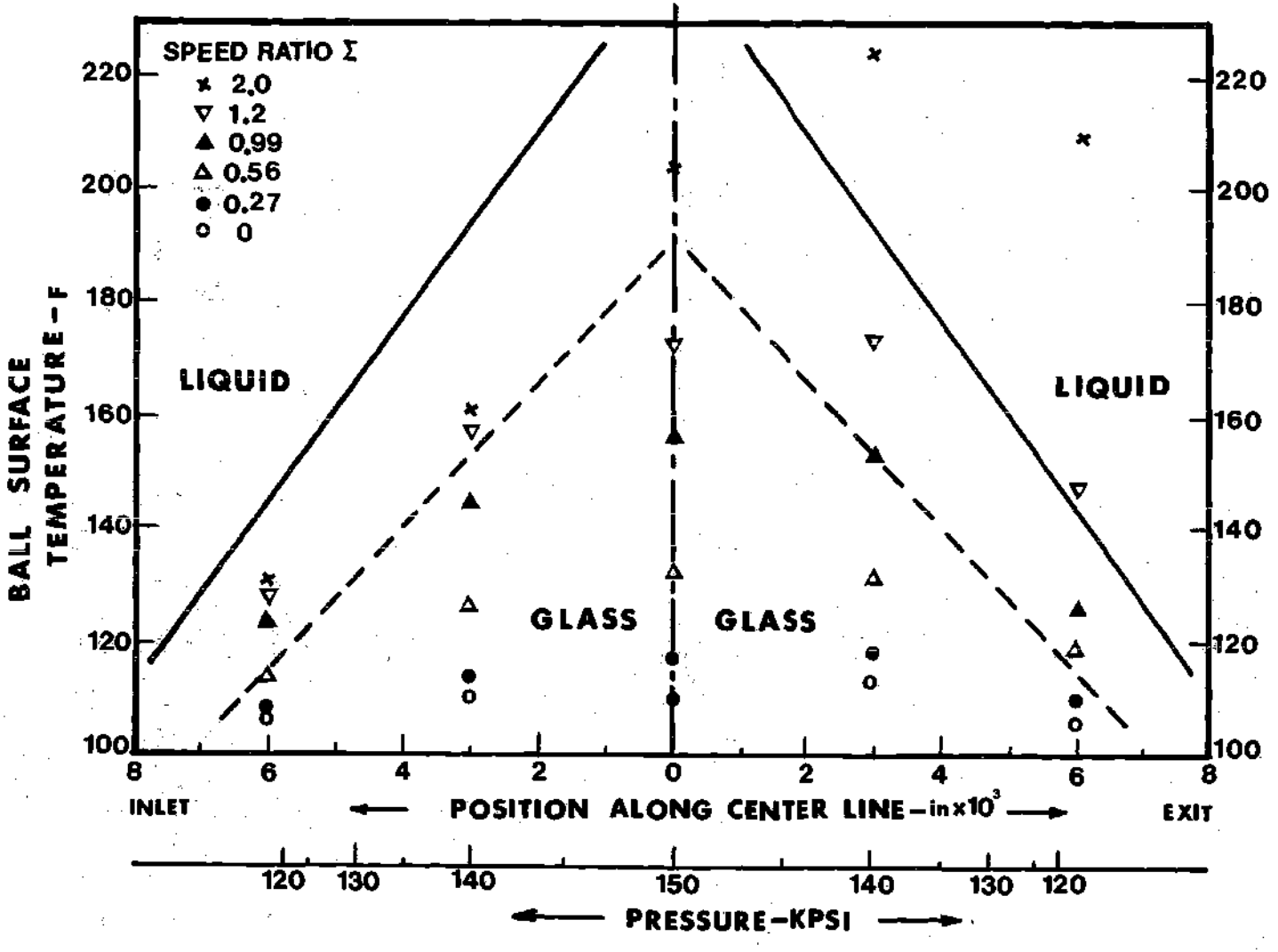

Figure 34. Physical State of Lubricant N1 Along the Contact Area at Different Slide-to-Roll Speed Ratios · - - - - - - and ——— Represent Light Scattering and Volumetric Transition Lines Respectively.

CHAPTER VI

CONCLUSIONS AND RECOMMENDATIONS

From the glass transition data obtained, the following conclusions are made:

1. Light-scattering technique is a useful tool in determining the transition between the liquid-like and solid-like behavior of materials in the giga cycle frequency range.

2. Lubricants in EHD contacts can exist in a glassy state at relatively high temperatures if the operating pressures are suitable.

3. Glass transition of lubricants and therefore the rheological behavior in the glassy state play a significant role in determining the rheological behavior of lubricants in EHD contacts.

4. Glass transition data may offer a basis for selecting lubricants for specific EHD applications.

5. Because the effective rate of pressurization in an EHD contact is relatively low compared to the gigacycle rate of the light-scattering technique, one should expect the glass transition to occur at temperatures low compared to the data obtained in this work.

6. Similarly, because the effective rate of pressurization in an EHD contact is relatively high compared to the volumetric measurements rate, one should expect the glass transition to occur at temperatures high compared to the volumetric measurements data.

7. Pressure and temperature ranges over which the glass

transition occurs are small compared to the ranges experienced in a typical EHD contact. Therefore, lubricants are primarily in the liquid state or the glassy state and not in viscoelastic state.

8. The glass transition data obtained for one of the experimental fluids are in good agreement with glass transition measurements of other techniques. The same result was obtained for the other fluids.

We believe that the present work will lead to new research areas in the elastohydrodynamic lubrication. A feasibility study of the role of the glass transition phenomena in EHD contacts should include:

1. Experimental investigations to study the rheological behavior of lubricants in the glassy state as a function of pressure, temperature, and glass formation history.

2. Analytical and experimental investigations into the effect of the glassy state behavior on the two most important operating variables of an EHD contact: the film thickness and traction.

APPENDICES

APPENDIX A

TABULATED DATA

The following tables list the detailed experimental results obtained. The velocity of sound and frequency shift reported in these tables represent the average value obtained from frequency spectra using the technique described in Chapter III.

Table A1-a. Frequency Shift and Sound Velocity as a Function of Pressure at 76F (history B) for 5P4E Fluid.

Date: December 26, 1975
Separation Distance = 0.50 cm
Resulting Pg = 24.7 kpsi

Spectrum Number	Pressure kpsi	Frequency Shift cm^{-1}	Frequency Shift GHZ	Refractive Index	Velocity of Sound, m/sec
1	4.78	0.33194	9.96	1.6405	2208
2	7.2	0.34034	10.21	1.6453	2258
3	10.46	0.35369	10.61	1.6518	2337
4	14.25	0.36805	11.04	1.6594	2421
5	16.80	0.37819	11.35	1.6645	2480
6	20.84	0.39429	11.83	1.6726	2573
7	23.12	0.40259	12.08	1.6772	2620
8	26.05	0.41204	12.36	1.6829	2672
9	28.20	0.41642	12.49	1.6873	2695
10	29.95	0.42067	12.62	1.6909	2715
11	31.50	0.42347	12.70	1.6939	2729

Table A1-b. Frequency Shift and Velocity of Sound (history A) at 30.5 kpsi for 5P4E Fluid.

Date: March 1, 1976
Separation Distance = 0.725 cm
Resulting Tg = 92.6 F

Spectrum Number	Temperature F	Frequency Shift cm^{-1}	Frequency Shift GHZ	Refractive Index	Velocity of Sound m/sec
11	119.3	0.39653	11.90	1.6807	2575
12	112.8	0.40107	12.03	1.6823	2602
13	107.9	0.40447	12.13	1.6836	2622
14	102.9	0.40841	12.25	1.6848	2645
15	97.1	0.41316	12.39	1.6863	2674
16	93.1	0.41575	12.47	1.6873	2689
17	90.0	0.41709	12.51	1.6881	2697
18	86.6	0.41824	12.55	1.6890	2703
19	82.0	0.41978	12.59	1.6901	2711

Table A1-c. Frequency Shift and Velocity of Sound (history A) at 36.0 kpsi for 5P4E Fluid.

Date: February 24, 1976
Separation Distance = 0.725 cm
Resulting Tg = 105.0 F

Spectrum Number	Temperature F	Frequency Shift cm^{-1}	Frequency Shift GHZ	Refractive Index	Velocity of Sound m/sec
21	120.5	0.41476	12.44	1.6914	2676
22	117.3	0.41673	12.50	1.6922	2688
23	113.0	0.42018	12.61	1.6933	2708
24	109.0	0.42277	12.68	1.6943	2723
25	105.0	0.42494	12.75	1.6953	2736
26	102.5	0.42611	12.78	1.6958	2742
27	99.5	0.42739	12.82	1.6967	2749
28	94.5	0.42909	12.87	1.6980	2758
29	89.8	0.43026	12.91	1.6991	2764
30	84.1	0.43197	12.96	1.7006	2772

Table A1-d. Frequency Shift and Velocity of Sound (history A) at 40.0 kpsi for 5P4E Fluid.

Date: March 1, 1976
Separation Distance = 0.725 cm
Resulting Tg = 115.6 F

Spectrum Number	Temperature F	Frequency Shift cm^{-1}	Frequency Shift GHZ	Refractive Index	Velocity of Sound m/sec
32	135.5	0.41632	12.49	1.6956	2680
33	131.2	0.41971	12.59	1.6967	2700
34	127.2	0.42110	12.63	1.6977	2714
35	122.2	0.42663	12.80	1.6989	2741
36	117.2	0.42986	12.90	1.7002	2760
37	111.9	0.43196	12.96	1.7015	2771
38	106.6	0.43430	13.03	1.7029	2783
39	102.4	0.43561	13.07	1.7040	2790
40	95.3	0.43766	13.13	1.7058	2800
41	90.1	0.43975	13.19	1.7071	2810

Table A1-e. Frequency Shift and Velocity of Sound (history A) at 46.5 kpsi for 5P4E Fluid.

Date: March 1, 1976
Separation Distance = 0.725 cm
Resulting Tg = 127.9 F

Spectrum Number	Temperature F	Frequency Shift cm^{-1}	Frequency Shift GHZ	Refractive Index	Velocity of Sound m/sec
43	154.7	0.42301	12.69	1.7037	2710
44	149.8	0.42688	12.81	1.7049	2732
45	145.4	0.42900	12.87	1.7061	2745
46	140.5	0.43250	12.98	1.7073	2765
47	136.5	0.43546	13.06	1.7083	2782
48	132.3	0.43751	13.13	1.7094	2794
49	124.0	0.44204	13.26	1.7115	2818
50	120.1	0.44369	13.31	1.7125	2821
51	115.5	0.44406	13.32	1.7136	2829
52	110.9	0.44532	13.36	1.7148	2830

Table A1-f. Frequency Shift and Velocity of Sound (history A) at 51.5 kpsi for 5P4E Fluid.

Date: March 8, 1976
Separation Distance = 0.725 cm
Resulting Tg = 138.7 F

Spectrum Number	Temperature F	Frequency Shift cm^{-1}	Frequency Shift GHZ	Refractive Index	Velocity of Sound m/sec
54	160.8	0.43323	13.00	1.7122	2762
55	155.3	0.43726	13.12	1.7135	2785
56	150.9	0.44009	13.20	1.7147	2802
57	145.5	0.44418	13.33	1.7160	2821
58	140.4	0.44752	13.43	1.7173	2844
59	134.6	0.44951	13.49	1.7188	2854
60	129.1	0.45096	13.53	1.7202	2862
61	123.1	0.45279	13.58	1.7217	2870
62	116.5	0.45462	13.64	1.7234	2879

Table A1-g. Frequency Shift and Sound Velocity (history A) at 59.0 kpsi for 5P4E Fluid.

Date: March 2, 1976
Separation Distance = 0.725 cm
Resulting Tg = 158.5 F

Spectrum Number	Temperature F	Frequency Shift cm^{-1}	Frequency Shift GHZ	Refractive Index	Velocity of Sound m/sec
64	180.3	0.43966	13.19	1.7222	2787
65	175.8	0.44236	13.27	1.7233	2801
66	170.8	0.44618	13.39	1.7246	2823
67	166.2	0.44973	13.49	1.7258	2844
68	161.0	0.45369	13.61	1.7271	2867
69	157.5	0.45511	13.65	1.7280	2875
70	152.9	0.45691	13.71	1.7292	2883
71	148.3	0.45789	13.74	1.7303	2888
72	144.5	0.45910	13.77	1.7313	2894
73	138.3	0.46064	13.82	1.7328	2901
74	132.5	0.46216	13.86	1.7343	2908

Table A2-a. Frequency Shift and Velocity of Sound as a Function of Pressure at 76 F (history B) for MCS-1218 Fluid.

Date: April 2, 1976
Separation Distance = 0.475 cm
Resulting: Pg = 23.7 kpsi

Spectrum Number	Pressure kpsi	Frequency Shift cm^{-1}	Frequency Shift GHZ	Refractive Index	Velocity of Sound m/sec
200	7.8	0.37366	11.21	1.5270	2671
201	10.0	0.38126	11.44	1.5314	2717
202	12.85	0.39455	11.84	1.5371	2782
203	15.7	0.40728	12.22	1.5428	2881
204	18.0	0.41720	12.52	1.5474	2943
205	21.0	0.43001	12.90	1.5534	3022
206	22.7	0.43798	13.14	1.5568	3071
207	24.4	0.44383	13.31	1.5602	3105
208	26.3	0.44733	13.42	1.5640	3.22
209	28.06	0.45071	13.52	1.5675	3139
210	31.0	0.45767	13.73	1.5734	3175

Table A2-b. Frequency Shift and Sound Velocity (history A) at 31.0 kpsi for MCS-1218 Fluid.

Date: April 5, 1976

Separation Distance = 0.625 cm

Resulting: Tg = 98.6 F

Spectrum Number	Temperature F	Frequency Shift cm^{-1}	Frequency Shift GHZ	Refractive Index	Velocity of Sound m/sec
211	118.3	0.43425	13.03	1.5639	3031
212	113.7	0.43830	13.15	1.5649	3057
213	109.8	0.44041	13.21	1.5657	3071
214	105.0	0.44537	13.36	1.5668	3103
215	100.2	0.44904	13.47	1.5679	3126
216	95.2	0.45141	13.54	1.5690	3140
217	90.4	0.45306	13.59	1.5700	3150
218	86.1	0.45396	13.62	1.5710	3154
219	82.0	0.45544	13.66	1.5719	3163
220	75.1	0.45747	13.72	1.5734	3174

Table A2-c. Frequency Shift and Sound Velocity (history A) at 37.0 kpsi for MCS-1218 Fluid.

Date: April 5, 1976
Separation Distance = 0.625 cm
Resulting: Tg = 116.3 F

Spectrum Number	Temperature F	Frequency Shift cm^{-1}	Frequency Shift GHZ	Refractive Index	Velocity of Sound m/sec
221	139.1	0.44403	13.32	1.5713	3084
222	133.5	0.44829	13.45	1.57225	3112
223	129.2	0.45141	13.54	1.5732	3132
224	124.1	0.45597	13.68	1.5744	3161
225	120.0	0.45915	13.77	1.5754	3181
226	113.1	0.46304	13.89	1.5766	3206
227	108.8	0.46403	13.92	1.5777	3210
228	103.5	0.46577	13.97	1.57875	3220
229	98.8	0.46757	14.03	1.5799	3230
230	91.5	0.46960	14.09	1.58095	3239

Table A2-d. Frequency Shift and Sound Velocity (history A) at 45.0 kpsi for MCS-1218 Fluid.

Date: April 6, 1976

Separation Distance = 0.625 cm

Resulting: Tg = 133.2 F

Spectrum Number	Temperature F	Frequency Shift cm^{-1}	Frequency Shift GHZ	Refractive Index	Velocity of Sound m/sec
231	154.5	0.46838	14.05	1.5838	3228
232	150.0	0.47137	14.14	1.5851	3246
233	144.5	0.47452	14.24	1.58605	3265
234	139.5	0.47783	14.33	1.5870	3286
235	136.7	0.48000	14.40	1.5880	3299
236	130.9	0.48220	14.47	1.5891	3312
237	126.4	0.48349	14.50	1.5903	3318
238	120.9	0.48454	14.54	1.5915	3323
239	115.0	0.48594	14.58	1.5926	3330
240	108.6	0.48938	14.68	1.5947	3339

Table A2-e. Frequency Shift and Sound Velocity (history A) at 50.0 kpsi for MCS-1218 Fluid.

Date: April 8, 1976
Separation Distance = 0.625 cm
Resulting: Tg = 145.3 F

Spectrum Number	Temperature F	Frequency Shift cm^{-1}	Frequency Shift GHZ	Refractive Index	Velocity of Sound m/sec
241	169.5	0.47086	14.13	1.5906	3231
242	164.0	0.47468	14.24	1.5919	3255
243	158.9	0.47788	14.34	1.5931	3271
244	153.7	0.48134	14.46	1.5940	3300
245	149.0	0.48492	14.55	1.5951	3318
246	142.7	0.48804	14.64	1.5965	3336
247	136.5	0.48891	14.67	1.5977	3340
248	131.4	0.49026	14.71	1.5989	3347
249	125.0	0.49164	14.75	1.6004	3353
250	117.9	0.49275	14.78	1.6020	3357

Table A2-f. Frequency Shift and Sound Velocity (history A) at 61.0 kpsi for MCS-1218 Fluid.

Date: April 8, 1976

Separation Distance = 0.625 cm

Resulting Tg = 170.8 F

Spectrum Number	Temperature F	Frequency Shift cm^{-1}	Frequency Shift GHZ	Refractive Index	Velocity of Sound m/sec
251	197.1	0.48924	14.68	1.6064	3324
252	192.2	0.49231	14.77	1.6076	3342
253	187.4	0.49444	14.83	1.6086	3355
254	182.5	0.49834	14.95	1.6097	3375
255	176.5	0.50196	15.06	1.6110	3401
256	170.4	0.50443	15.13	1.6124	3415
257	165.2	0.50617	15.19	1.6135	3424
258	160.2	0.50724	15.22	1.6146	3429
259	154.5	0.50836	15.25	1.6159	3433
260	149.5	0.50870	15.26	1.6170	3434
261	143.1	0.51023	15.31	1.6184	3441

Table A2-g. Frequency Shift and Sound Velocity (history A) at 67.0 kpsi for MCS-1218 Fluid.

Date: April 9, 1976
Separation Distance = 0.625 cm
Resulting Tg = 189.4 F

Spectrum Number	Temperature F	Frequency Shift cm^{-1}	Frequency Shift GHZ	Refractive Index	Velocity of Sound m/sec
262	210.0	0.49761	14.93	1.6157	3362
263	204.3	0.50129	15.04	1.6169	3384
264	198.5	0.50527	15.16	1.6181	3408
265	192.2	0.50899	15.27	1.6195	3430
266	187.4	0.51108	15.33	1.6207	3442
267	181.2	0.51172	15.35	1.6219	3451
268	176.0	0.51412	15.42	1.6232	3457
269	169.5	0.51526	15.46	1.6246	3461
270	164.5	0.51594	15.48	1.6258	3464
271	156.0	0.51785	15.54	1.6276	3473

Table A3-a. Frequency Shift and Sound Velocity as a Function of Pressure at 76 F (history B) for N1 Fluid.

Date: December 22, 1976
Separation Distance = 0.40 cm
Resulting Pg = 68.8 kpsi

Spectrum Number	Pressure kpsi	Frequency Shift cm^{-1}	Frequency Shift GHZ	Refractive Index	Velocity of Sound m/sec
100	0.0	0.23520	7.06	1.5033	1707
101	6.90	0.27808	8.34	1.5165	2001
102	10.65	0.29726	8.92	1.5246	2128
103	16.50	0.32854	9.86	1.52363	2334
104	21.20	0.35107	10.53	1.5477	2475
105	25.15	0.36860	11.06	1.5562	2585
106	29.85	0.38299	11.49	1.5630	2674
107	33.10	0.39446	11.83	1.5695	2743
108	37.30	0.40957	12.29	1.5779	2833
109	40.15	0.41667	12.50	1.5836	2872
110	43.85	0.42559	12.77	1.5910	2920
111	47.05	0.43444	13.03	1.5974	2969
112	50.90	0.44510	13.35	1.6051	3027
113	54.40	0.45383	13.61	1.6121	3073
114	58.00	0.46316	13.89	1.6193	3122
115	60.55	0.47110	14.12	1.6244	3165
116	63.95	0.47895	14.37	1.6312	3204
117	66.90	0.48774	14.63	1.6371	3252
118	69.35	0.49363	14.81	1.6420	3281
119	72.90	0.49948	14.98	1.6491	3306
120	75.70	0.50374	15.11	1.6547	3323

Table A3-b. Frequency Shift and Sound Velocity (history A) at 80.0 kpsi for N1 Fluid.

Date: March 23, 1976
Separation Distance = 0.635 cm
Resulting Tg = 93.0 F

Spectrum Number	Temperature F	Frequency Shift cm^{-1}	Frequency Shift GHZ	Refractive Index	Velocity of Sound m/sec
122	120	0.48559	14.57	1.6529	3206
123	115.2	0.48899	14.67	1.6540	3227
124	111.0	0.49258	14.78	1.6549	3249
125	105.8	0.49686	14.91	1.65615	3274
126	100.4	0.50965	15.29	1.6574	3299
127	96.2	0.50447	15.13	1.6584	3320
128	91.6	0.50733	15.22	1.6594	3337
129	87.1	0.50856	15.26	1.6605	3343
130	81.3	0.51042	15.31	1.6618	3352
131	75.2	0.51211	15.36	1.6633	3360
132	70.1	0.51333	15.40	1.6644	3366

Table A3-c. Frequency Shift and Sound Velocity (history A) at 86.0 kpsi for N1 Fluid.

Date: March 24, 1976
Separation Distance = 0.635 cm
Resulting Tg = 102.6 F

Spectrum Number	Temperature F	Frequency Shift cm^{-1}	Frequency Shift GHZ	Refractive Index	Velocity of Sound m/sec
133	129.8	0.49046	14.71	1.6626	3220
134	135.5	0.49378	14.81	1.6636	3239
135	120.5	0.49769	14.93	1.6647	3263
136	115.8	0.50141	15.04	1.6658	3285
137	110.7	0.50506	15.15	1.6670	3307
138	104.5	0.50985	15.30	1.66845	3335
139	100.5	0.51187	15.36	1.6694	3347
140	94.6	0.51368	15.41	1.67075	3356
141	88.7	0.51515	15.45	1.6721	3363
142	83.5	0.51705	15.51	1.6733	3373
143	80.0	0.51812	15.54	1.6741	3178

Table A3-d. Frequency Shift and Sound Velocity (history A) at 92.0 kpsi for N1 Fluid.

Date: March 25, 1976
Separation Distance = 0.635 cm
Resulting Tg = 113.3 F

Spectrum Number	Temperature F	Frequency Shift cm^{-1}	Frequency Shift GHZ	Refractive Index	Velocity of Sound m/sec
144	134.5	0.49858	14.96	1.6735	3252
145	130.4	0.50148	15.04	1.6744	3269
146	124.5	0.50595	15.18	1.6758	3296
147	119.1	0.51042	15.31	1.6771	3322
148	114.3	0.51411	15.42	1.6782	3344
149	109.8	0.51670	15.50	1.6792	3359
150	102.2	0.51894	15.57	1.6810	3370
151	96.2	0.52079	15.62	1.0824	3379
152	90.9	0.52249	15.67	1.6836	3387
153	82.1	0.52509	15.75	1.68565	3400

Table A3-e. Frequency Shift and Sound Velocity (history A) at 100.0 kpsi for N1 Fluid.

Date: March 26, 1976

Separation Distance = 0.635 cm

Resulting Tg = 123.2 F

Spectrum Number	Temperature F	Frequency Shift cm^{-1}	Frequency Shift GHZ	Refractive Index	Velocity of Sound m/sec
154	146.3	0.50596	15.18	1.6868	3274
155	140.5	0.50996	15.30	1.6881	3297
156	135.7	0.51368	15.41	1.6892	3319
157	131.8	0.51670	15.50	1.6901	3337
158	125.7	0.52191	15.66	1.6915	3363
159	120.7	0.52381	15.71	1.6927	3377
160	114.0	0.52568	15.77	1.69425	3386
161	107.5	0.52721	15.82	1.6958	3393
162	100.8	0.52859	15.86	1.6973	3399
163	93.2	0.53124	15.94	1.6991	3412

Table A4-a. Frequency Shift and Sound Velocity as a Function of Pressure at 76 F (history B) for N2 Fluid.

Date: April 30, 1976
Separation Distance = 0.415 cm
Resulting Pg = 63.5 kpsi

Spectrum Number	Pressure kpsi	Frequency Shift cm^{-1}	Frequency Shift GHZ	Refractive Index	Velocity of Sound m/sec
300	17.2	0.32553	9.77	1.5346	2315
301	20.2	0.33781	10.13	1.5407	2395
302	23.7	0.35125	10.54	1.5476	2477
303	27.1	0.36447	10.93	1.5544	2559
304	30.7	0.37699	11.31	1.5619	2635
305	35.0	0.39214	11.76	1.5702	2726
306	39.8	0.40724	12.22	1.5798	2814
307	43.3	0.41663	12.50	1.5868	2866
308	47.0	0.42679	12.80	1.5942	2922
309	50.9	0.43727	13.12	1.6020	2979
310	53.9	0.44637	13.39	1.6080	3030
311	57.2	0.45512	13.65	1.6146	3077
312	60.8	0.46440	13.93	1.6218	3126
313	64.0	0.47211	14.16	1.6283	3165
314	67.1	0.47889	14.37	1.6344	3198
315	69.9	0.48419	14.53	1.6400	3222
316	71.9	0.48758	14.63	1.6439	3237
317	74.8	0.49289	14.79	1.6498	3261
318	77.1	0.49709	14.91	1.6545	3279

Table A4-b. Frequency Shift and Sound Velocity (history A) at 76.0 kpsi for M2 Fluid.

Date: May 4, 1976
Separation Distance = 0.625 cm
Resulting Tg = 100.5 F

Spectrum Number	Temperature F	Frequency Shift cm^{-1}	Frequency Shift GHZ	Refractive Index	Velocity of Sound m/sec
320	122.3	0.47927	14.38	1.6421	3186
321	118.0	0.48150	14.45	1.6430	3199
322	114	0.48347	14.50	1.6439	3210
323	109.6	0.48664	14.60	1.6448	3229
324	105.1	0.48896	14.67	1.6457	3243
325	100.2	0.49174	14.75	1.6468	3259
326	95.2	0.49298	14.79	1.6479	3265
327	90.0	0.49430	14.83	1.6490	3272
328	85.5	0.49583	14.87	1.6500	3280
329	80.0	0.49707	14.91	1.6511	3286
330	73.5	0.49861	14.96	1.6520	3294

Table A4-c. Frequency Shift and Sound (history A) at 80.0 kpsi for N2 Fluid.

Date: May 3, 1976
Separation Distance = 0.625 cm
Resulting Tg = 105.0 F

Spectrum Number	Temperature F	Frequency Shift cm^{-1}	Frequency Shift GHZ	Refractive Index	Velocity of Sound m/sec
331	126.1	0.48356	14.51	1.6493	3200
332	121.8	0.48551	14.57	1.6502	3211
333	117.2	0.48883	14.66	1.6512	3231
334	112.0	0.49138	14.74	1.6523	3246
335	107.0	0.49437	14.83	1.6534	3263
336	102.1	0.49647	14.89	1.6544	3275
337	97.1	0.49802	14.94	1.6555	3283
338	91.9	0.49955	14.99	1.6566	3291
339	87.5	0.50106	15.03	1.6575	3299
340	82.8	0.50201	15.06	1.6585	3303
341	76.5	0.50438	15.13	1.660	3316

Table A4-d. Frequency Shift and Sound Velocity (history A) at 86.0 kpsi for N2 Fluid.

Date: May 3, 1976
Separation Distance = 0.625 cm
Resulting Tg = 116.2 F

Spectrum Number	Temperature F	Frequency Shift cm^{-1}	Frequency Shift GHZ	Refractive Index	Velocity of Sound m/sec
342	143.6	0.48638	14.59	1.6586	3201
343	138.2	0.48937	14.68	1.6597	3218
344	133.3	0.49127	14.74	1.6608	3228
345	128.5	0.49437	14.83	1.6618	3247
346	124.0	0.49617	14.89	1.6628	3257
347	119.3	0.49923	14.98	1.6638	3275
348	114.5	0.50078	15.02	1.6648	3283
349	109.0	0.50261	15.08	1.6660	3293
350	103.7	0.50416	15.12	1.6671	3301
351	98.6	0.50481	15.14	1.6682	3303
352	93.5	0.50630	15.19	1.6693	3310
353	88.4	0.50744	15.22	1.6703	3316

Table A4-e. Frequency Shift and Sound Velocity (history A) at 91.0 kpsi for N2 Fluid.

Date: May 4, 1976
Separation Distance = 0.625 cm
Resulting Tg = 124.0 F

Spectrum Number	Temperature F	Frequency Shift cm^{-1}	Frequency Shift GHZ	Refractive Index	Velocity of Sound m/sec
354	152.9	0.48855	14.66	1.6659	3201
355	146.8	0.49127	14.74	1.6670	3217
356	141.0	0.49495	14.85	1.6682	3238
357	135.8	0.49707	14.91	1.6693	3250
358	130.4	0.49954	14.99	1.6705	3264
359	125.3	0.50329	15.10	1.6715	3286
360	120.1	0.50454	15.14	1.6726	3292
361	115.0	0.50514	15.15	1.6737	3294
362	110.0	0.50696	15.21	1.6747	3304
363	102.5	0.50876	15.26	1.6763	3312
364	95	0.51046	15.31	1.6779	3321

Table A4-f. Frequency Shift and Sound Velocity (history A) at 100.0 kpsi for N2 Fluid.

Date: May 13, 1976
Separation Distance = 0.625 cm
Resulting Tg = 139.7 F

Spectrum Number	Temperature F	Frequency Shift cm^{-1}	Frequency Shift GHZ	Refractive Index	Velocity of Sound m/sec
365	165.5	0.49737	14.92	1.6809	3230
366	160.1	0.49977	14.99	1.6820	3243
367	155.8	0.50162	15.05	1.6831	3253
368	151.0	0.50490	15.15	1.6840	3272
369	146.5	0.50750	15.23	1.6850	3287
370	141.5	0.50957	15.29	1.6860	3299
371	136.5	0.51151	15.35	1.6871	3309
372	131.9	0.51236	15.37	1.6881	3313
373	127.2	0.51405	15.42	1.6891	3321
374	122.0	0.51526	15.46	1.6902	3327
375	117.0	0.51609	15.48	1.6913	3331
376	111.9	0.51730	15.52	1.6923	3337
377	107.0	0.51851	15.56	1.6934	3342
378	100.2	0.52010	15.60	1.6943	3349
379	91.2	0.52254	15.68	1.6968	3361

APPENDIX B

DESCRIPTION OF EXPERIMENTAL FLUIDS AND REFRACTIVE INDEX DETERMINATION

Description of Experimental Fluids

The following table summarizes the oils investigated in this research and gives characteristic data for each oil.

Experimental Fluids

Symbol	Description
5P4E	Polyphenyl Ether
MCS-1218	Cycloaliphatic Hydrocarbon
N1	Naphthenic Base Oil R-620-15
N2	N1 + 2.2 percent Polybutane LF-5346

Fluid Characterization

Symbol: 5P4E

Type: Five-ring Polyphenyl Ether

Source: Monsanto Company

Properties:		
	Viscosity at 100F, cs	363
	Viscosity at 210F, cs	13.1
	Density at 72F, g/cc	1.205
	Density at 100F, g/cc	1.19
	Flash Point, F	550
	Pour Point, F	40

Symbol:	MCS-1218	
Source:	Monsanto Company	
Type:	Cycloaliphatic Hydrocarbon	
Properties:	It is a combination of two components each have a molecular weight less than 1000.	
	Viscosity at 100F, cs	1418
	Viscosity at 210F, cs	18.37
	Density at 75F, gm/cc	0.94

Symbol:	N1	
Source:	Sun Oil Company	
Type:	Naphthenic Base Oil R-620-15	
Properties:	Viscosity at 100F, cs	24
	Viscosity at 210F, cs	3.728
	Viscosity Index (ASTM D-2270)	-13
	Flash Point, F	315
	Pour Point, F	-45
	Density at 68F, gm/cc	0.9157
	Molecular Weigh	305

Symbol:	LF 5346, used as additive in lubricant N1	
Type:	Polybutane in oil solution	
Source:	American Oil Company	
Properties:	Density at 25C, gm/cc	0.8656
	Viscosity at 100F, cs	8041
	Viscosity at 210F, cs	637

Viscosity Index	123.5
Flash Point, F	400
Dilute Oil Content, percent	80
Dilute Oil Viscosity at 100F, cs	18
Weight Average Molecular Weight	50,000

The percent additive reported above (2.2 percent by volume) is the percent polymer in the final solution.

Refractive Index Determination

Temperature and pressure variations of the refractive index, n_i, are required to calculate the sound velocity from the measured frequency shift as indicated by equation (11). The measurements of the refractive index as a function of temperature (25 to 85C) were made by using a precision Abbe "60" Refractometer using Sodium D_1 line ($\lambda = 5896\text{Å}$). Heating the sample in the refractometer was accomplished by circulating heated oil through the prism. A coper-constantan thermocoulpe was embedded in the oil sample and the temperature was measured with an Omega digital thermometer. The results of these measurements are shown in Table B1. Table B2 gives the value of $\frac{dn_i}{dT}$ and the least square expressions obtained.

Since it was not possible to measure the variation of the refractive index with pressure, it was assumed that $\frac{dn_i}{dP}$ for all experimental oils investigated has a constant value of 2×10^{-3} per thousand psi. This value was estimated from information available in the literature. Dill[26] et al. utilized density data taken from literature in conjunction with the values of n_i measured at atmospheric pressure to calculate the

pressure dependence of the index by applying the Lorentz-Lorenz relation

$$n_i(P) = \frac{(1 + 2A)^{\frac{1}{2}}}{1 - A} \qquad \text{(B-1)}$$

where

$$A = \frac{\rho(P)}{\rho} \frac{n_\alpha^2 - 1}{n_\alpha^2 + 2} \qquad \text{(B-2)}$$

ρ and ρ_α are the densities at pressure P and atmospheric pressure respectively and n_α is the refractive index at atmospheric pressure. The results of the above procedure applied to their fluid (5P4E) show that $\frac{dn_i}{dP}$ has a constant value of about 2.2×10^{-3} per thousand psi for pressures up to 50,000 psi.

The deviation of the assumed value of $\frac{dn_i}{dp}$ from the actual value does not affect the glass transition as measured from the velocity of sound because the glass transition is related to the change in slope of the data not the absolute value. Any other estimate for $\frac{dn_i}{dp}$ will only shift the velocity of sound up or down without changing the location of the glass transition.

Figures B1-a through B1-d show the refraction index as a function of temperature for 5P4E, MCS-1218, N1, and N2 respectively.

Table B1. Variation of the Refractive Index with Temperature for all Experimental Fluids.

5P4E		MCS-1218		N1		N2	
Temperature F	n_i	Temperature F	n_i	Temperature F	n_i	Temperature F	n_i
75.0	1.6309	75	1.51140	75.0	1.5033	75.0	1.5002
84.6	1.6287	85.6	1.5092	86.2	1.5007	84.5	1.4982
96.1	1.6257	94.3	1.5071	99.3	1.4976	93.8	1.4962
108.0	1.6226	105.8	1.5046	114.4	1.4942	102.2	1.4944
120.0	1.6195	117.1	1.5024	124.3	1.4919	111.3	1.4924
131.6	1.6169	129.3	1.4995	132.6	1.4901	121.6	1.4904
142.6	1.6140	139.8	1.4972	144.2	1.4872	130.2	1.4885
153.2	1.6113	152.3	1.4945	154.2	1.4850	139.6	1.4864
162.0	1.6090	163.5	1.4921	164.5	1.4828	152.8	1.4834
		177.0	1.4893			164.0	1.4812

Table B2. Least Square Expression for the Refractive Index of the Experimental Fluids as a Function of Temperature.

Experimental Fluid	Least Square Expression for n_i, T in F
5P4E	$n_i = 1.6499 - 2.52 \times 10^{-4} T$
MCS-1218	$n_i = 1.5277 - 2.2 \times 10^{-4} T$
N1	$n_i = 1.5205 - 2.3 \times 10^{-4} T$
N2	$n_i = 1.5163 - 2.1 \times 10^{-4} T$

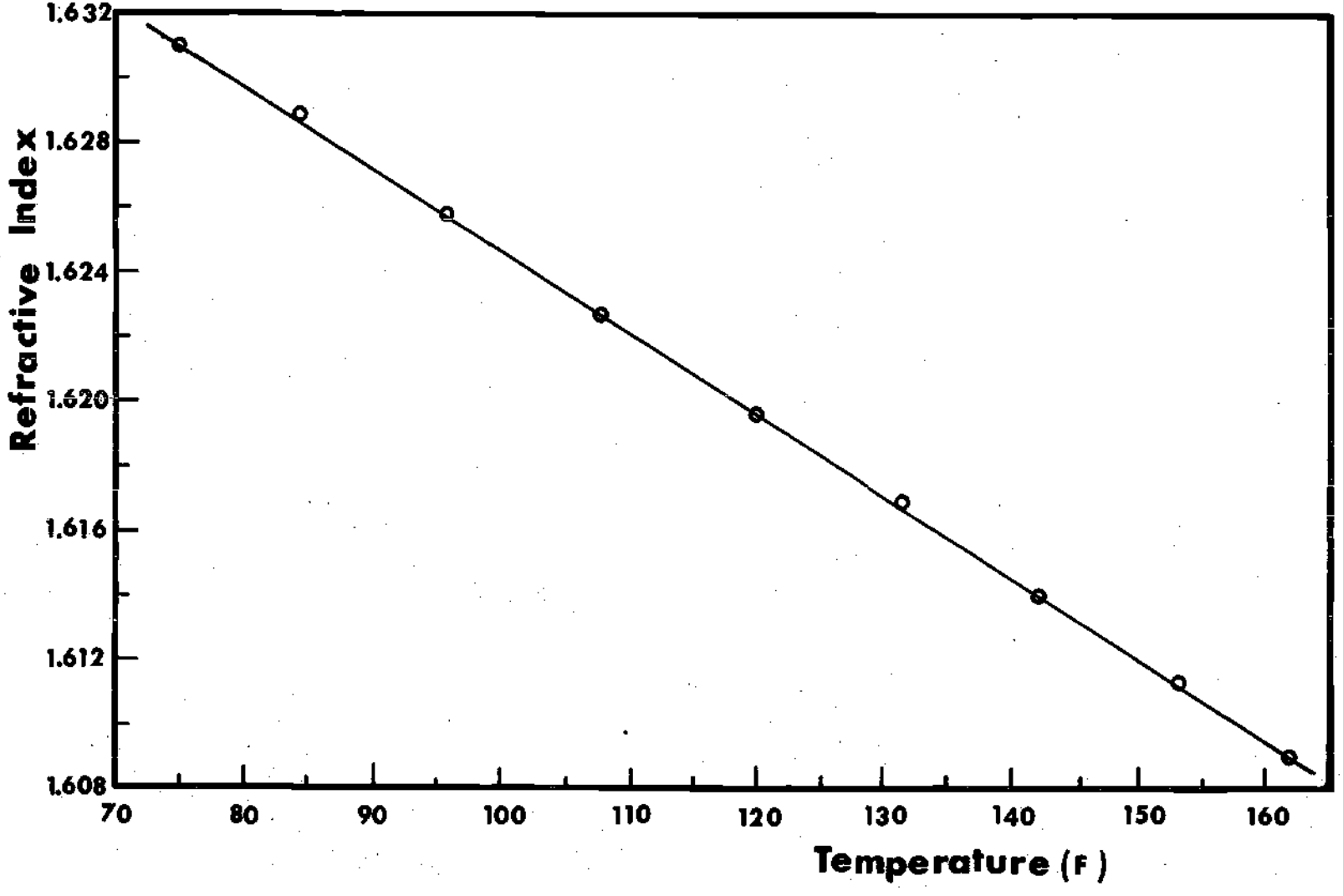

Figure B1-a. Variation of the Refractive Index of 5P4E Fluid with Temperature (λ = 5896 Å).

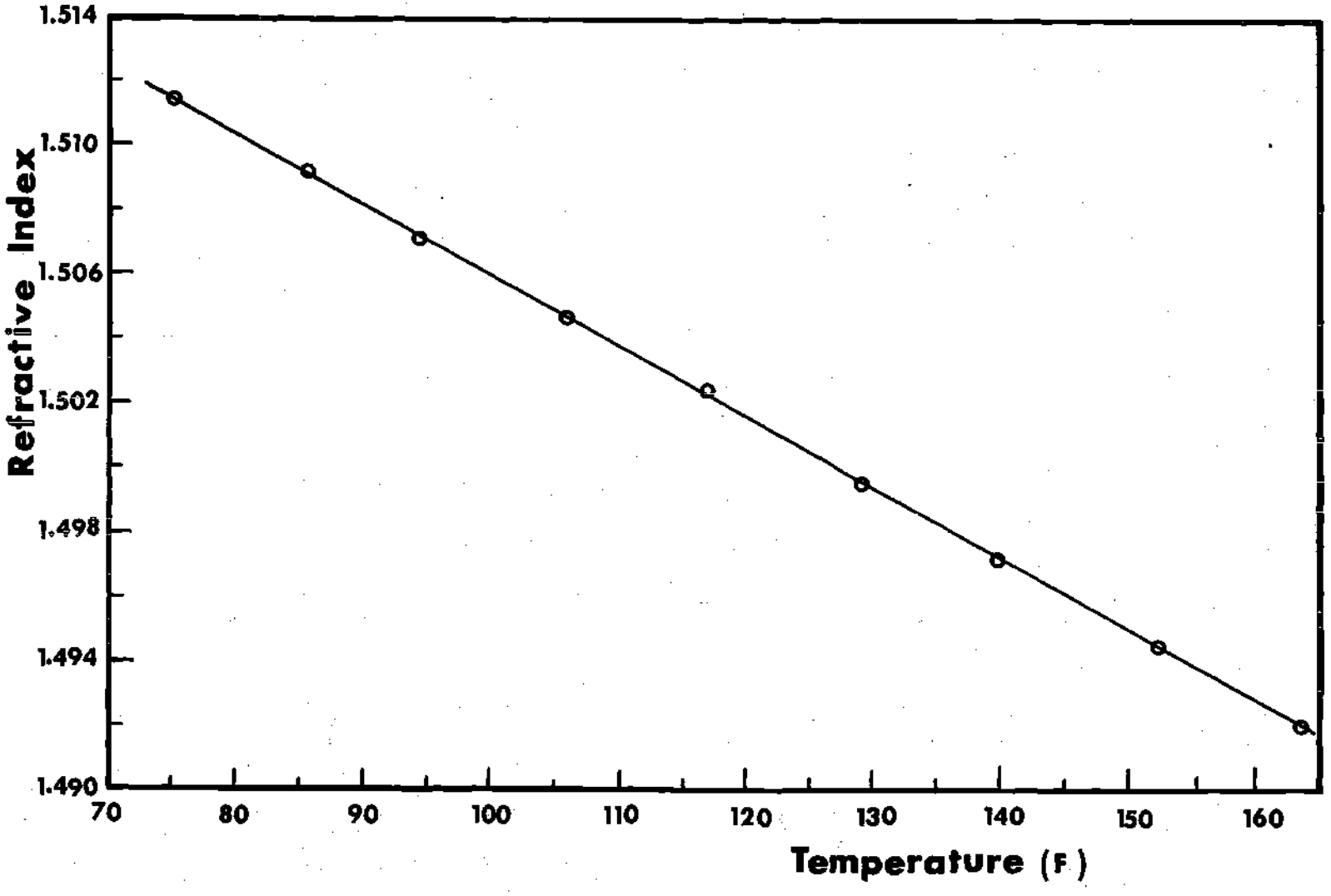

Figure B1-b. Variation of the Refractive Index of MCS-1218 Fluid with Temperature (λ = 5896 Å).

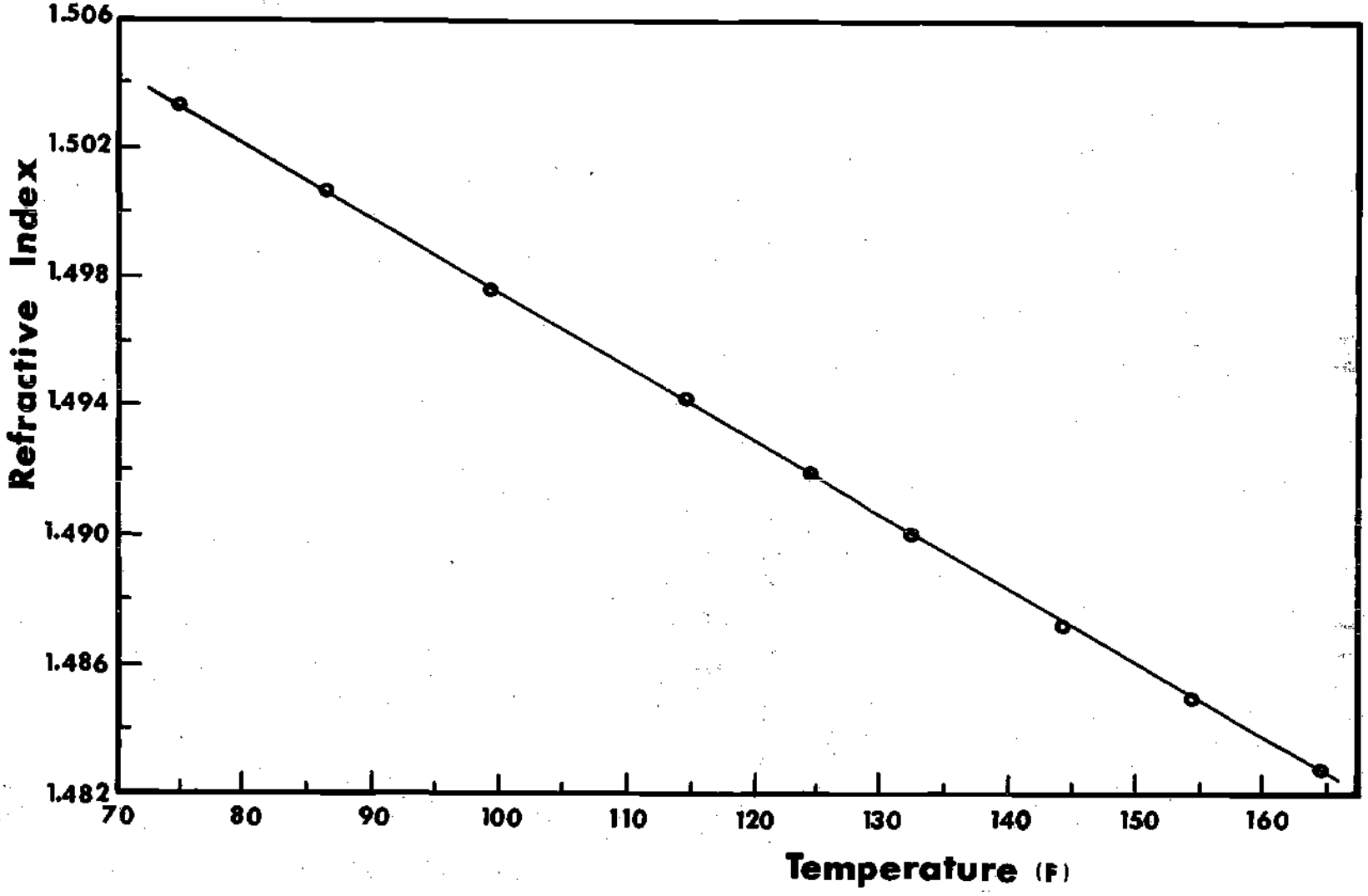

Figure B1-c. Variation of the Refractive Index of N1 Fluid with Temperature (λ = 5896 Å).

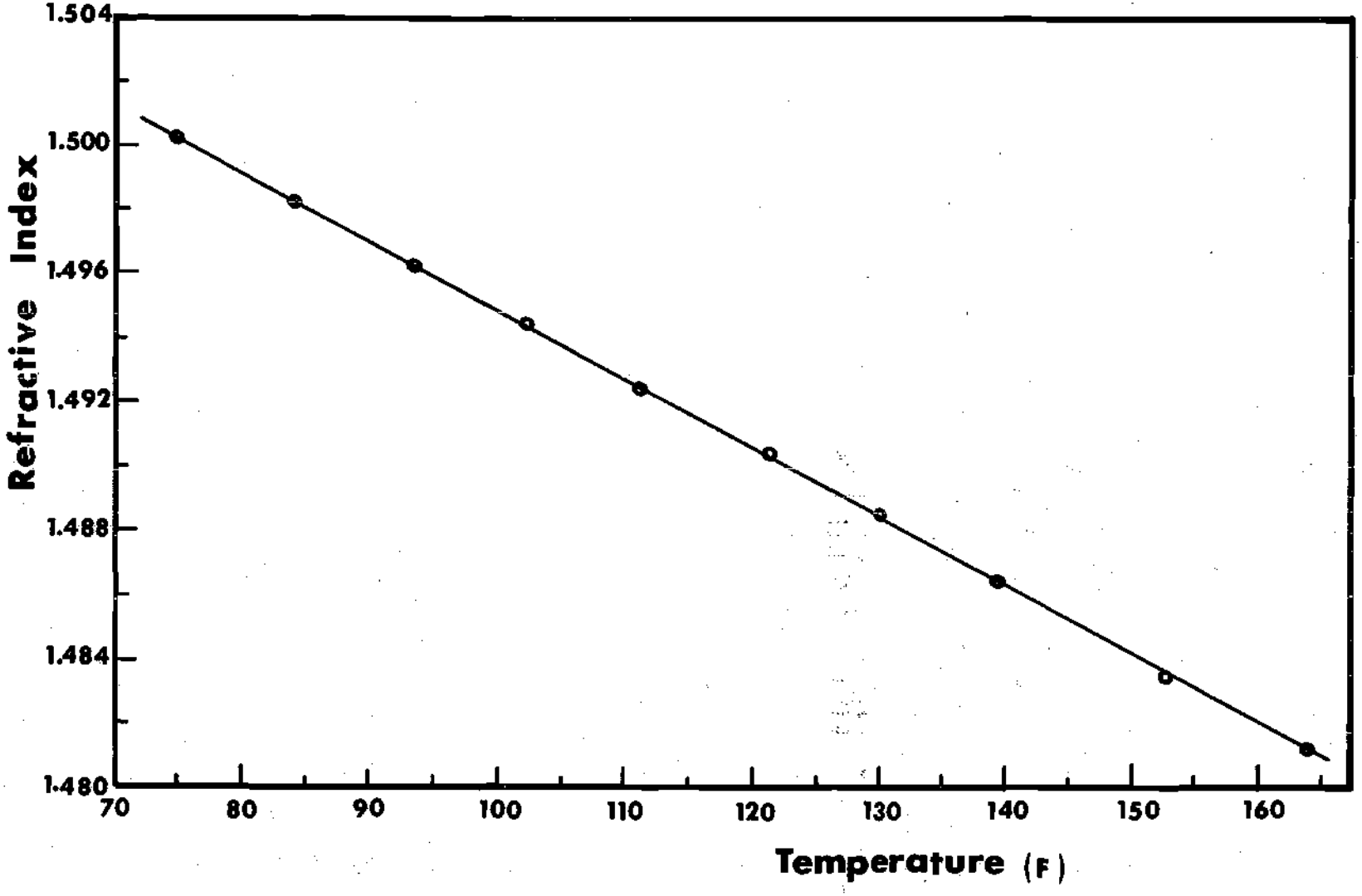

Figure B1-d. Variation of the Refractive Index of N2 Fluid with Temperature ($\lambda = 5896\text{Å}$).

APPENDIX C

PRESSURE AND TEMPERATURE SENSING EQUIPMENT

Pressure Transducer Specifications and Calibration Data

(i) Pressure Transducer Specifications

The strain gauge pressure transducer was Norwood Pressure Transducer, Model 114 manufactured by the advanced Technology Division of American-Standard. The general performance specifications are given below:

Bridge	Four active arms
Non-linearity	Less than 1.0 percent of full scale
Hysteresis	Less than 0.5 percent of full scale
Repeatability	Better than 0.1 percent of full scale
Resolution	Infinite
Temperature Range	-65 to 250F uncooled, 2000F cooled Mounting thread temperature 250F maximum
Thermal Zero Shift (0 to 200F)	Less than 0.02 percent F. S. per F change
Thermal Sensitivity Shift (0 to 200F)	Less than 0.02 percent F. S. per F change
Pressure Range	100,000 psig
Pressure Limit	150 percent F. S. for static pressures. Full scale for dynamic pressures.
Burst Pressure	Above 200 percent F. S.
Recommended Excitation	10 volts DC or AC, 17 volts maximum

Cooling Air	2 cfm at 15 to 20 psig clean, dry air
Negative Pressure	Usable to full vacuum
Material	347 stainless steel diaphragm and 17-4PH stainless steel body
Mounting Torque	42 ft.lbs. maximum

The transducer pin identification is shown in Figure C1.

(ii) Pressure Transducer Calibration

The schematic arrangements used during the calibration procedure are shown in Figure C2. The pressure transducer was calibrated by reading the transducer output in millivolt and reading the corresponding pressure from a 100,000 psi Heise Bourdon Pressure gage. Intervals of 5000 psi each were used. A six volt battery was used to excite the transducer. The excitation voltage was measured during the calibration procedure and was constant to within 0.4 percent. The transducer output was measured with a Leeds and Northrup Type K-4 Potentiometer and an electronic null defector (Leeds and Northrup Model 9834). The following accessory equipment were necessary to detect the transducer output: Constant Power Supply (Leeds and Northrup Model 9879), standard cell with 1.01942 volt and internal resistance less than 500 ohms, and electronic null detector (Leeds and Northrup Model 9874). Specifications for the potentiometer, the constant power supply, and the null detector are given in Section 2.

Figure C3 shows the external connections of the potentiometer to the accessory components described above. A detector reverse key gives a means of checking any thermal emfs in the external detector

circuit. This check is performed after each measurement by adjusting for a null zero with and without the detector reverse key. The average of both readings was taken to represent the transducer output.

The transducer calibration data is given in Table C1 and shown in Figure C4. The relation between the pressure gage reading and the transducer output is linear above 10,000 psi. The slope was calculated using linear least square fit of the form

$$Y = A + B\,P$$

to the transducer calibration data where; Y is the transducer output in millivolt, P is the corresponding pressure in KPsi. The least square expression obtained is

$$Y = -2.106 + 0.6379P$$

The above equation was used in pressure range of 10 to 100 kpsi. Below 10 kpsi, the following equation was obtained and used

$$Y = -2.09 + 0.6344\,P$$

Table C1. Calibration Data of the Pressure Transducer.

Gage Pressure kpsi	Transducer Output Without Revised Key mv	Transducer Output With Revised Key mv	Average Transducer Output, mv	Excitation Voltage Volts
atm.	-2.075	-2.085	-2.08	6.65
5.00	1.080	1.070	1.075	6.65
9.80	4.12	4.115	4.12	6.65
17.55	9.04	9.045	9.04	6.66
20.25	10.79	10.77	10.78	6.66
25.35	14.05	14.04	14.045	6.66
30.35	17.25	17.245	17.25	6.66
35.30	20.435	20.415	20.42	6.66
40.75	23.95	23.94	23.945	6.66
45.30	26.83	26.83	26.83	6.67
50.25	29.95	29.94	29.945	6.67
53.40	32.00	31.98	31.99	6.67
55.85	33.43	33.41	33.42	6.67
57.20	34.40	34.38	34.39	6.68
60.15	36.175	36.165	36.17	6.68
63.30	38.30	38.29	38.295	6.68
64.25	38.81	38.79	38.80	6.68

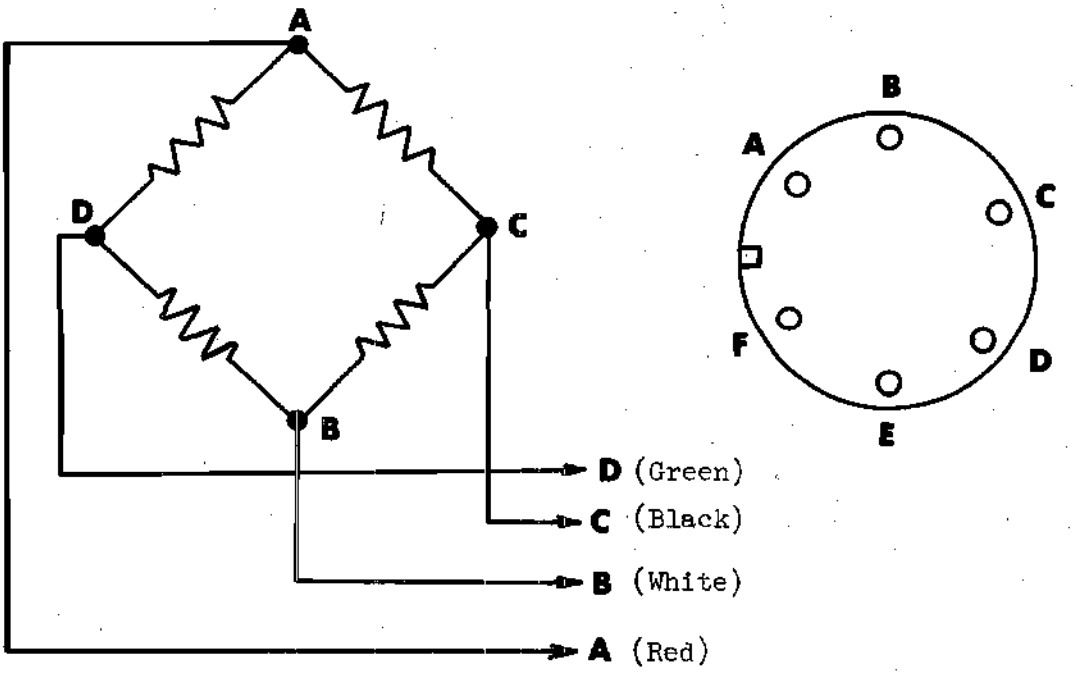

Figure C1. Pressure Transducer Pin Identification.

A(red) = Signal (+)
B(white) = Signal (-)
C(Black) = Excitation (-)
D(Green) = Excitation (+)
E = External Shunt
F = External Shunt

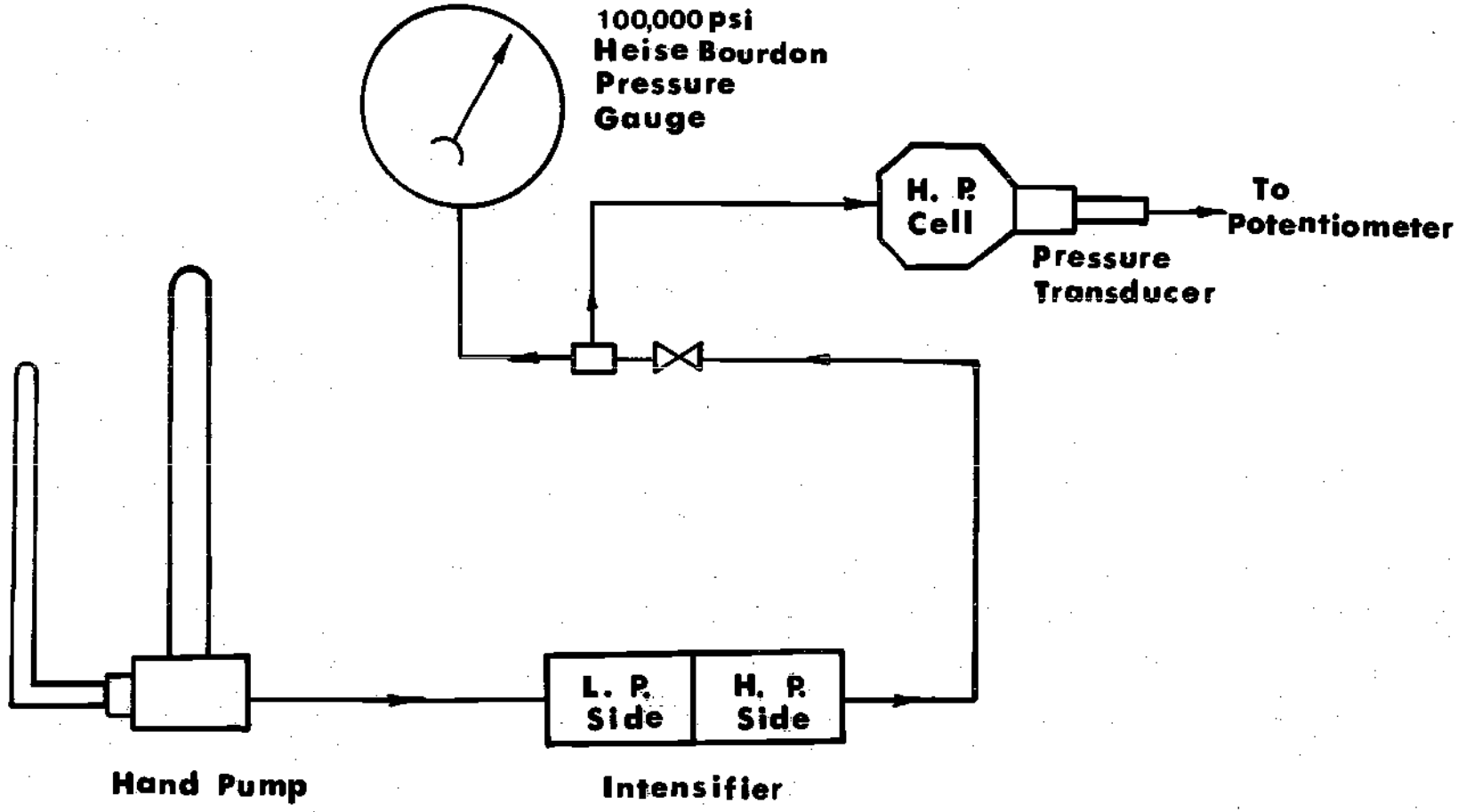

Figure C2. Schematic Arrangement for the Pressure Transducer Calibration.

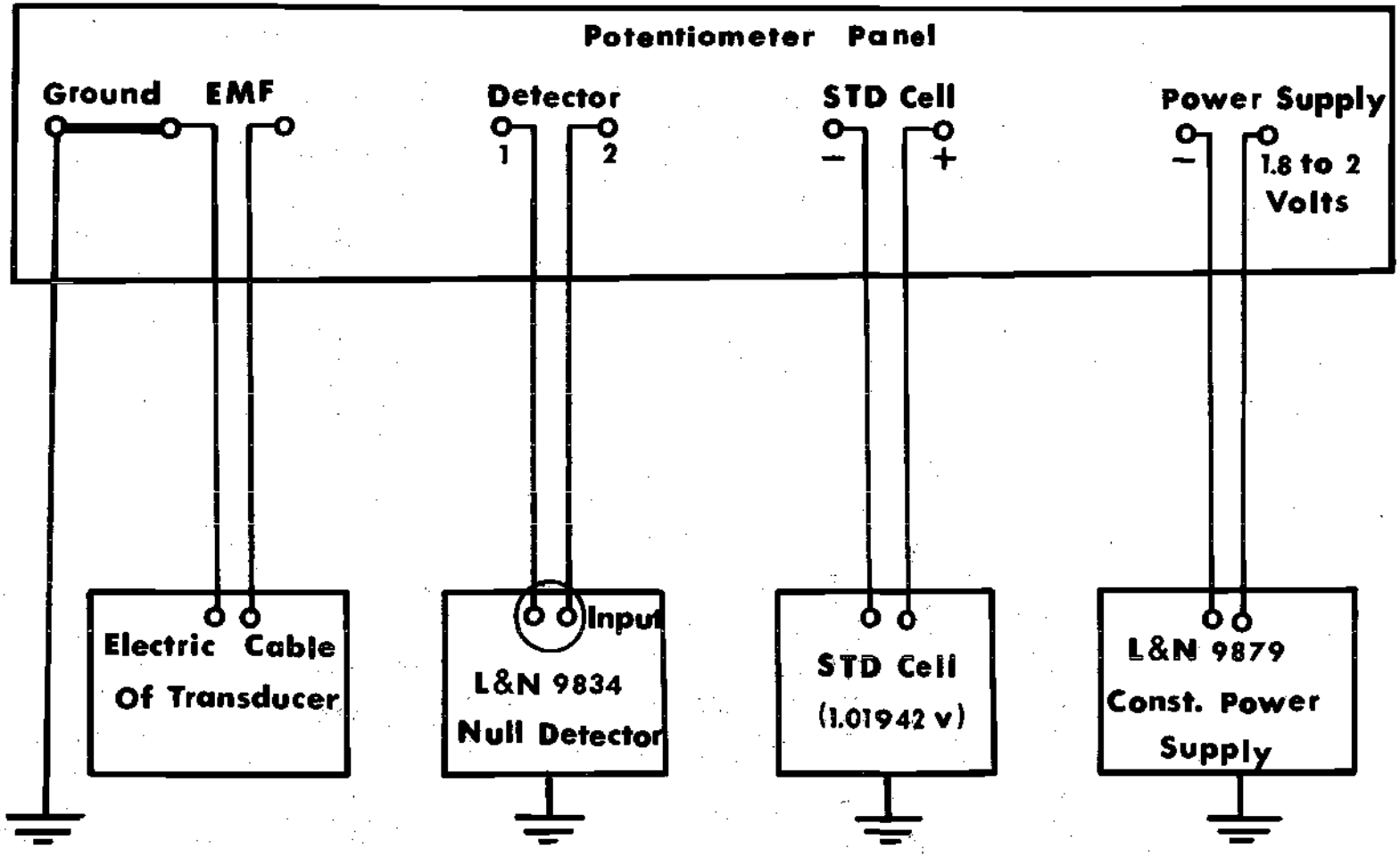

Figure C3. External Connections of the Potentiometer to the Accessory Components.

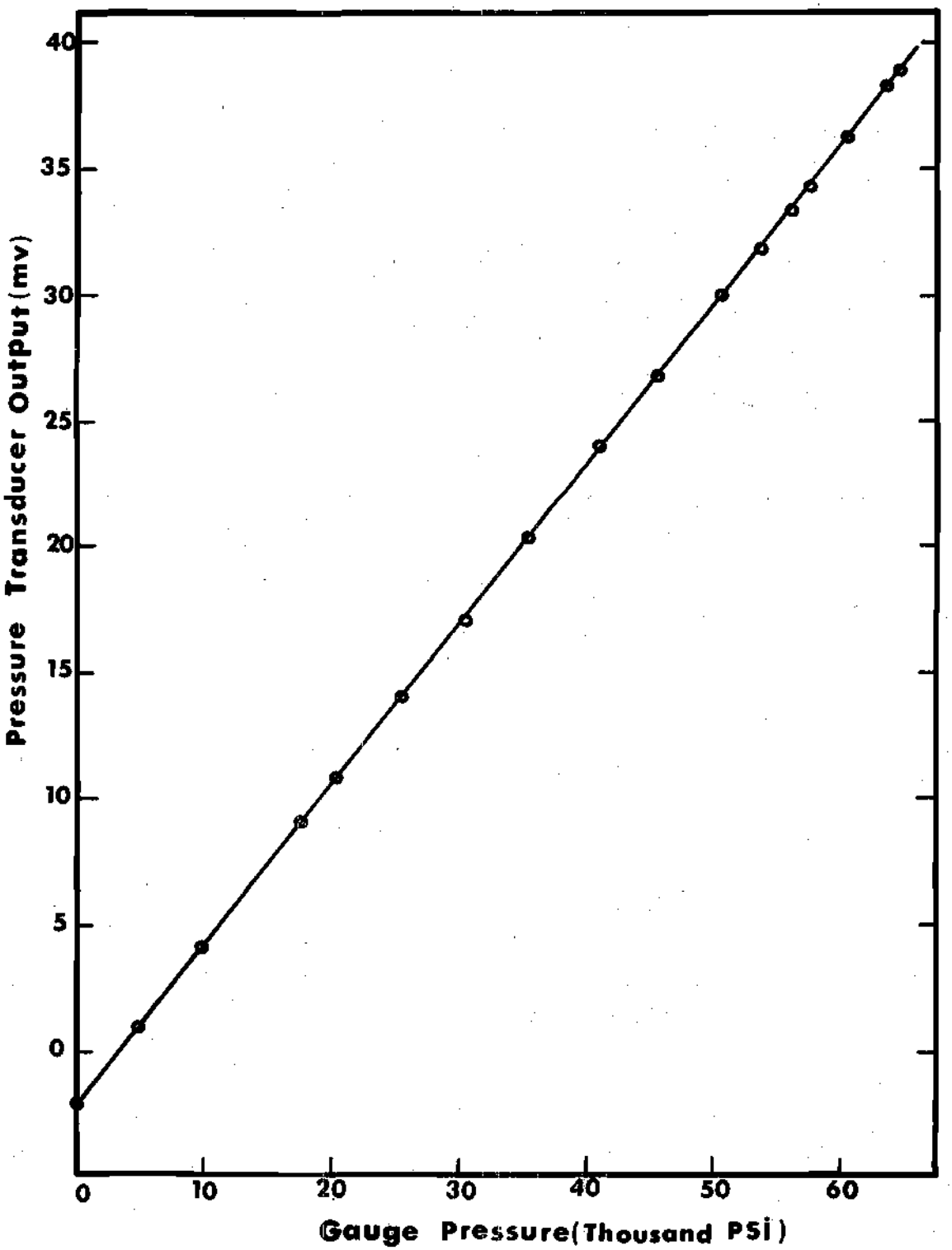

Figure C4. Calibration Curve for the Pressure Transducer.

Accessory Equipment for Transducer Calibration

(i) Type K-4 Potentiometer (Model 7554)

SPECIFICATIONS

RANGES

1.6 (high):	-0.0005 to + 1.6105 volts
0.16 (medium):	-0.00005 to + 0.16105 volt
0.016 (low):	-0.000005 to + 0.016105 volt.

LIMIT OF ERROR

1.6 Range:	± (0.005 percent of reading + 20 microvolts)
0.16 Range:	± (0.007 percent of reading + 2 microvolts)
0.016 Range:	± (0.007 percent of reading + 0.5 microvolt).

TRANSIENT THERMAL EMFS

Less than 0.1 microvolt of very short duration during normal operation of switch A or B, and less than 0.1 microvolt within 1 second after normal operation of slidewire C.

DETECTOR KEYS

Two tap keys permit selection of either full sensitivity of detector or 1/400 of full sensitivity. A normal-reverse key permits the effect of any thermal emfs in the detector circuit to be eliminated from the measurement.

INTERNAL RESISTANCE

Resistance across emf input therminals depends on dial settings; varies between 10 and 280 ohms, approximately.

POWER SUPPLY REQUIREMENTS

12.1 milliamperes, 1.8 to 2.3 volts d-c.

STANDARD CELL ADJUSTMENT

Adjusts reference emf to be equal to standard cell emf. Resolution is better than 0.8 ppm for standard cell emfs between 1.0175 and 1.0205 volts.

CURRENT STANDARDIZATION

Provided by one COARSE rheostat and one ten-turn FINE rheostat. Resolution is better than 0.5 ppm.

GUARDED CIRCUITS

Power supply, standard cell, and detector circuits are guarded to intercept leakage currents, thus assuring accurate measurements even under humid conditions.

(ii) Electronic Null Detector (Model 9834)

SPECIFICATIONS

SENSITIVITY
Sensitivity decreases as source resistance increases.
Minimum sensitivity (position 0) is approximately 30 μv/mm or 45 μv/scale division with source resistance up to 2000 ohms.

LINEARITY
2 percent of full scale for 80 percent deflection either side of scale zero.

ZERO DRIFT
Conditions: Temperature of 68 ± 10F and 30 minute warm-up before operation.
Maximum drift during first hour of operation: 1 μv or 10 divisions at maximum sensitivity.
Maximum rate of drift after 5 hours operation: 0.1 μv/hour or one division/hour at maximum sensitivity.

NOISE LEVEL
Less than 0.1 microvolt, peak to peak.

SPEED OF RESPONSE
Less than 2 seconds for source resistances up to 1000 ohms, increasing to 4 seconds at 100,000 ohms.

INPUT RESISTANCE
25,000 ohms.

OUTPUT RESISTANCE
1,000 ohms.

INSULATION RESISTANCE
Guard to chassis or case -- over 10,000 megohms.
Chassis to line circuit or case -- over 300 megohms.

OUTPUT
-0.5 to 0 to +0.5 volt.

LINE VOLTAGE REQUIRED
120 volts, 50/60 cycles.

POWER CONSUMPTION
18 watts.

(iii) Constant Voltage Supply (Model 9879)

SPECIFICATIONS

INPUT
117 volts, ± 10 percent, 50/60 Hz, 3 volt-amperes.

OUTPUT
2.0 volts dc ± 2 percent at 12.10 milliamperes.

LINE REGULATION
0.0005 percent (maximum) immediate change of output per 10-volt line change (20-30 C).
0.001 percent (maximum) final change of output per 10-volt line change (20-30 C).

TEMPERATURE COEFFICIENT
Less than 0.0005 percent per degree C (20-30 C).

DRIFT (STABILITY) AT CONSTANT TEMPERATURE AND INPUT VOLTAGE
0.01 percent per year.
0.001 percent per 24 hours.
0.0005 percent per hour (after one hour warmup).
0.0002 percent per minute (after one hour warmup).

CONNECTIONS
6-foot shielded line cord with 3-prong plug and a 2-prong adapter with grounding lead. Two binding posts for connections to potentiometer. Negative output binding post connected to guard internally.

Omega Digital Thermometer (Model 2809)

SPECIFICATIONS

Temperature Measuring Range Selector	5 Calibrations; T, J, E, K, and R
Input Terminal	Thermocouple is connected between -ve (red) and +ve (black).
Digital Display	Output is displayed in four digits plus a decimal point.
Power Connector	3-Pin Power Connector with Center Pin grounded to case.
Power Supply	115 Volts AC, 50/60 HZ.
Response Time	Approximately 1.5 sec.
Display Temperature	In degrees F.

Measuring Range used and Resolution are as follows:

Thermocouple	+ve Terminal (Black)	-ve Terminal (Red)	Measuring Range F	Resolution F
T	Copper	Constantan	-60 to 400	0.1

APPENDIX D

DSC MEASUREMENTS ON N1 AND 5P4E

The DSC technique was employed in the early stages of this research to measure the glass transition temperature at atmospheric pressure which, together with the estimated range of $\frac{dTg}{dP}$ from Reference [8], permitted the prediction of the glass transition temperature at elevated pressures.

Thermograms for N1 and 5P4E were obtained using a Perkin-Elmer instrument (DSC-2) and are shown in Figures D1 and D2. These thermograms were obtained by controlled heating from the glassy state to the liquid state. The glass transition temperatures determined by this technique are shown in Table D1. For both oils examined, the sample size was about 10 mg and the scan rate was 20K/min.

Figure D2 shows evidence of an endothermic peak in the transition region. The observed endothermic effect may be explained as due to bulk stress relaxation in the sample. However, the presence of this peak offers no difficulty in the measurement of Tg. In this case the post-transition baseline is extrapolated through the peak and Tg is measured in the conventional manner.

Table D1. DSC Values of Glass Transition Temperatures for N1 and 5P4E.

Sample	Onset Transition Temperature, K	Extrapolated Transition Temperature, K
N1	209 (-83F)	214 (-74F)
5P4E	248 (-13F)	252 (- 6F)

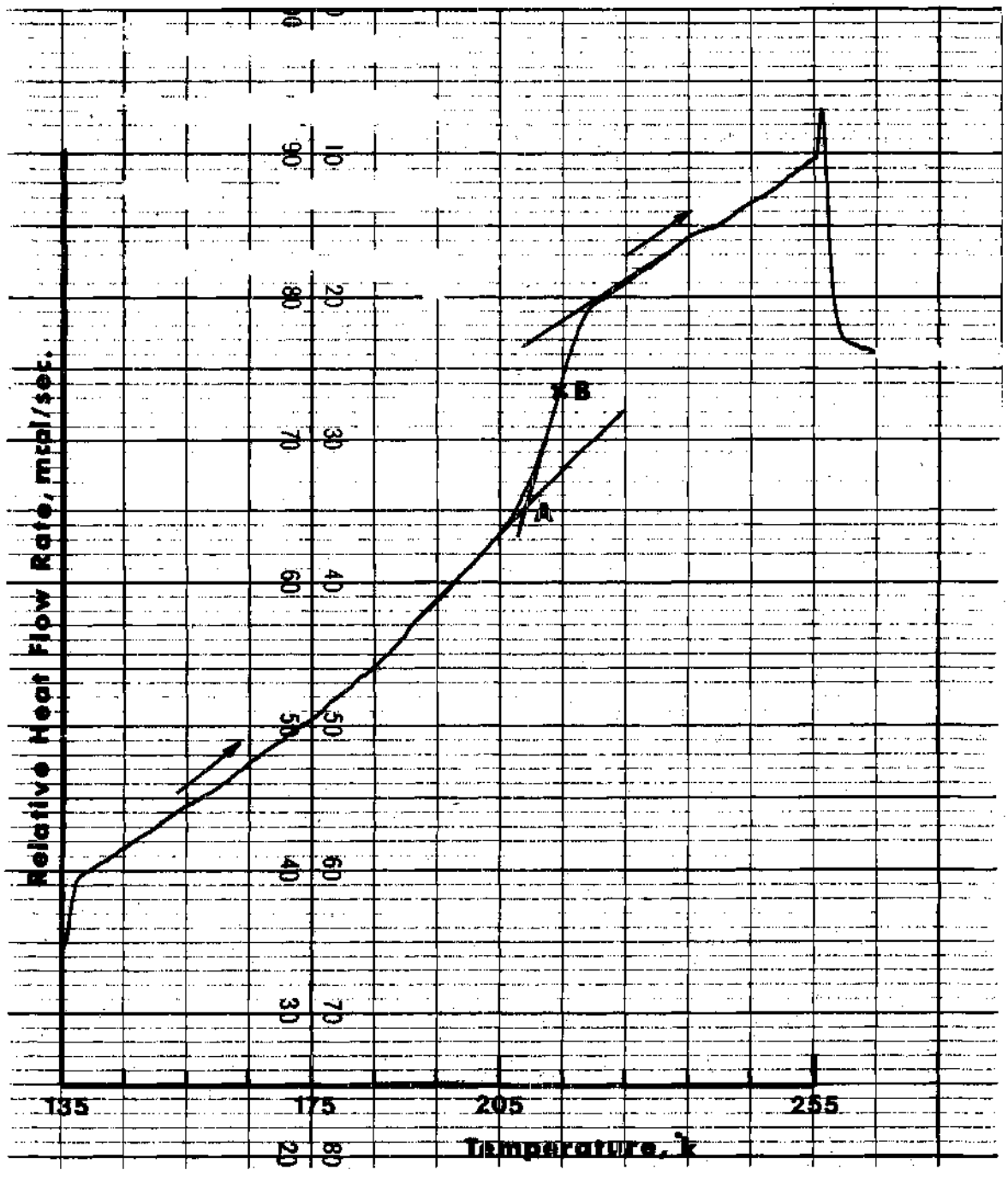

Figure D1. Thermogram Run for N1 Fluid, Scan Rate = 20K/min, Range = 2.5 mcal/sec., Sample Weight = 9.36 mg, A and B Represent Onset and Extrapolated Glass Transition Temperatures Repsectively.

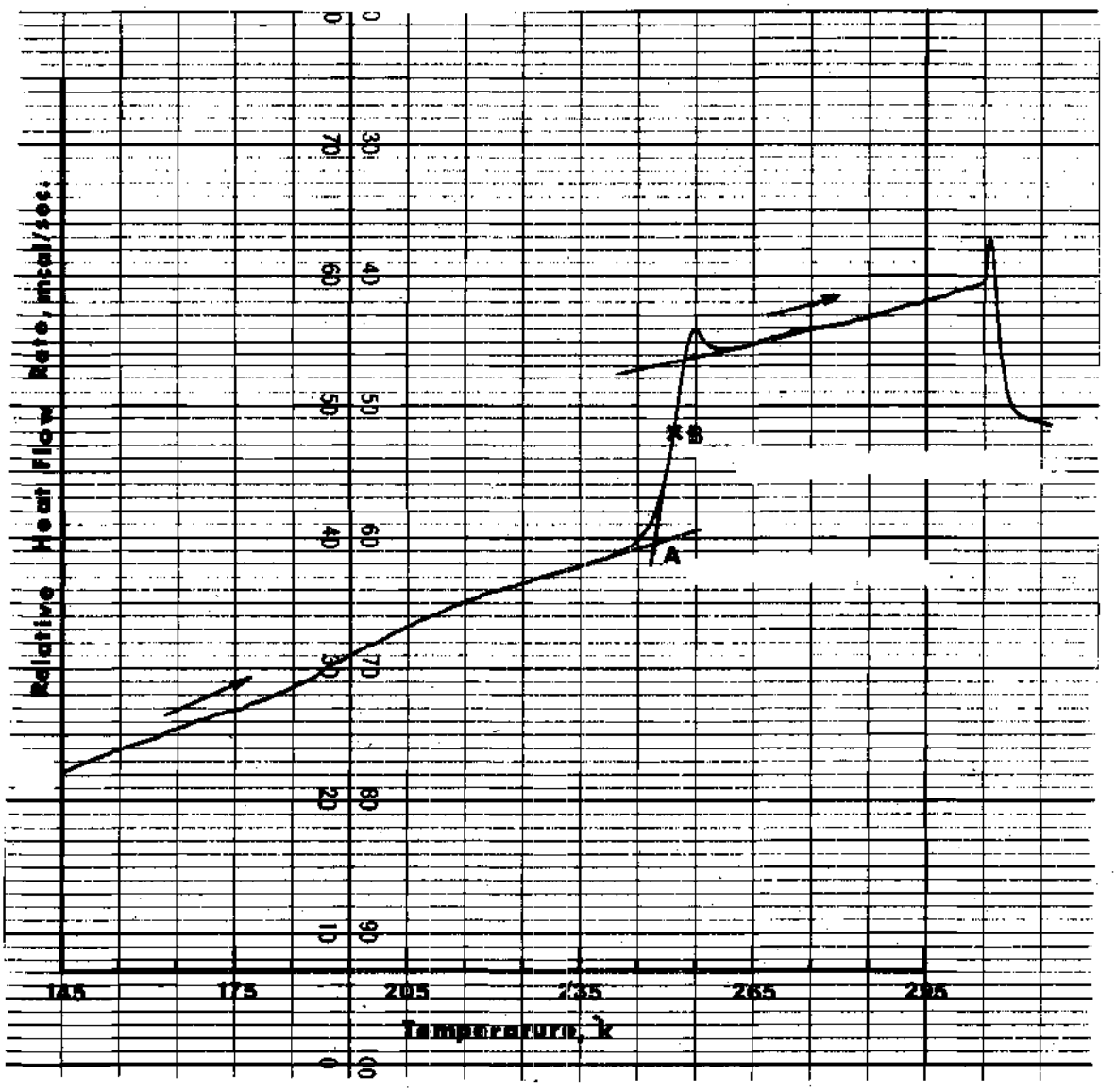

Figure D2. Thermogram Run for 5P4E Fluid; Scan Rate = 20K/min., Range = 2.5 mcal/sec., Sample Weight = 10.58 mg, A and B Represent Onset and Extrapolated Glass Transition Temperatures Respectively.

APPENDIX E

REPRESENTATIVE FREQUENCY SPECTRA

Frequency spectra representing the formation histories A and B for MCS-1218, N1 and N2 fluids are shown in Figures E1-a-c and Figures E2-a-c respectively. Representative spectra of 5P4E were reproduced in Chapter III (Figures 13 and 15). The spectra shown are typical in general appearance for all spectra obtained.

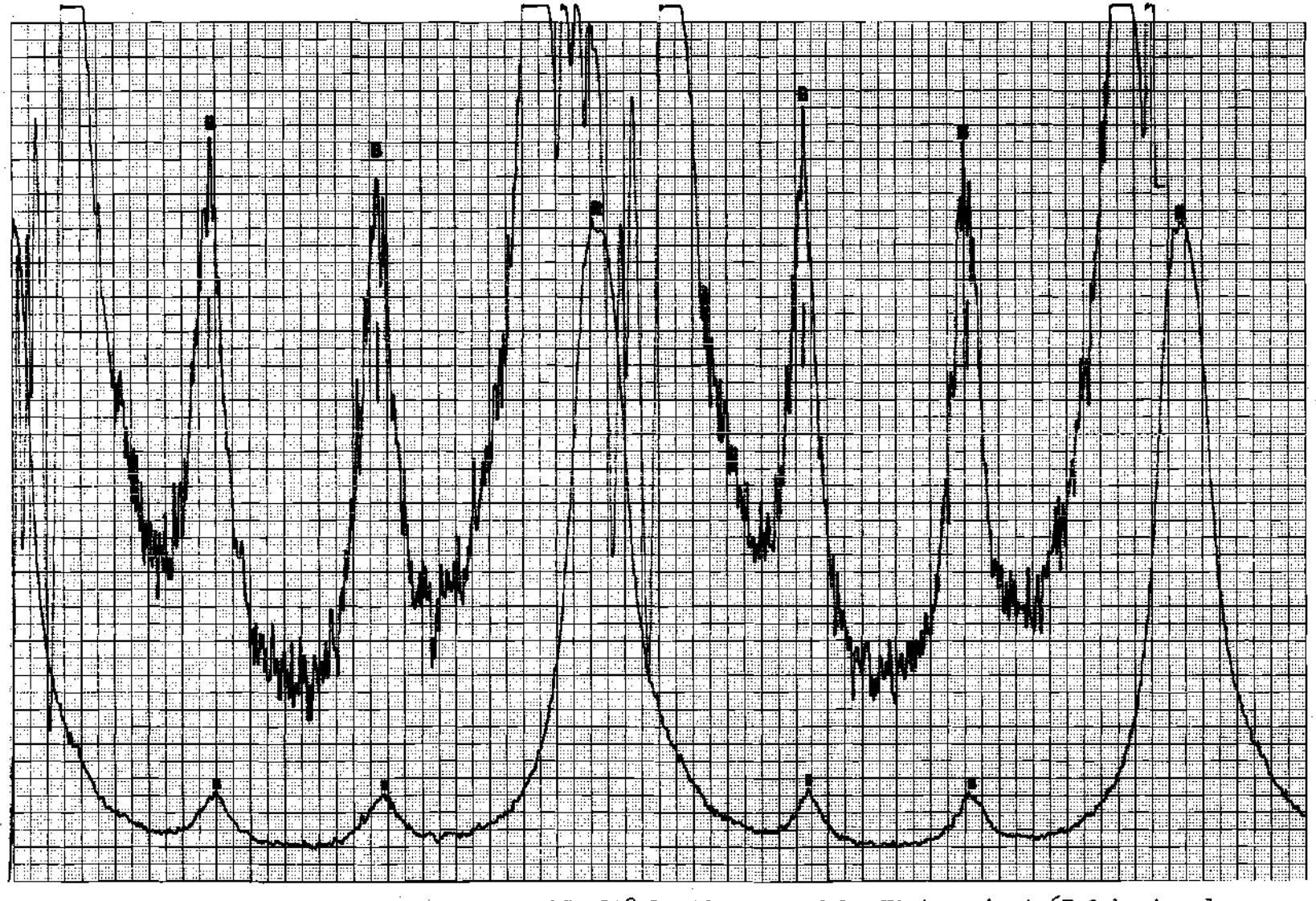

Figure E1-a. Frequency Spectrum of MCS-1218 Fluid Obtained by History A at 67.0 kpsi and 176F. B and R Represent the Brillouin and Rayleigh Components Respectively.

Figure E1-b. Frequency Spectrum for N1 Fluid Obtained by History A at 100.0 kpsi and 100.8F. B and R Represent the Brillouin and Rayleigh Components Respectively.

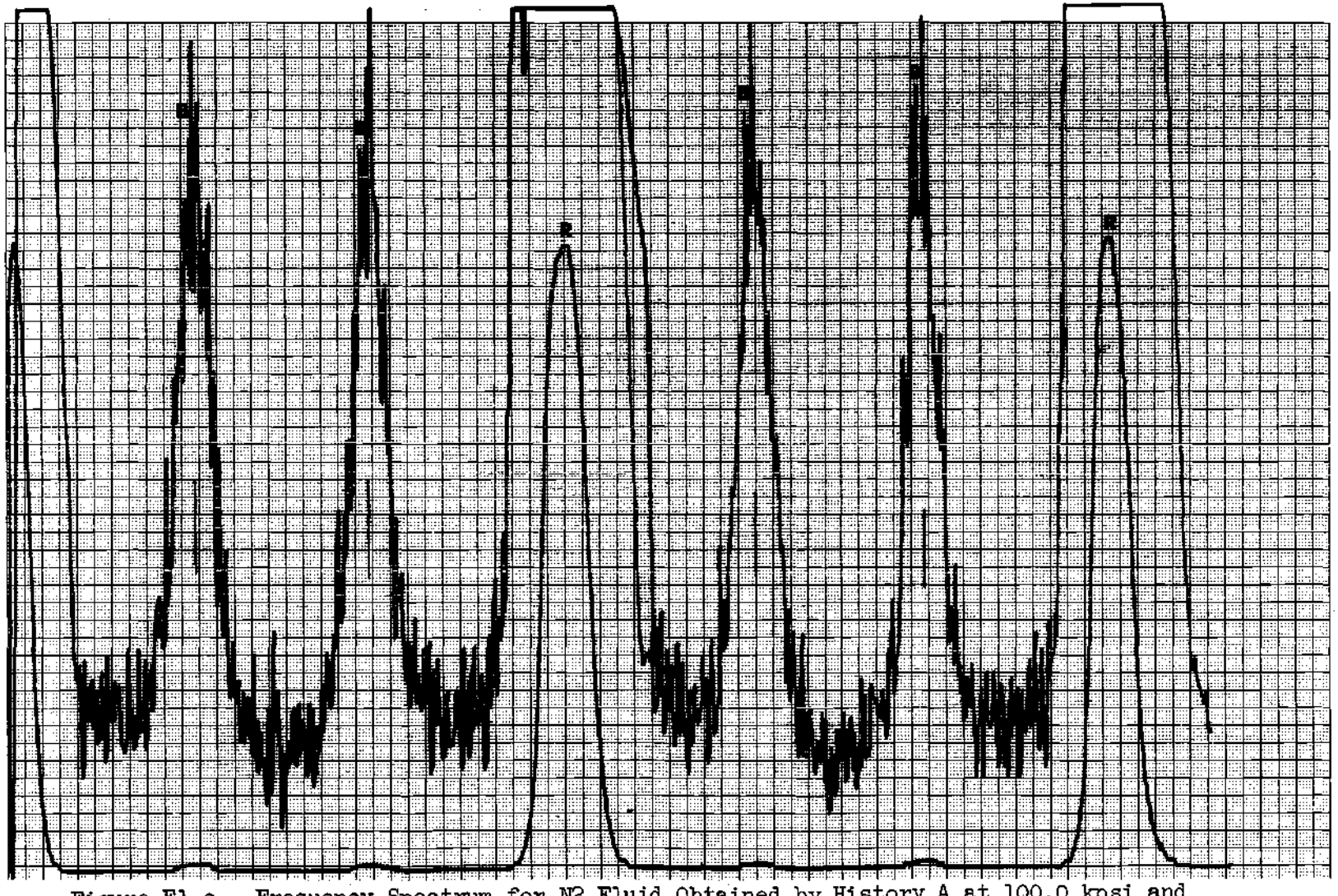

Figure E1-c. Frequency Spectrum for N2 Fluid Obtained by History A at 100.0 kpsi and 151F. B and R Represent the Brillouin and Rayleigh Components Respectively.

Figure E2-a. Frequency Spectrum for MCS-1218 Fluid Obtained by History B at 24.4 kpsi. B and R Represent the Brillouin and Rayleigh Components Respectively.

Figure E2-b. Frequency Spectrum for N1 Fluid Obtained by History B at 40.15 kpsi. B and R Represent the Brillouin and Rayleigh Components Respectively.

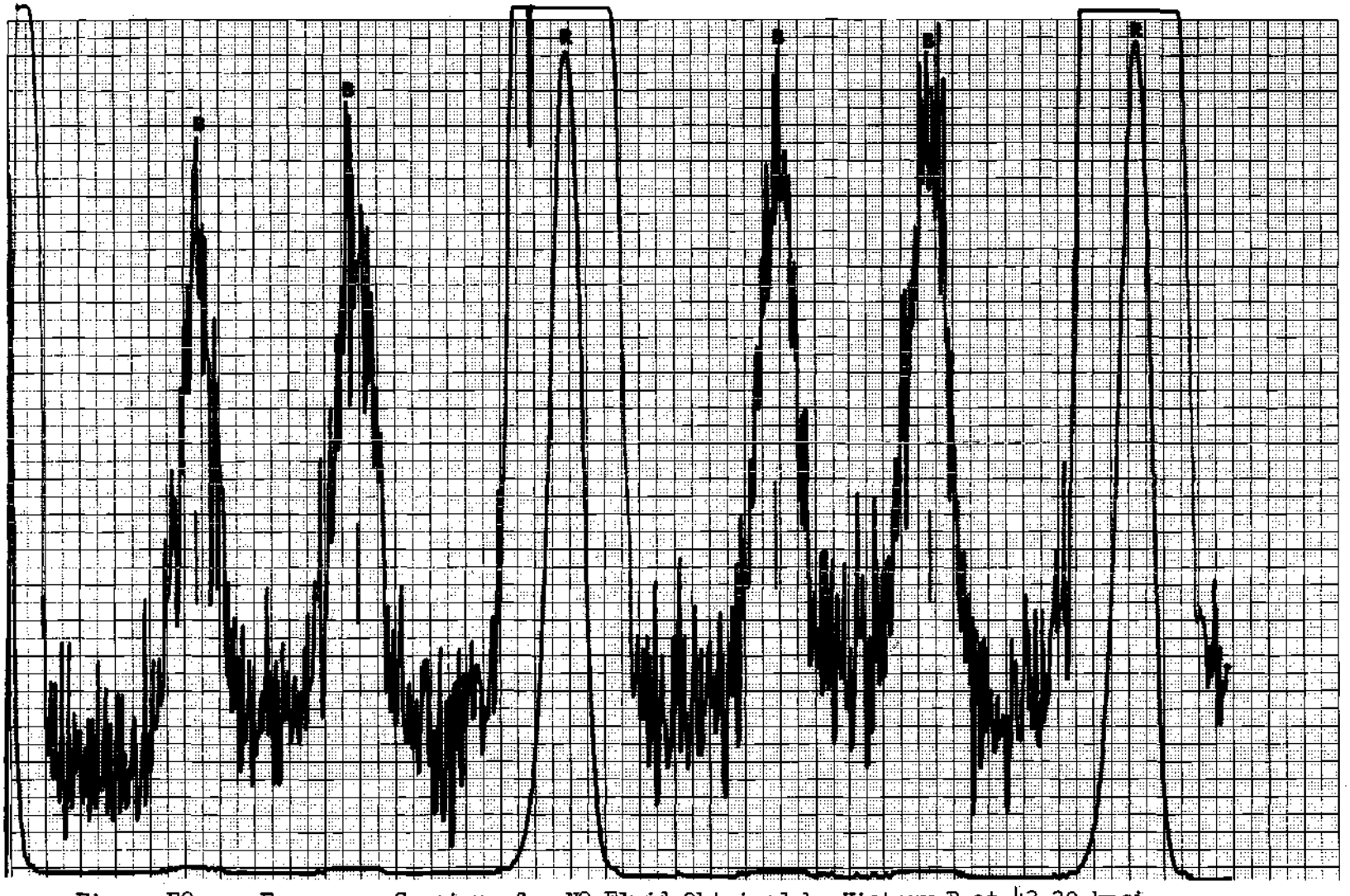

Figure E2-c. Frequency Spectrum for N2 Fluid Obtained by History B at 43.30 kpsi. B and R Represent the Brillouin and Rayleigh Components Respectively.

BIBLIOGRAPHY

1. F. W. Smith, "Lubricant Behavior in Concentrated Contact - Some Rheological Problems," ASLE Transaction, 3, 18, 1960.

2. K. L. Johnson and A. D. Roberts, "Observation of Viscoelastic Behavior of an EHD Lubricant Film," Proc. Roy. Soc. Lond. A-337, 217, 1974.

3. K. L. Johnson and R. Cameron, "Shear Behavior of Electohydrodynamic Oil Films at High Rolling Contact Pressures," Proc. Inst. Mech. Engrs., 182, Pt. 1, 307, 1967/1968.

4. John Lamb, "Experimental Linear Viscoelastic Measurements for Liquids," Symposium on Lubricant Properties in Thin Lubricating Films, April 1976 (to be published).

5. W. Hirst and A. J. Moore, "The Elastohydrodynamic Behavior of Polyphenyl Ether," Proc. Roy. Soc Lond., A-344, 403, 1975.

6. F. Noel, "Thermal Analysis of Lubricating Oils," Thermonica Act., 4, 377, 1972.

7. E. O. Stejskal and A. Cameron, "Optical Interferometry Study of Film Formation in Lubrication of Sliding and/or Rolling Contacts," Report No. NASA CR-120842, 1972.

8. ASME, Pressure-Viscosity Report, I, II, A Report Prepared by the ASME Research Committee on Lubrication, N.Y., ASME, 1953.

9. R. N. Haward, "The Physics of Glassy Polymers," New York, Wiley and Sons, Inc., 1973.

10. D. Turnbull, Contemp. Phys. 10, 473, 1969.

11. J. D. Ferry, "Viscoelastic Properties of Polymers," New York, Wiley and Sons, Inc., 1961.

12. A. J. Kovacs, J. Polym. Sci., 30, 131, 1958.

13. S. Matsuaka and B. Maxwell, J. Poly. Sci., 32, 131, 1958.

14. J. E. McKinny and M. Goldstein, "PVT Relationships for Liquid and Glassy Poly(Vinyl Acetate)," Journal of Research of the NBS-Physics and Chemistry, 78A, 331, 1974.

15. W. O. Winer, D. M. Sanborn, H. S. Nagaraj, and V. K. Ausherman, "Infrared Temperature Mapping in EHD Lubrication," Paper No. 75-Lub-17, Presented at the ASLE-ASME Joint Lubrication Conference, Miami Beach, Florida, October 1975.

16. I. L. Fabelinskii, Molecular Scattering of Light, Plenum Press, New York, 1968.

17. P. Debye, Ann. Physik, 39, 789, 1912.

18. L. Brillouin, Ann. Phys. (Paris) 17, 88, 1922.

19. L. Landua and G. Placzek, Z. Phys. Sowjetunion, 5, 172, 1934.

20. D. H. Rank, E. M. Kiess, and U. Fink, "Brillouin Spectra of Viscous Liquids," J. Opt. Soc. Am. 56(2), 103, 1966.

21. D. A. Pinnow, S. J. Candau, I. T. LaMacchia, and T. A. Litovitz, "Brillouin Scattering: Viscoelastic Measurements in Liquids," J. Acoust. Soc. Am., 43, 13, 1968.

22. D. H. Rank, E. M. Kiess, U. Fink and T. A. Wiggins, J. Opt. Soc. Am., 54, 1286, 1964.

23. H. Z. Cummins and R. W. Gammon, "Rayleigh and Brillouin Scattering in Liquids: The Landau-Placzek Ratio," J. Chem. Phys., 44(7), 2785, 1966.

24. J. R. Stevens, D. A. Jackson, and J. V. Champion, "Evidence for Ordered Regions in P ly(n-butyl) Methacrylate from Light Scattering Studies," Molecular Physics, 29(6), 1893, 1975.

25. R. W. Coakley, R. S. Mitchell, J. R. Stevens and J. L. Hunt, "Rayleigh-Brillouin Light Scattering Studies on Atactic Polystrene," A paper presented at the American Physical Society Conference, Atlanta, Georgia, April, 1976.

26. J. F. Dill, P. W. Drake, and T. A. Litovitz, "The Study of Viscoelastic Properties of Lubricants Using High Pressure Optical Techniques," ASLE, 18(3), 202, 1975.

27. D. A. Jackson, H. T. A. Pentecost, and J. G. Powels, "Hypersonic Absorption in Amorphous Polymers by Light Scattering," Molecular Physics, 23(2), 425, 1972.

28. A. B. Romberger, D. P. Eastman, and J. L. Hunt, "Evidence for Structure in Plastics from Light Scattering," J. Chem. Phys., 51(9), 3723, 1969.

29. Richard N. Work, "On the Discontinuity in the Temperature Coefficient of the Velocity of Ultra Waves in Polymeric Materials," J. Appl. Phys., 27(1), 69, 1956.

30. R. S. Mitchell, and J. E. Guillet, "Brillouin Scattering in Amorphous Polymeric Solid," J. Polymer Sci.: Polymer Phys. Ed., 12, 713, 1974.

31. E. A. Friedman, A. J. Ritger, and R. D. Andrews, "Brillouin Scattering Near the Glass Transition of Polymethyl Methacrylate," J. Appl. Phys., 40(11), 4243, 1969.

32. D. C. O'Shea, W. R. Callen, and W. T. Rhodes, "A Laser Textbook-An Introduction to Lasers and their Applications," Georgia Institute of Technology Bookstore, 1973.

33. J. D. Novak, "An Experimental Investigation of the Combined Effects of Pressure, Temperature, and Shear Stress Upon Viscosity," Ph.D. Thesis, University of Michigan, 1968.

34. J. Jakobsen, "Lubricant Rheology at High Shear Stress," Ph.D. Thesis, Georgia Institute of Technology, 1973.

35. G. Gee, "The Glassy State in Polymers," Contemp. Phys., 11(4), 313, 1974.

36. J. B. Yourtee and S. L. Cooper, "Properties of Densified Amorphous Polystyrene," J. Appl. Polym. Sci., 18, 897, 1974.

37. R. J. Greet and D. Turnbull, "Glass Transition in O-Terphenyl," J. Chem. Phys., 46(4), 1967.

38. E. M. Barrall, II, R. S. Porter, and J. F. Johnson, "Heat of Transition for Some Cholesteryl Esters by Differential Scanning Calorimetry," J. Phys. Chem., 71(5), 1224, 1967.

39. G. P. Johari and M. Goldstein, "Viscous Liquids and the Glass Transition," J. Chem. Phys., 55(9), 4245, 1971.

40. O. Yano and Y. Wada, "Dynamic and Dielectric Relaxations of Polysterene Below the Glass Temperature," J. Polym. Sci., 9(A2), 669, 1971.

41. D. M. Sanborn, "An Experimental Investigation of the Elasto-hydrodynamic Lubrication of Point Contacts in Pure Sliding," Ph.D. Thesis, University of Michigan, 1969.

42. G. R. Paul and A. Cameron, Proc. Roy. Soc. (Lond.), A331, 171, 1972.

43. J. J. Filliben and J. E. McKinny, "Confidence Limits for the Abscissa of Intersection of Two Linear Regressions," J. Res. Nat. Bur. Stand. (U.S.), 768 (Math. Sci.), 179, 1972.

44. P. R. Bevington, "Data Reduction and Error Analysis for the Physical Sciences," McGraw-Hill, New York, 1969.

45. W. W. Hines and D. C. Montgomery, "Probability and Statistics," Ronald Press, New York, 1972.

46. Private Communication of Concurrent Work to be Published, W. O. Winer, S. Bair and M. A. Alsaad.

47. H. Nagaraj, Ph.D. Thesis, School of Mechanical Engineering, Georgia Institute of Technology, Atlanta, Georgia, to be published.

48. G. Harrison, "The Dynamic Properties of Supercooled Liquids," Academic Press, New York, 1976.

VITA

Mohammed Ahmad Alsaad was born in Um-Elfahm, Palestine, on November 1, 1940. In 1948, he moved out of Palestine to the West Bank of Jordan and obtained a Jordanian citizenship. In 1961, he graduated from High School. He obtained his B.Sc in Mechanical Engineering from Cairo University, Cairo, Egypt in 1966. After graduating, he worked in the State of Kuwait in the oil industry for five years. In 1971, he decided to pursue his graduate studies in the United States where he obtained his Master's Degree in Mechanical Engineering at the George Washington University, Washington D.C. in 1973. He then enrolled in Georgia Institute of Technology, Atlanta, Georgia to continue graduate education toward the Ph.D degree in Mechanical Engineering. His educational emphasis has been in the area of the thermal and fluid sciences.